NUREG/CR-3190
SAND82-1580
R3
Printed April 1984

PLUGM
A Coupled Thermal-Hydraulic Computer Model for Freezing Melt Flow in a Channel

Marty Pilch

Peter K. Mast
Science Applications, Inc.
Albuquerque, NM

Prepared by
Sandia National Laboratories
Albuquerque, New Mexico 87185 and Livermore, California 94550
for the United States Department of Energy
under Contract DE-AC04-76DP00789

Prepared for
U. S. NUCLEAR REGULATORY COMMISSION

Available from

GPO Sales Program
Division of Technical Information and Document Control
U.S. Nuclear Regulatory Commission
Washington, D.C. 20555

and

National Technical Information Service
Springfield, Virginia 22161

NUREG/CR-3190

SAND82-1580

PLUGM

A Coupled Thermal-Hydraulic Computer Model for Freezing Melt Flow in a Channel

Marty Pilch
Peter K. Mast*

April 1984

Sandia National Laboratories
Albuquerque, NM 87185
Operated by
Sandia Corporation
for the U.S. Department of Energy

Prepared for
Division of Engineering Technology
and
Division of Accident Evaluation
Office of Nuclear Regulatory Research
U.S. Nuclear Regulatory Commission
Washington, DC 20555
Under Memorandum of Understanding DOE 40-550-75
NRC FIN No. A1247

---

* Science Applications, Inc., Albuquerque, NM.

Abstract

PLUGM models the flow and freezing of molten material in a nonmelting channel. PLUGM is being developed for applications in Sandia's Ex-Vessel Core Retention Materials Assessment Program and in Sandia's LMFBR Transition-Phase Program.

PLUGM models time-dependent flow from a reservoir, through a channel and possibly into a catch tank. Three user-specified geometry options enable realistic modeling of melt flow and freezing in tubes, thin slits, and particle beds. Axial variation of relevant channel parameters is possible.

Melt flow is driven or hindered by gravity, applied pressure, and capillary pressure. Hydrodynamic losses due to friction, area changes, and flow direction changes are modeled. Also modeled are the competing effects of mass addition to the reservoir, mass drainage into the channel, and slug depletion by film and crust deposition on the channel wall.

Cooldown of a superheated melt occurs by material transport down the channel and by convective heat transfer to the channel walls or crust. Axial conduction and volumetric heating within the bulk melt are not modeled.

Crust deposition on the channel wall is controlled by the competing effects of convective heat transfer from the bulk melt to the crust surface and the conduction limited removal of heat from the crust into the wall. An external coolant may further enhance this heat removal by limiting the temperature increase in the wall.

Sample problems, pertaining to ex-vessel core retention and LMFBR transition phase, illustrate features and capabilities of the code.

Table of Contents

List of Figures

List of Tables

List of Symbols

A_f,	cross-sectional flow area of node
A_s,	wetted surface area of node
c_p,	specific heat of crust
c_{pb},	specific heat of bulk melt
c_{pw},	specific heat of wall
$D_h(t)$,	hydraulic diameter of channel
D_p,	particle diameter
D_w,	wall thickness
f(t),	Fanning friction factor at the bulk-melt/crust interface or the bulk-melt/wall interface if no crust exists
g,	acceleration due to gravity
h(t),	heat transfer coefficient from the bulk melt to the crust or to the wall if no crust exists
h_{fb},	heat of fusion of bulk melt
h^*_{fb},	modified heat of fusion of bulk melt
$h_w(t)$,	heat transfer coefficient from the wall to the external coolant
K,	nonrecoverable, hydrodynamic loss coefficient associated with area changes or flow direction changes
k,	thermal conductivity of crust
k_b,	thermal conductivity of bulk melt
k_w,	thermal conductivity of wall
NLEAD,	node index for the partially filled leading edge node
NTRAIL,	node index for the partially filled trailing edge node

$Nu = \frac{hD_h}{k_b}$, Nusselt number

p, pressure

$Pr = \frac{c_{pb}\mu_b}{k_b}$, Prantl number

$Re_h = \frac{\rho_b v D_h}{\mu_b}$, Reynolds number

s, distance from the initial reservoir/channel interface

$T_b(t)$, temperature of bulk melt

T_{bm}, fusion temperature of bulk melt

$T_c(t)$, temperature at the crust/wall interface or bulk-melt/wall interface if no crust exists

$T_s(t)$, temperature at bulk-melt/crust interface or bulk-melt/wall interface if no crust exists

T_w^o, initial temperature of the wall and external coolant

$T_{wb}(t)$, interface temperature between wall and external coolant

V, volume of node

$v(t)$, velocity of bulk-melt

z, vertical elevation relative to the initial reservoir/channel interface

α, thermal diffusivity of crust

α_w, thermal diffusivity of wall

$\beta(t)$, shape parameter of the crust temperature profile

$\beta_w(t)$, shape parameter of the wall temperature profile

$\delta(t)$, crust thickness

$\delta_w(t)$, wall thermal layer thickness

ε, porosity

Δs, node size

Δt, time step

ρ, density of crust

ρ_b, density of bulk melt

ρ_w, density of wall

σ, surface tension of bulk melt

μ, viscosity

Superscripts

n, time level index

Subscripts

i, node index

l, node index of leading edge node

t, node index of trailing edge node

1. Introduction

The phenomenon of freezing liquid flow in cold channels is of importance in two reactor safety programs at Sandia National Laboratories: The Core Retention Materials Assessment Program and the LMFBR Transition Phase Program. PLUGM, a coupled thermal-hydraulic computer model of this phenomenon, has been developed. Application to each of the programs is described in the following subsections.

An overview of the code is presented in Chapter 2. Chapters 3, 4, and 5 treat melt hydrodynamics, bulk melt cooldown, and crust-growth, respectively. Chapter 6 discusses development plans for a code in which additional transition-phase phenomena are coupled to the freezing phenomenon treated by PLUGM.

An input description to the code is provided in Appendix A. Finally, a number of sample problems are used in Appendies B, C, and D to illustrate unique features of PLUGM.

1.1 Ex-Vessel Core Retention

The Core Retention Material Assessment Program at Sandia, sponsored by the U. S. Nuclear Regulatory Commission, involves both experiments and analyses designed 1) to determine the fundamental limitations of candidate core retention materials and concepts, and 2) to develop a data base for use by the NRC in licensing review of proposed ex-vessel core retention devices. The program is currently focused on magnesia brick crucibles, thoria and alumina particle beds, and high alumina concrete liners.

The function of ex-vessel core retention is to reduce the risk of a severe nuclear accident by

1. reducing the probability of early above-ground containment failure;

2. eliminating long-term sources of fission-product-laden aerosols and combustible gases associated with debris/concrete interactions, and

3. preventing basemat penetration in those reactors, such as a floating nuclear plant, having major liquid pathways for fission product release.

All facets of this function require that core debris is prevented from coming into contact with concrete in the basemat and in the sidewall of the reactor cavity. As such, both initial and secondary penetration of a core retention device by molten core debris is of extreme importance. Application of PLUGM to melt

penetration of cracks and spaces in refractory brick crucibles and of the voids in particle beds is discussed below.

Refractory Brick Crucibles

Offshore Power Systems proposed a magnesia brick crucible for their floating nuclear plants [14]. A refractory brick crucible was also proposed for the Clinch River Breeder Reactor parallel design [21]. This concept has been investigated experimentally at Argonne National Laboratories, at Atomics International, and at Sandia National Laboratories. The primary advantage of the refractory brick concept is that it represents an inexpensive technique commonly practiced in the steel industry. The concerns with the concept include premature penetration of the cracks and spaces in the brick matrix of molten debris, gross failure of the crucible by flotation of bricks in the more dense debris, and the difficulty of assuring long-term coolability of the device and the contained debris.

Earlier analyses had treated the refractory brick crucibles as monolithic structures [2,3,4,10]. Such treatment ignores the fundamental concern with the concept. Thermal and mechanical stresses can lead to cracks in the crucible when melt falls from the reactor vessel onto the crucible. Furthermore, interbrick gaps are an engineering necessity so that thermal expansion of the bricks can be accommodated. Melt seepage through cracks and interbrick gaps could initiate catastrophic and rapid failure of the crucible by eroding the interlocking network and freeing bricks to float away. In addition to brick flotation, melt seepage in cracks and gaps could lead to premature contact of the melt with the concrete basement or any active cooling system which may be imbedded in the crucible.

PLUGH can model the freezing and plugging of melt as it flows through the tortuous flow paths of a brick matrix. The code incorporates such important features as:

1. representation of cracks using a thin slit geometry option,

2. the ability to account for hydrodynamic losses when the flow suddenly changes direction,

3. providing time dependent account of the gravity head, which drives the flow, even though the channel consists of vertical and horizontal sections.

Particle Beds

Particle-bed core retention devices were originally proposed for retrofitting existing light water reactors [18,19]. A conceptual design for a thoria particle-bed core retention device was performed by EG G, Idaho [15]. They found the expense of such a device prohibitive. Extensive investigation of the particle-bed concept at Sandia [8,9] has indicated that a device composed primarily of inexpensive alumina aggregate can contain molten core debris for several hours without any cooling, and indefinitely once coolant is added. In fact, because alumina melts, it provides a better thermal barrier than thoria. Currently, particle-bed core retention devices are being considered for new and advanced reactors as well as for existing light water reactors.

Both experiments and analyses (see sample calculation in Appendix B) have shown that a properly designed particle bed must consist of three layers. Molten core material is distributed, diluted, and quenched as it penetrates a top layer of relatively large particles (1-3 cm in diameter). Initial penetration is stopped by a middle layer of relatively small particles (0.3-0.4 cm in diameter). An additional layer of large particles at the bottom of the bed provides pathways for coolant.

In modeling flow and freezing of melt in a particle bed, the PLUGM code incorporates such important features as

1. appropriate hydrodynamic losses for a particle bed,
2. the incorporation of capillary forces for wetting or nonwetting melts,
3. and an appropriate heat transfer coefficient from the melt to the particles.

Experiments at Sandia with both steel and urania melts have confirmed PLUGM predictions of the effectiveness of a layer of small particles in stopping initial melt penetration.

1.2 Molten Fuel Relocation During the Transition Phase of an LMFBR Core Disruptive Accident

The analysis of hypothetical core disruptive accidents (CDAs) in Liquid Metal Fast Breeder Reactors (LMFBRs) has been primarily concerned with identifying those accident scenarios that could generate sufficiently high energetics (high core temperature and pressure resulting from neutronic burst) to threaten the integrity of the reactor vessel. Recent analysis [16] of low sodium void worth cores (the CRBR hetrogeneous core, for example) have indicated that the greatest potential for accident energetics in these reactors exists if the core were to melt

down, with limited removal of fuel from the active core region. "Sloshing" of such a high-fuel-inventory molten pool may be neutronically unstable such that amplification of any initial disturbance could lead to eventual large fuel-motion reactivity ramp rates and unacceptable energetics.

Crucial to the assessment of such molten-pool energetics is a determination of how much fuel inventory reduction has occurred prior to the formation of a neutronically coherent pool. Fuel inventory reduction because of fuel dispersal through several available escape paths may occur during the transition from intact pin geometry to the core-wide molten pool (referred to as the transition phase of the accident). A removal of 40% of the initial fissile fuel inventory would ensure subcriticality for any molten pool that does form. However, even smaller amounts of fuel removal could limit the pool-"sloshing" reactivity ramp rates, such that vessel-threatening energetics would not be expected.

The two potential fuel removal paths that become available earliest in the accident sequence are the flow channels in the upper axial blanket (UAB) region of the core and the intersubassembly gaps between adjacent internal blanket assemblies. The UAB flow channels are available to the extent that they have not been blocked because of prior cladding relocation. Some open UAB flow channels are to be expected, and these are available for fuel removal as soon as the fuel becomes mobile. The gaps between adjacent internal blanket assemblies become available for fuel removal only after melting of the neighboring driver assembly can walls. Thus, there is less time available for fuel removal through these gaps before complete disruption of the core occurs.

These important questions of the timing and magnitude of fuel removal through the UAB and intersubassembly gaps are being addressed in the SNL LMFBR Transition-Phase program. Needed experimental data on fuel removal and freezing is being provided by a series of in-pile experiments using actual reactor materials under prototypic temperature and pressure conditions. Complementary to the experiments is the development of the PLUGM code, which is being used to aid in the interpretation of the SNL experiments and to extrapolate from the experiment results to predictions of behavior in actual LMFBR accident scenarios.

The PLUGM code incorporates all known relevant transition-phase fuel removal phenomena into a consistent framework. Important features of the code include,

1. the ability to model finite liquid mass effects such as film deposition onto a crust surface,

2. the ability to model external cooling of the channel in which fuel freezing is occurring (relevant to fuel flow in intersubassembly gaps when the adjacent subassemblies have not yet experienced Na voiding),

3. allowing for all driving forces (applied pressure, gravity) and potential pressure loss mechanisms (flow area changes, flow direction changes, etc.).

The character of the fuel-freezing process is highly dependent on whether melting and entrainment of the flow channel walls occur. The version of the PLUGM code described in this report is applicable to the analysis of fuel freezing in a non-melting channel, where conduction-freezing of the fuel onto the channel walls is expected. For LMFBR transition-phase analyses, a future version of the PLUGM code is planned that will incorporate wall melting and entrainment phenomena.

2.0 Overview of PLUGM

The PLUGM code models the time-dependent flow of a molten material through a user-specified flow channel, taking into account heat transfer between the molten material and the channel wall and possible constriction of the channel due to surface crust formation. The three major aspects of the calculation are:

1. bulk-melt hydrodynamics,
2. bulk-melt cooldown,
3. crust growth (remelt) and wall heatup.

The following time-dependent information is calculated at each melt-containing channel node:

1. bulk-melt temperature,
2. crust thickness,
3. crust temperature profile,
4. wall temperature profile,
5. crust/wall or melt/wall contact temperature,
6. bulk-melt velocity.

From this information, the complete history of melt penetration into the channel can be constructed. Integral information such as final total penetration and total plugging time are also provided to the user.

2.1 Geometry

The user-specified flow channel may be defined in one of three geometries:

1. tube,
2. thin-slit, or
3. particle bed.

For the tube-geometry option, useful for the analysis of most transition-phase plugging and freezing experiments, the channel diameter and channel wall thickness define the geometry. For the thin-slit geometry option, useful for the analysis of brick crucibles and the transition-phase intersubassembly-gap fuel removal analysis, the slit spacing, slit width and channel wall

thickness define the geometry. Particle-bed geometry is more difficult to treat. Bulk-melt hydrodynamics and bulk-melt cooldown are handled in an appropriate manner for particle-bed geometry. Crust growth (remelt) and wall heat are handled by modeling a typical flow path through a particle bed as a tube with equivalent hydraulic diameter. The equivalent wall thickness is chosen in a manner consistent with the hydraulic diameter and the particle-bed porosity.

External cooling of the channel walls may also be modeled for the tube and thin-slit geometry options. The coding assumes the existence of an external coolant, the temperature of which remains fixed in time at the initial wall temperature. Heat transfer to this external coolant can be specified via a user-supplied (axially varying) heat transfer coefficient. For the particle bed geometry option, the external coolant is nonphysical. Thus, the external coolant heat transfer coefficient is automatically set to zero (overriding the user input) to preset an adiabatic boundary at the center of the particle.

Overall problem geometry is divided into a number of regions in order to specify the axial variation of input parameters:

1. flow direction (with gravity, against gravity, or horizontal),
2. initial channel diameter (or slit-spacing, slit-width) and wall thickness,
3. initial wall temperature,
4. initial melt temperature,
5. external-coolant heat-transfer coefficient.

In its most elementary form, PLUGM models three regions:

1. reservoir,
2. channel, and
3. catch tank.

Figure 2.1 depicts the arrangement.

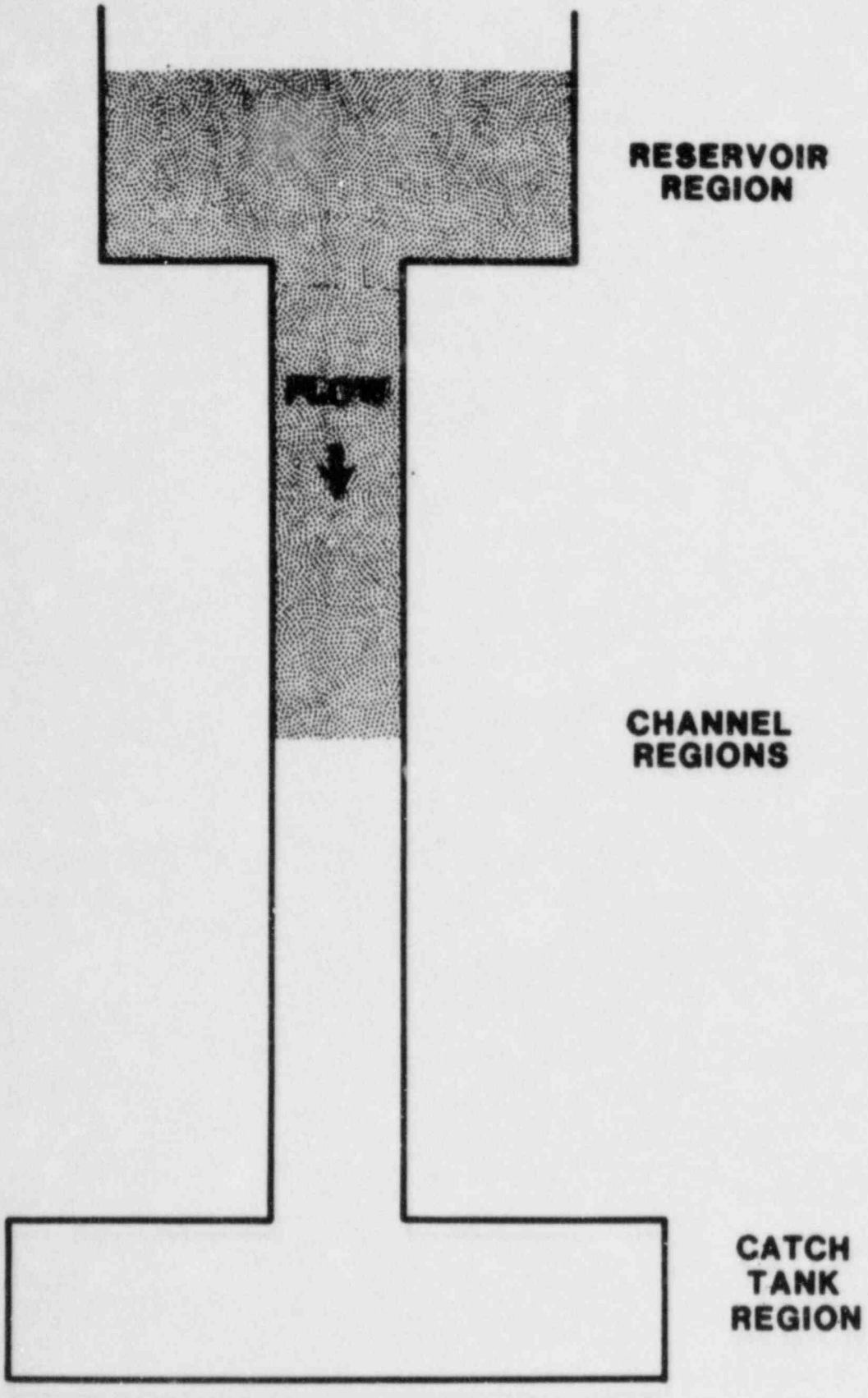

Figure 2.1 Regions Modeled by PLUGH

Reservoir

The reservoir is the first defined region. In general, all the melt is contained in the reservoir at the start of the problem. PLUGM offers three reservoir options: rigid-boundary reservoir, pool-type reservoir, and constant-mass reservoir.

For a rigid-boundary reservoir, heat transfer and friction losses are calculated for all reservoir nodes (except the node adjacent to the free surface). The time-dependent depth of the reservoir is determined from the user-specified mass-addition rate and the code-calculated drainage rate into the channel.

An example illustrates a pool-type reservoir. If melt is poured onto a particle bed, then a pool-type reservoir represents the unit cell of melt situated over a flow channel into the particle bed. A pool-type reservoir has no rigid boundaries, and heat transfer to the boundary and friction losses are not calculated. The time dependent depth of the reservoir is also calculated for this option.

A constant-mass reservoir is treated as a pool-type reservoir; i.e., no heat transfer or friction losses. However, the melt level in the reservoir remains constant in time regardless of how much melt is added to the reservoir or drained into the channel. This reservoir option, which models a nonphysical situation, is useful when trying to reproduce results obtained from existing analytic solutions for freezing and plugging.

Channel

Melt drains from the reservoir into the channel. The channel itself can be broken into an arbitrary number of regions, thus providing more resolution in any parameters that vary axially.

Catch Tank

Melt leaving the channel enters the catch tank, which is the last defined region. PLUGM offers three catch tank options:

1. treat catch tank like channel, calculate heat transfer and hydrodynamic losses, melt expands from channel to fill entire flow area of catch tank,

2. heat transfer and hydrodynamic losses are <u>not</u> calculated, melt expands from channel to fill entire flow area of catch tank, and

3. heat transfer and hydrodynamic losses are <u>not</u> calculated, fluid jets from last channel region into

catch tank, the jet diameter does not change regardless of catch tank diameter.

Each of the user-specified regions may be further subdivided into an arbitrary number of axial nodes for the actual PLUGM calculations. These nodes define the axial resolution on the code-calculated crust growth, temperature, and velocity distributions.

2.2 Coupled Solution Procedure

There are three major parts of the PLUGM calculational procedure:

1. bulk-melt hydrodynamics,
2. bulk-melt cooldown,
3. crust growth (remelt) and wall heatup.

In the PLUGM formalism, the coupling between these three calculations is done explicitly.

Bulk-melt Hydrodynamics

PLUGM's hydrodynamics calculations are based on a finite-difference axial (in direction of flow) formulation. Inertial effects are included by solving an approximation to the one-dimensional momentum equation. An alternate quasi-steady flow option is available in which a modified Bernoulli equation is used to calculate consistent velocities at the end of each time step.

Melt flow is driven by one or more of the following:

1. applied pressure,
2. gravity, or
3. capillary pressure.

Note that any of these can also be a retarding force depending on the problem. PLUGM's hydrodynamics also account for

1. friction losses (laminar or turbulent flow),
2. recoverable Bernoulli losses due to flow area changes, and
3. nonrecoverable losses due to expansions, contractions, or changes in flow direction (i.e., elbow losses).

PLUGM allows for arbitrary mass addition to the reservoir or trailing edge node. PLUGM also accounts for the film deposition at the trailing edge of the flow in the event that mass addition is insufficient to prevent draining of the inlet reservoir. Thus, mass depletion of the liquid material by crust and liquid-film deposition is calculated.

The quantities calculated by the hydrodynamics module are the time-dependent bulk-melt velocity distribution and leading-edge and trailing-edge positions of the bulk-melt slug. The principle parameter needed from the other solution modules is the crust-thickness distribution, which is required to determine the time-dependent hydraulic diameters and hence friction factors. Because constant material properties are used in the analysis, there is no direct feedback on the hydrodynamics calculation from the time-varying bulk-melt temperature. A detailed description of the hydrodynamics solution procedure is found in Section 3 of this document.

Bulk-Melt Cooldown

The axial temperature distribution in the bulk melt changes in time as a result of

1. material transport of bulk melt down the channel, and

2. convective heat transfer to the channel walls or crust.

Axial (in direction of flow) conduction and volumetric heating within the bulk melt are not modeled. An axial finite-difference formulation of the heat transport within the bulk-melt is used. The needed boundary conditions of bulk-melt velocity and crust (or wall, if no crust) surface temperature distributions are obtained explicitly from the hydrodynamics and crust growth/wall-heatup modules.

The initial bulk-melt temperature can be either saturated or superheated: an important feature for most reactor-safety applications. Convective heat transfer to the crust or wall surface can be either laminar or turbulent depending on the code-calculated local Reynolds number. The calculation of local bulk-melt to crust (or wall) heat transfer coefficient also accounts for the Prandtl number of the fluid (liquid metal versus normal fluid).

Crust Growth (Remelt) and Wall Heatup

Crust deposition on the channel wall is controlled by the competing effects of convective heat transfer from the bulk melt to the crust surface and the conduction limited removal of heat from the crust into the wall. An external coolant may further enhance this heat removal by limiting the temperature increase in the wall.

The solution for the coupled crust-growth (or remelt) and wall heatup is obtained from a numerical solution of the integral energy equations in the crust and wall. The solution procedure assumes that both the crust and wall temperature profiles can be described by second order polynomials (in spatial coordinate) with time-dependent coefficients. User-input, constant material properties are used in the analysis. The use of these assumed profiles in the integral energy equations results in a system of coupled first-order differential equations for the time-dependent coefficients that must be solved for at each axial node. The equations account for the time-dependent heat flux from the bulk-melt into the growing (or remelting) crust as well as the possible heat transfer between the outer wall surface and the external coolant.

The time-dependent crust/wall contact temperature at each axial node is uniquely defined by the coupled equations. These temperatures indicate the axial extent over which channel wall melting is to be expected. The PLUGM code as described herein does not account for the effect of wall melting (i.e., heat of fusion) on the crust-growth/wall-heatup solutions. This is not required for the core retention applications. However, a future version of the code will account for this effect for transition-phase applications.

The quantities calculated by the crust-growth/wall-heatup module are the time-dependent axial crust-thickness distribution and the crust and wall temperature distributions. The principle parameters needed from the other solution modules are the bulk-melt temperature and the bulk-melt velocity (for determining heat transfer coefficients). A detailed description of the crust-growth/wall-heatup solution scheme is found in Chapter 5 of this document.

2.3 Node Indexing

The reservoir region and each channel region consists of one or more nodes, the catch-tank region consists of only one node. Nodes are indexed consecutively from the reservoir to the catch tank as depicted in Figure 2.2. The index of the partially filled trailing edge node is called NTRAIL, and the index of the partially filled leading edge node is called NLEAD. The following parameters are node centered.

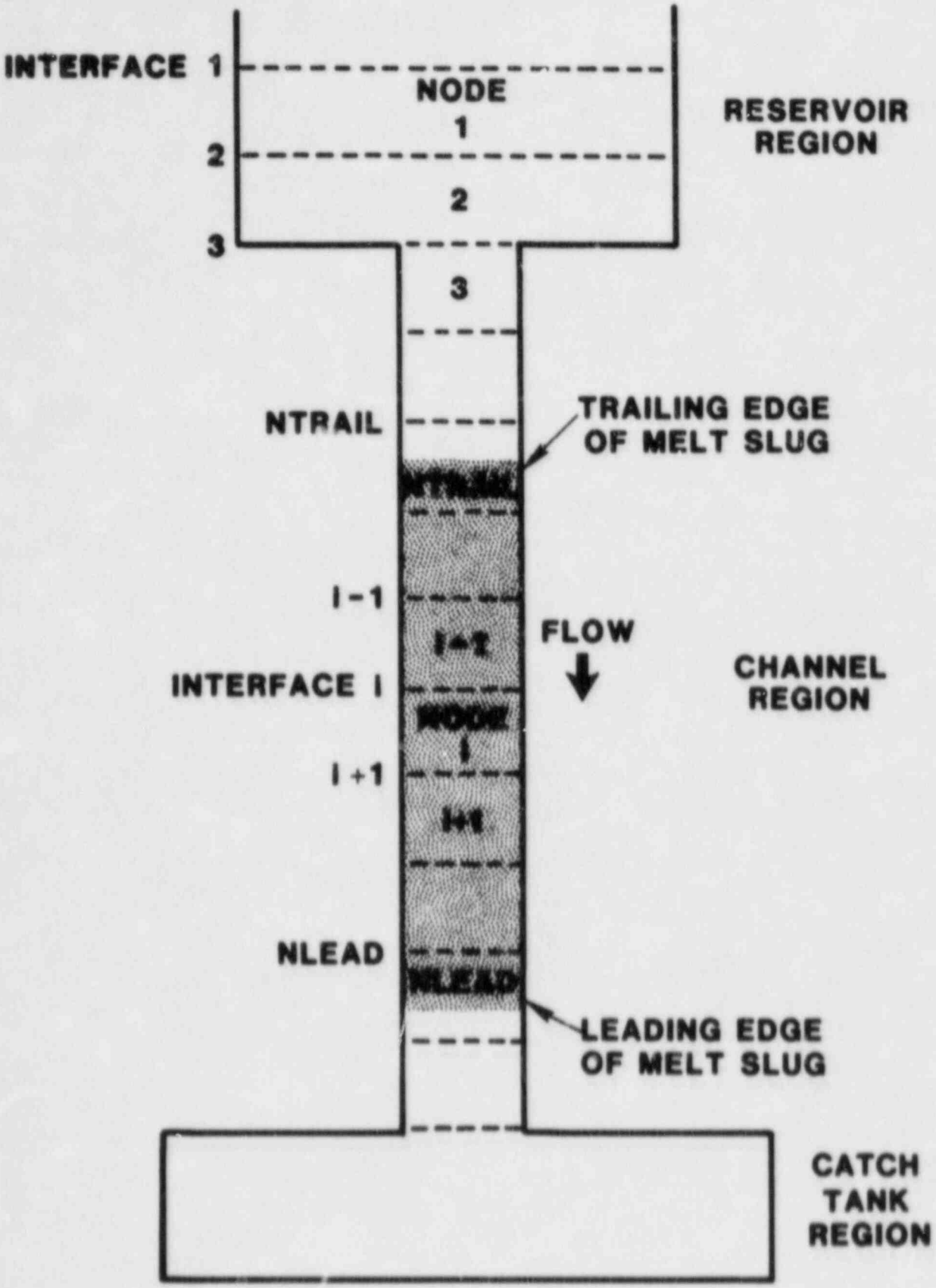

Figure 2.2. Node Indexing

D, channel diameter or slit spacing

δ, crust thickness

δ_w, wall thermal-layer thickness

D_w, wall thickness

D_h, channel hydraulic diameter*

A_f, channel cross-sectional flow area*

T_b, Temperature of bulk melt

v, velocity of bulk melt

h, heat transfer coefficient from the bulk-melt to the crust or the wall if no crust exists.

f, friction factor at the bulk melt/crust interface or the bulk-melt/wall interface if no crust exists

T_c, temperature of crust/wall interface

T_w^o, initial temperature of the wall and external coolant

T_{wb}, temperature of outer wall surface

h_w, heat transfer coefficient from the wall to the external coolant

The following parameters are defined at axial node interfaces:

s, total distance from he initial reservoir/channel interface

z, total vertical elevation relative to initial reservoir/channel interface

K, hydrodynamic loss coefficient associated with expansions, contractions, of flow direction changes

As shown in Figure 2.3, a typical node is composed of bulk melt, crust, heated wall, unheated wall, and external coolant. In some problems, the crust may disappear, and the heated wall may extend to the external coolant.

*These quantities are defined in Section 2.4.

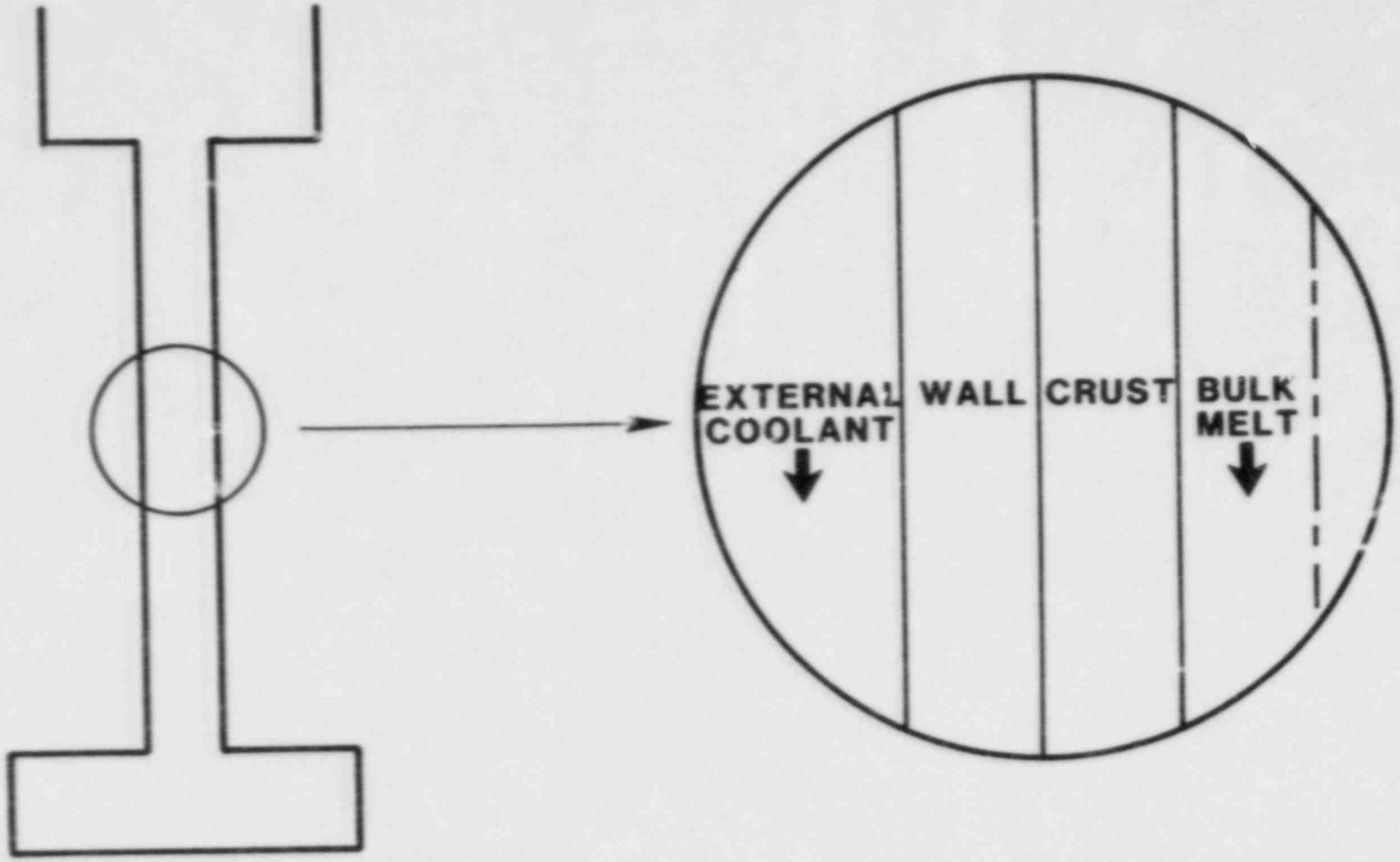

Figure 2.3. Composition of a Typical Node

2.4 Definition of Hydraulic Diameter and Channel Flow Area

The axially-dependent channel hydraulic diameter and flow area are used extensively in the calculations and in the detailed descriptions of the three PLUGM code modules that follow in the subsequent chapters. They are defined here for each of the three geometry options available in the code.

Tube Geometry

At any point in time, the effective channel diameter, D', can be expressed in terms of the initial channel diameter, D, and the bulk-melt crust thickness, δ, as

$$D' = D - 2\delta \quad . \qquad 2.4.1$$

The hydraulic diameter and channel flow area are then simply described by

$$D_h = D' \qquad 2.4.2$$

and

$$A_f = \frac{\pi}{4} (D')^2 \quad . \qquad 2.4.3$$

Thin-Slit Geometry

At any point in time, the effective slit spacing, D', can be expressed in terms of the initial slit-spacing, D, and the bulk-melt crust thickness, δ, as

$$D' = D - 2\delta \quad . \qquad 2.4.1$$

Because a thin slit has been assumed in the analysis, the length of the slit, W, is assumed to be unaffected by crust growth. Thus, the hydraulic diameter and channel flow area are given by

$$D_h = \frac{2WD'}{(W + D')} \qquad 2.4.2$$

and

$$A_f = WD' \qquad 2.4.3$$

Particle Bed

A particle bed geometry is described in PLUGM by an equivalent tube-geometry picture. Thus, Equations 2.4.1-3 are applicable.

The user must input an appropriate tube diameter, D, such that this represents the initial hydraulic diameter in the particle bed. Thus, the user-supplied value for D can be expressed in terms of the bed porosity, ε, and particle diameter, D_p, as

$$D = \frac{2}{3} \frac{\varepsilon}{1 - \varepsilon} D_p \quad . \qquad 2.4.4$$

For a particle bed, an effective wall thickness, D_w, must also be supplied by the user such that the ratio of initial channel flow area to cross-sectional wall area is consistent with the given bed porosity. This implies that

$$\varepsilon = \frac{\pi D^2}{\pi(D + 2D_w)^2} \qquad 2.4.5$$

so that the user supplied value for the effective wall thickness should be given by

$$D_w = \frac{D}{2}\left[\varepsilon^{-1/2} - 1\right] \qquad 2.4.6$$

This definition of D_w ensures that thermal mass ratio between the bulk melt and the wall is the same for the actual particle bed and the tube geometry model of the particle bed. When a pool of liquid initially sits on top of a particle bed, the reservoir (i.e., first melt-filled region) represents the liquid associated with one flow channel into the particle bed. Thus, the flow area in the reservoir should equal the total cross-sectional area associated with the channel (flow area plus associated particles) at the entrance to the particle bed. Thus, the reservoir diameter in this case is simply given by

$$D(res) = D + 2D_w \qquad 2.4.7$$

and the wall thickness in the reservoir is zero.

$$D_{w(res)} = 0 \qquad 2.4.8$$

3. Bulk-Melt Hydrodynamics

PLUGM's hydrodynamics calculations are based on a finite-difference, axial formulation assuming incompressible flow. Three options are available to the user to specify the type of hydrodynamics calculation to be performed:

1. transient velocity calculation including inertial effects with an initial velocity of zero,.
2. transient velocity calculation including inertial effects with a quasi-steady initial velocity,
3. quasi-steady velocity calculated by simply balancing driving forces with loss terms.

Included in the hydrodynamics calculation is the treatment of possible mass addition to the melt flow and mass depletion (by crust growth and film deposition) at the trailing edge of the flow.

Melt flow is driven by one or more of the following:

1. applied pressure,
2. gravity,
3. capillary forces.

Note that any of these forces may also retard the flow depending on the problem. PLUGM's hydrodynamics also account for

1. friction losses (laminar or turbulent flow),
2. recoverable Bernoulli losses due to flow area changes,
3. nonrecoverable losses due to expansions, contractions, or changes in flow direction (elbow losses).

3.1 Mass Addition and Depletion

As mentioned above, both mass addition and mass depletion are accounted for in the PLUGM hydrodynamics treatment. An example of where mass addition would have to be modeled is a simple reservoir/channel/catch-tank configuration where material is poured into the reservoir at some mass flow rate $\dot{m}$. In that case, the total melt mass is increasing with time, thereby affecting the hydrostatic head that produces melt flow into the channel. In the PLUGM code, such mass addition is always assumed to occur at the trailing edge of the melt flow. Thus, it is not possible to model the possible situation of multiple slugs of liquid moving through the channel.

For the case of no mass addition to the reservoir, or for the case of limited mass addition, the trailing edge of the flowing melt moves through the defined problem geometry, leaving behind any frozen crust that had formed. Such a draining of liquid would also leave a residual liquid film on the crust surface, which subsequently solidifies. This is illustrated in Figure 3.1. Thus, in such a finite liquid-mass situation, the mass of the liquid "slug" moving down the channel is continually being depleted by crust formation and film deposition at the trailing edge of the flow.

In general, the thickness of liquid film deposited at the trailing edge of a constant-velocity (or near-constant) liquid slug is a function of the bulk-melt velocity, the material properties (viscosity and surface tension in particular), and the channel geometry. However, a detailed prediction of film thickness based on these parameters is not done in PLUGM. Rather, the code uses a simple correlation based on the results of single-bubble slug-ejection experiments [7,11]. In these experiments, a gas bubble was forced through various simulant fluids (water and Freon) in cylindrical and annular flow channels with hydraulic diameters of 5-8 mm. For high bubble velocities such that the liquid flow was clearly turbulent, the residual liquid film on the channel walls was characterized by a liquid fraction (fraction of available flow area occupied by the liquid film) of 0.13-0.15. This result tended to be independent of the material used, channel diameter, or bubble velocity (so long as the flow was turbulent). The resulting liquid fraction was consistent with the explanation that only the central portion of the liquid flow for which the local velocity is greater than the radial mean velocity remains with the liquid slug. The flowing liquid near the channel walls remains as the trailing film. For lower bubble velocities, where the liquid flow regime was laminar, the residual liquid film was characterized by a liquid fraction of as high as 25% of the flow area. For the laminar flow regime cases, however, the liquid film thickness was not as independent of material properties and flow channel geometry as was the case for turbulent flow.

The PLUGM code utilizes these results and assumes the residual film thickness at the trailing edge of a near-constant-velocity liquid slug occupies 15% and 25% of the available flow area depending upon whether the flow is turbulent or laminar.

If the liquid slug is accelerated through the flow channel by a lower density fluid, then Taylor instabilities at the trailing edge of the liquid slug will cause the lighter-density fluid to penetrate into the heavier density liquid slug. This might be expected in LMFBR transition-phase analyses where fuel or steel vapor is the driving force for the flow of molten corium through the various flow channels. Such Taylor instabilities

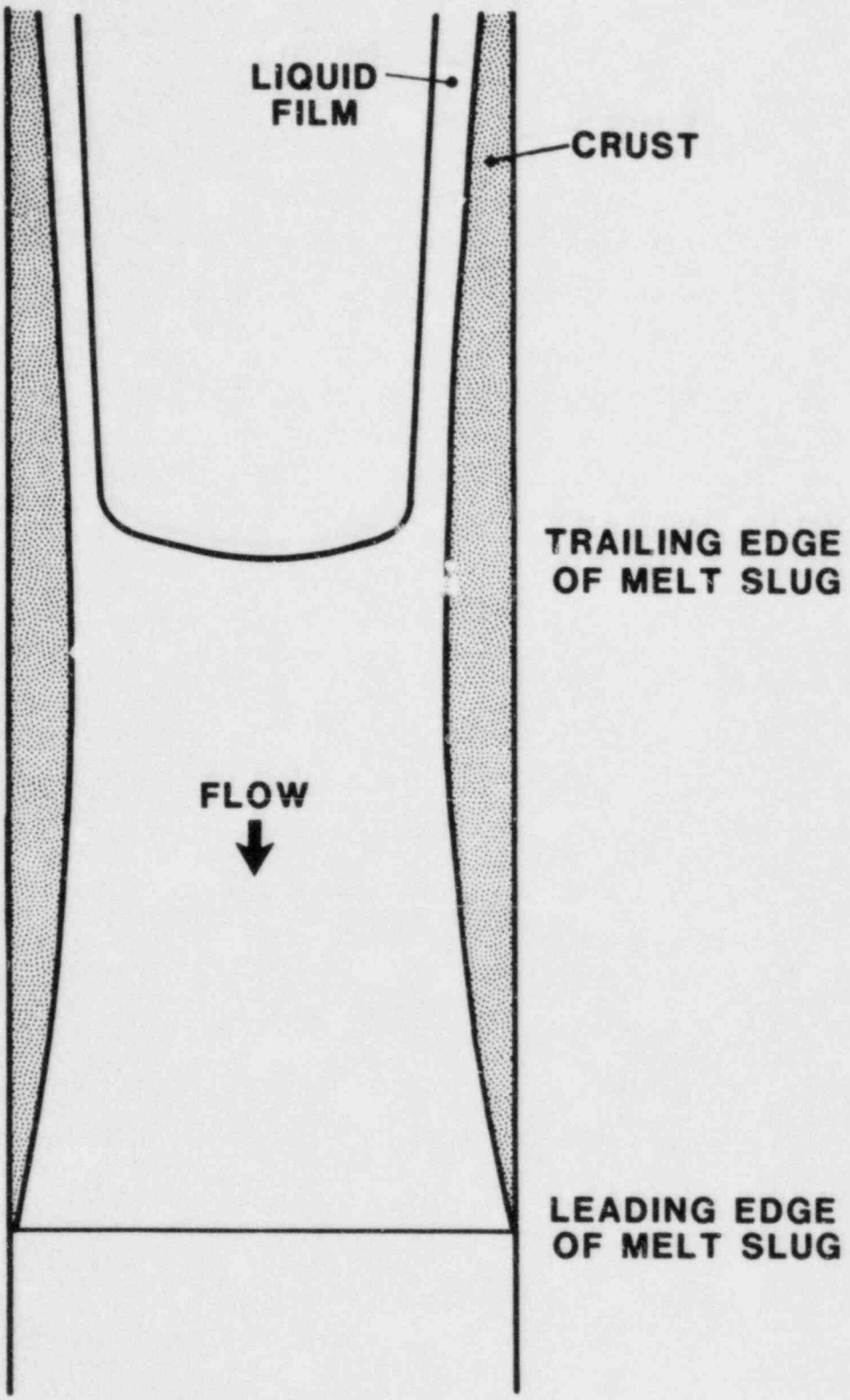

Figure 3.1. Mass Depletion Modeling in PLUGM

would result in the deposition of a thicker liquid film than predicted by the steady-state deposition described previously.

An estimate of the liquid film thickness left by such Taylor instabilities can be obtained by considering the relative velocity between the trailing edge of the flow (the "bubble" velocity) and the bulk liquid velocity near the trailing edge [20]. An upper bound for this relative velocity is obtained from the growth rate of the fastest growing instability wavelength in the channel. Given this relative velocity, it is a simple matter to calculate the resulting film thickness. The procedure used to calculate this film thickness (as well as the steady-state result previously described) is described by the following equations.

Given a trailing edge velocity of v_{trail} and a bulk material velocity of v_{bulk} near the trailing edge of the flow, the residual liquid film is characterized by a liquid fraction, F, of

$$F = 1 - \frac{v_{trail}}{v_{bulk}} \qquad 3.1.1$$

For steady-state film deposition, the trailing edge velocity is thus given by

$$v_{trail}(ss) = \left[\frac{1}{1 - F_{ss}} \right] v_{bulk} \qquad 3.1.2$$

where $F_{ss} = 0.25$ for $Re < 3500$. 3.1.3

$F_{ss} = 0.15$ for $Re > 3500$. 3.1.4

If the liquid slug is being accelerated through the channel, the trailing edge velocity must be increased by the relative velocity between the lighter density fluid (bubble) and the liquid slug, v_{Taylor}. Thus,

$$v_{trail} = v_{trail}(ss) + v_{Taylor} \qquad 3.1.5$$

An upper-bound estimate for the relative velocity V_{Taylor} can be expressed in terms of the bulk slug acceleration, a_{bulk}, and the longest Taylor wavelength, λ, as

$$V_{Taylor} = C_{Taylor} \cdot (a_{bulk} \cdot \lambda)^{1/2} \qquad 3.1.6$$

The constant, C_{Taylor}, and the longest wavelength, λ, are dependent upon the channel geometry. For slit geometry, these parameters are expressed in terms of the slit spacing, D, and the slit width, W, as

$$\lambda = W \qquad 3.1.7$$

$$C_{Taylor} = 0.23 + 0.13\frac{D}{W} \qquad 3.1.8$$

For cylindrical geometry these parameters are expressed in terms of the channel diameter, D, as

$$\lambda = D \qquad 3.1.9$$

$$C_{Taylor} = 0.345 \qquad 3.1.10$$

It should be pointed out that these criteria for film thickness are applied not only in tube and slit geometry, where the experimental data is relevant, but also for the case of particle bed geometry. The 0.15 and 0.25 liquid fraction criterion have no experimental or theoretical basis for particle bed geometry, and thus caution is urged in interpreting the film deposition results in particle bed geometry.

3.2 Transient Hydrodynamics Solution

For certain applications of the PLUGM code, the total bulk-melt mass (by mass depletion) varies significantly in time such that accounting for inertial effects is important in order to accurately calculate the bulk-melt velocity. This section describes the finite-difference formalism used in PLUGM to

calculate bulk-melt velocity as a function of position along the assumed one-dimensional (in direction of flow) channel.

At any location, s, along the flow channel, the one-dimensional momentum equation may be written as

$$\rho_b \frac{\partial v}{\partial t} + \rho_b \frac{\partial}{\partial s}\left(\frac{v^2}{2}\right) = - \frac{dp^*}{ds} + \rho_b g_s \qquad 3.2.1$$

where g_s is that component of gravity in the direction of the flow. The dp^*/ds term represents applied external pressures, capillary forces, and losses due to friction, area changes, and flow direction changes.

For each of the defined finite-difference nodes (see Section 3.2 for a description of node notation), one can integrate Equation 3.2.1 over the length of node i to obtain an expression for the time derivative of the velocity in the i^{th} node.

$$\begin{aligned} \rho_b \Delta s_i \frac{dv_i}{dt} = & - \frac{\rho_b}{2}(v_{i+1}^2 - v_i^2) \\ & + (p_i - p_{i+1}) + \rho_b g (z_{i+1} - z_i) \\ & + 4\sigma_b \left(\frac{1}{D_{h,i+1}} - \frac{1}{D_{h,i}}\right) \\ & - \left(K_{i+1} + f_i \frac{A_{s,i}}{A_{f,i}}\right) \frac{1}{2}\rho_b v_i^2 \end{aligned} \qquad 3.2.2$$

where,

$\Delta s_i = s_{i+1} - s_i$

$z_{i+1} - z_i$ = elevation change between s_{i+1} and s_i

K_{i+1} = loss coefficient between nodes i and i+1 due to expansions, contractions, and elbows

f_i = friction factor in node i.

Note that the pressure term dp^*/ds was expanded into its component terms.

In order to obtain a simplified solution to the transient velocity distribution, the approximation is made that the mass flow rate is constant everywhere in the channel during a time step. Thus,

$$A_{f,i}\, v_i = A_{f,i+1}\, v_{i+1} \,. \qquad 3.2.3$$

Using this approximation, Equation 3.2.2 can be rewritten in terms of the velocity at the trailing edge of the flow for any arbitrary point in the flow.

$$\rho_b \Delta s_i \frac{A_{f,t}}{A_{f,i}} \frac{dv_t}{dt} = -\frac{\rho_b}{2}\left[\left(\frac{A_{f,t}}{A_{f,i+1}}\right)^2 - \left(\frac{A_{f,t}}{A_{f,i}}\right)^2\right] v_t^2$$

$$+ (p_i - p_{i+1}) + \rho_b g (z_{i+1} - z_i) \qquad 3.2.4$$

$$+ 4\sigma_b \left(\frac{1}{D_{h,i+1}} - \frac{1}{D_{h,i}}\right)$$

$$- \left(K_{i+1} + f_i \frac{A_{s,i}}{A_{f,i}}\right) \left(\frac{A_{f,t}}{A_{f,i}}\right)^2 \frac{1}{2} \rho_b v_t^2$$

Note that it has been assumed in the above equation that the approximation

$$\frac{d}{dt}\left(\frac{A_{f,t}}{A_{f,i}}\right) = 0 \qquad 3.2.5$$

is valid.

Given Equation 3.2.4, it is then possible to sum over all hydrodynamics nodes from trailing edge (node t) to leading edge

(node 1) to obtain an expression from the time derivative of the trailing edge velocity.

$$\frac{dv_t}{dt} = \left[\sum_i \Delta s_i \frac{A_{f,t}}{A_{f,i}} \right]^{-1} \left[\frac{1}{2} \left(1 - \frac{A_{f,t}}{A_{f,1}} \right)^2 v_t^2 \right.$$

$$+ \frac{(p_t - p_1)}{\rho_b}) + g(z_1 - z_t) + \frac{4\sigma_b}{\rho} \left(\frac{1}{D_{h,1}} - \frac{1}{D_{h,t}} \right) \qquad 3.2.6$$

$$\left. - \frac{1}{2} v_t^2 \sum_i (K_{i+1} + f_i \frac{A_{s,i}}{A_{f,i}}) \frac{A_{f,t}}{A_{f,i}}^2 \right]$$

In PLUGH, an explicit (in time) finite-difference representation of Equation 3.2.6 is used to calculate v_t at time t^{n+1} in terms of v_t at time t^n. Mass addition and/or depletion are automatically accounted by recalculating $z_1 - z_t$, Δs_1, and Δs_t.

The assumption of uniform mass flow rate is then used to calculate the bulk-melt velocity for the other nodes.

$$v_i = \frac{A_{f,t}}{A_{f,i}} v_t \qquad 3.2.7$$

The initial (start of problem) velocity may either be specified as zero or a quasi-steady-state value (see Section 3.3).

3.3 Quasi-Steady Hydrodynamics Solution

The previous section presented the method used in PLUGH to calculate the bulk-melt velocity distribution when inertial effects are important. For many applications, the velocity can be approximated by simply balancing driving pressure (applied pressure, capillary forces, and gravity head) with the loss terms (friction, area changes, and elbows). This is done by setting the time derivative in Equation 3.2.6 to zero and solving for the velocity v_t directly.

$$v_t^2 = \frac{2\,\frac{p_t - p_1}{\rho_b} + 2g(z_1 - z_t) + \frac{8\sigma_b}{\rho_b}\left(\frac{1}{D_{h,1}} - \frac{1}{D_{h,t}}\right)}{1 - \left(\frac{A_{f,t}}{A_{f,1}}\right)^2 - \sum_i \left[(K_{i+1} + f_i \frac{A_{s,i}}{A_{f,i}})\left(\frac{A_{f,t}}{A_{f,i}}\right)^2 \right]} \qquad 3.3.1$$

Again, Equation 3.2.7 is used to calculate the velocity in the other nodes.

The quasi-steady solution (Eqn. 3.2.8) may also be used to initialize the velocity at the start of the problem even though the transient velocity solution (Eqn. 3.2.6) is used thereafter.

3.4 Friction Factors

PLUGM calculates friction losses for both laminar and turbulent flow. These friction losses give rise to a pressure drop given by

$$\Delta p = f\tfrac{1}{2}\rho_b v^2 \frac{A_s}{A_f} \quad . \qquad 3.4.1$$

Here, f is the Fanning friction factor. In general, the friction factor is a function of the Reynolds number (Re_h).

$$Re_h = \frac{\rho_b v D_h}{\mu_b} \qquad 3.4.2$$

The wetted-surface-area-to-flow-area ratio (A_s/A_f) is given by

$$\frac{A_{s,i}}{A_{f,i}} = \frac{4\,\Delta s_i}{D_{h,i}} . \qquad 3.4.3$$

This expression is formulated in terms of the hydraulic diameter (D_h) and thus is valid for all geometries.

Thin Slit Geometry

Fanning friction factors, which are appropriate for thin slit geometry, are presented in Rohsenow [17].

Laminar Flow

$$f = \frac{24}{Re_h} \qquad Re_h \leq 2400 \qquad 3.4.4$$

Transition flow

$$f = .01 \qquad 2400 \leq Re_h \leq 5220 \qquad 3.4.5$$

Turbulent flow

$$f = \frac{.085}{Re_h^{.25}} \qquad 5220 \leq Re_h \qquad 3.4.6$$

Tube Geometry

Fanning friction factors, appropriate for tube geometry, are presented in Rohsenow [14].

Laminar flow

$$f = \frac{16}{Re_h} \qquad Re_h \leq 1600 \qquad 3.4.7$$

Transition flow

$$f = .01 \qquad 1600 \leq Re_h \leq 3895 \qquad 3.4.8$$

Turbulent flow

$$f = \frac{.079}{Re_h^{.25}} \qquad 3895 \leq Re_h \qquad 3.4.9$$

Particle Bed Geometry

Friction factors for particle beds are given by the Ergun equation [6], which is rewritten here in a form consistent with Equation 3.4.1.

$$f = \frac{2}{3}\left(\frac{50}{Re_h} + .875\right) \qquad 3.4.10$$

3.5 Nonrecoverable Pressure Losses Due To Contractions, Expansions, and Sudden Changes in Flow Direction

PLUGM's hydrodynamics calculations include the affects of nonrecoverable pressure losses. Contractions and expansions are assumed to occur gradually from node to node. This is the case where there is a continuous variation in crust thickness along the channel. PLUGM's methodology, which assumes gradual contractions or expansions, can approximate the actual losses associated with large, sudden contractions or expansions, however, the success of the approximate result is somewhat node-size dependent.

All nonrecoverable losses can be expressed in the following form.

$$\Delta p = K\frac{1}{2}\rho_b v^2 \qquad 3.5.1$$

All nonrecoverable losses are based on the upstream velocity. A further assumption is that the loss coefficient (K) is independent of geometry.

Gradual Expansions

Loss coefficients for gradual expansions are given in Baumeister [5]. Consider the expansion loss incurred in going from node i to node i+1, Figure 3.2 depicts the geometry.

The loss coefficient for a gradual expansion is given by

$$K_{i+1} = K' \left[1 - \frac{A_{f,i}}{A_{f,i+1}}\right]^2 . \qquad 3.5.2$$

The coefficient K' is a function of the expansion rate from node i to node i+1. The expansion rate is characterized by the parameter ξ.

$$\xi = \frac{D_{i+1} - 2\delta_{i+1} - (D_i - 2\delta_i)}{\Delta s_{i+1} + \Delta s_i} \qquad 3.5.3$$

Note that ξ becomes infinite for a sudden contraction.

The functional relationship between K' and ξ is given approximately by

$$K' = \min \begin{cases} 1 \\ 2.8607\xi - 1.2143\xi^2 \end{cases} . \qquad 3.5.4$$

Gradual Contractions

Loss coefficients for gradual contractions are given in Babcocks and Wilcox [1]. Consider the contraction loss incurred in going from node i to node i+1. The loss coefficient for a gradual contraction is given by

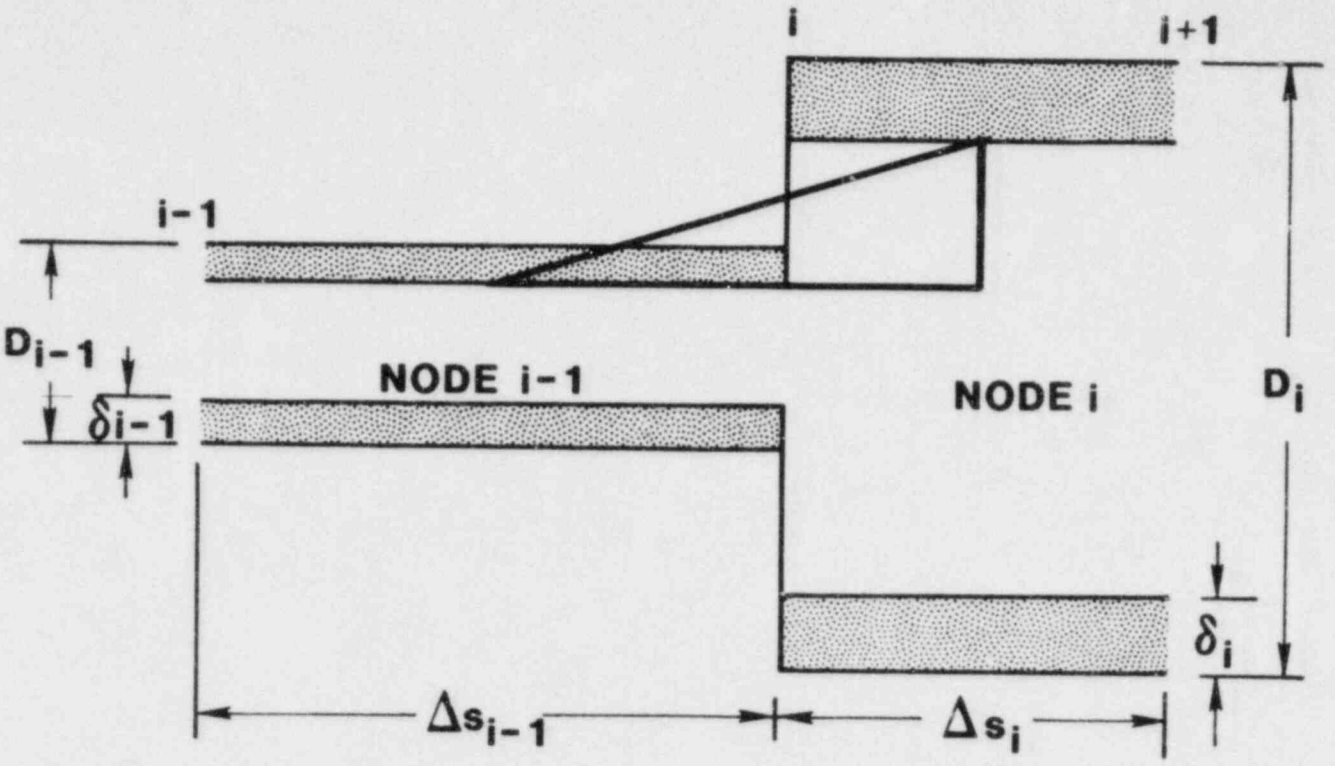

Figure 3.2 Calculation of Expansion Losses

$$K = K' \left[\frac{A_{f,i}}{A_{f,i+1}}\right]^2 . \qquad 3.5.5$$

Here, K' is the loss coefficient for a gradual contraction when based on the downstream velocity. The area ratio in Equation 3.5.5 is required because PLUGM bases all nonrecoverable losses on the upstream velocity.

The coefficient K' is a function of the contraction rate from node i to node i+1. The contraction rate is characterized by the parameter ξ.

$$\xi = \frac{D_i - 2\delta_i - (D_{i+1} - 2\delta_{i+1})}{\Delta s_{i+1} + \Delta s_i} \qquad 3.5.6$$

This is just the negative of the expansion rate parameter (Equation 3.5.3).

The functional relationship between K' and ξ is given approximately by the following.

For $\xi \leq .267949$

$$K' = .05 \left(\frac{\xi}{.267949}\right) \qquad 3.5.7$$

For $.267949 < \xi$ and $0 \leq \frac{A_{f,i+1}}{A_{f,i}} \leq .72$

$$K' = .5\left(1 - .80556 \frac{A_{f,i+1}}{A_{f,i}}\right) \qquad 3.5.8$$

For $.267949 < \xi$ and $.72 < \frac{A_{f,i+1}}{A_{f,i}} \leq 1$

$$K' = .75\left(1 - \frac{A_{f,i+1}}{A_{f,i}}\right) \qquad 3.5.9$$

Sudden Changes in Flow Direction

The loss coefficient for a 90 degree elbow is given in John and Haberman [10].

$$K = .75 \qquad 3.5.10$$

4. Bulk-Melt Energy Transfer

The initial bulk-melt temperature can be either saturated or superheated, an important feature for most reactor-safety applications. Convective heat transfer to the crust or wall surface can be either laminar or turbulent depending on the code-calculated local Reynolds number. The calculation of local bulk-melt to crust (or wall) heat transfer coefficient also accounts for the Prandlt number of the fluid (liquid metal versus normal fluid).

4.1 Finite-Difference Heat Transfer Formulation

The axial temperature distribution in the bulk melt changes in time as a result of

1. material transport of bulk melt down the channel, and
2. convective heat transfer to the channel walls or crust.

Axial (in direction of flow) conduction and volumetric heating within the bulk melt are not modeled. An axial finite-difference formulation of the heat transport (within the bulk-melt) is used. The needed boundary conditions of bulk-melt velocity and crust (or wall, if no crust) surface temperature distributions are obtained explicitly from the hydrodynamics and crust growth/wall-heatup modules.

Melt Filled Nodes

Energy conservation for the i^{th} melt filled node is expressed below.

For i = NTRAIL+1 to NLEAD-1

$$\rho_b c_{pb}(T^{n+1}_{b,i} - T^{n}_{b,i})V^{n}_{i} = \rho_b c_{pb}\, T^{n+1}_{b,i-1}\, v^{n}_{i-1}\, A^{n}_{f,i-1}\, \Delta t - \rho_b c_{pb}\, T^{n+1}_{b,i}\, v^{n}_{i}\, A^{n}_{f,i}\, \Delta t - h^{n}_{i}(T^{n+1}_{b,i} - T^{n}_{s,i})\, A^{n}_{s,i}\, \Delta t \qquad 4.1.1$$

Here, ρ_b is the density of the bulk melt; c_{pb} is the specific heat of the bulk melt, T_b is the temperature of the bulk melt, V is the melt volume, A_f is the cross-section flow area; Δt is the time increment, h is the heat transfer coefficient between the bulk melt and the crust or wall if no crust exists, T_s is the

bulk-melt/crust or bulk-melt/wall interface temperature, and A_s is the wetted surface area.

If crust is present, then the bulk-melt/crust interface temperature is given by the fusion temperature of the melt.

$$T^n_{s,i} = T_{bm} \qquad 4.1.2$$

But if crust does not exist, then the bulk-melt/wall interface temperature is given by a time dependent interface temperature that is determined from wall heatup solutuions, which are discussed in Section 5.

$$T^n_{s,i} = T^n_{c,i} \quad . \qquad 4.1.3$$

During any given time step, the mass flow rate is assumed constant at all axial locations in the channel.

$$v^n_i \, A^n_{f,i} = v^n_{i-1} \, A^n_{f,i-1} \qquad 4.1.4$$

The updated temperature of the bulk melt is obtained from Equations 4.1.1-3.

For i = NTRAIL+1 to NLEAD-1

$$T_{b,i}{}^{n+1} = \frac{T_{b,i}{}^{n} + A_{l,i} T^n_{s,i} + A_{l,i} T^{n+1}_{b,i-1}}{1 + A_{l,i} + A_{l,i}} \qquad 4.1.5$$

where,

$$A_{l,i} = \frac{h^n_i}{\rho_b c_{pb}} \frac{A^n_{s,i}}{V^n_i} \Delta t \qquad 4.1.6$$

$$A_{1,i} = v_i^n \frac{A_{f,i}^n}{V_i^n} \Delta t \qquad 4.1.7$$

The flow-area-to-flow-volume ratio has a common form for PLUGM's three geometries.

$$\frac{A_{f,i}^n}{V_i^n} = \frac{1}{\Delta s_i} \qquad 4.1.8$$

Likewise, the wetted-surface-area-to-flow-volume ratio can also be expressed in a common form for PLUGM's three geometries.

$$\frac{A_{s,i}^n}{V_i^n} = \frac{4}{D_{h,i}^n} \qquad 4.1.9$$

Partially Filled Trailing-Edge Node (i=NTRAIL)

There is no material motion into the trailing-edge node. Material motion out of the trailing-edge node decreases its total energy, but not its temperature. Energy conservation for the trailing-edge node is given below.

$$\rho_b c_{Pb} (T_{b,i}^{n+1} - T_{b,i}^n) V_i^n =$$

$$- h_i^n (T_{b,i}^{n+1} - T_{s,i}^n) A_{s,i}^n \Delta t \qquad 4.1.10$$

The updated bulk temperature is obtained directly from Equation 4.1.10.

$$T_{b,i}^{n+1} = \frac{T_{b,i}^{n} + A_i T_{s,i}^{n}}{1 + A_i} \qquad 4.1.11$$

Here, $T_{s,i}^{n}$ and A_i are still given by Equation 4.1.2-3 and Equation 4.1.6 respectively. Although the trailing-edge node is only partially filled, the wetted-surface-area-to-flow-volume ratio is still given by Equation 4.1.9.

Partially Filled Leading-Edge Node (i=NLEAD)

There is no material motion out of the leading-edge node. Energy conservation for the leading-edge node is given below.

$$\rho_b c_{pb} (T_{b,i}^{n+1} - T_{b,i}^{n}) V_i^{n} = \rho_b c_{pb} T_{b,i-1}^{n+1} v_{i-1}^{n} A_{f,i}^{n} \Delta t - h_i^{n} (T_{b,i}^{n+1} - T_{s,i}^{n}) A_{s,i}^{n} \Delta t \qquad 4.1.12$$

Assume again a constant mass flow rate during a time step (Eq. 4.1.4). The updated bulk-melt temperature is obtained from Equation 4.1.12.

$$T_{b,i}^{n+1} = \frac{T_{b,i}^{n} + A_i T_{s,i}^{n} + B_i T_{b,i-1}^{n+1}}{1 + A_i} \qquad 4.1.13$$

Here, $T_{s,i}^{n}$, A_i, and B_i are still given by Equations 4.1.2-3, Equation 4.1.6, and Equation 4.1.7 respectively. Although the leading-edge node is only partially filled, the wetted-surface-area-to-flow-volume ratio is still given by Equation 4.1.9. The flow-area-to-flow-volume ratio is modified for the partially-filled leading-edge node.

$$\frac{A_{f,i}}{V_i} = \frac{1}{\text{PFILL} \cdot \Delta s_i} \; . \qquad 4.1.14$$

Here PFILL is the fraction of the leading-edge node that remains filled ($0 < PFILL < 1$).

4.2 Heat Transfer Coefficients

PLUGM models time-dependent, convective heat transfer from the melt to the crust or directly to the channel wall if no crust exists. The flow can be laminar or turbulent. The heat transfer coefficient is incorporated into the dimensionless Nusselt number (Nu) which in turn is a function of the Reynolds number (Re_h) and the Prandtl number (Pr).

$$Nu = \frac{hD_h}{k_b} \qquad 4.2.1$$

$$Re_h = \frac{\rho_b v D_h}{\mu_b} \qquad 4.2.2$$

$$Pr = \frac{c_{pb}\mu_b}{k_b} \qquad 4.2.3$$

The fluid can be a normal fluid or a liquid metal. A normal fluid has a Prandtl number (Pr) greater than .5, and a liquid metal has a Prandtl number less than .03. Some fluids, such as molten steel, have Prandtl numbers which lie between .5 and .03. For these fluids, PLUGM performs a linear interpolation between the normal-fluid heat-transfer coefficient and the liquid-metal heat-transfer coefficient.

$$Nu = Nu_{nf} + (Nu_{lm} - Nu_{nf}) \frac{.5 - Pr}{.5 - .03} \qquad 4.2.4$$

Thin Slit Geometry

Heat transfer coefficients appropriate for thin slit geometry are summarized by Rohsenow [14].

Normal Fluid .5 $\leq$ Pr

$$Nu_{nf} = 7.5407 + .021\ Re_h^{.8}Pr \qquad 4.2.5$$

Liquid Metal Pr $\leq$ .03

For $Re_hPr \leq 40$

$$Nu_{lm} = 7.5407 \qquad 4.2.6$$

For $40 \leq Re_hPr$

$$Nu_{lm} = 6.5767 + .015(Re_hPr)^{0.8} \qquad 4.2.7$$

Tube Geometry

Heat transfer coefficients appropriate for tube geometry are also summarized by Rohsenow [14].

Normal Fluid .5 $\leq$ Pr

$$Nu_{nf} = 3.656 + .021Re_h^{0.8}Pr^{0.6} \qquad 4.2.8$$

Liquid Metal Pr $\leq$ .03

For $Re_hPr \leq 40$

$$Nu_{lm} = 3.656 \qquad 4.2.9$$

For $40 \leq Re_hPr$

$$Nu_{lm} = 4.8 + .025\ (Re_hPr)^{0.8} \qquad 4.2.10$$

Particle Bed

Heat transfer coefficients appropriate for particle-bed geometry are summarized by Whitaker [20]. The laminar-limit heat transfer coefficient for an isothermal tube is added to Whitaker's turbulent flow correlaton. Furthermore, Whitaker's

correlation is rewritten slightly to be consistent with notation used in this report.

Normal Fluid .5 $\pm$ Pr

$$Nu_{nf} = 3.656 + \left[.408Re_h^{1/2} + .115\ Re_h^{2/3}\right] Pr^{1/3} \qquad 4.2.11$$

No liquid metal heat transier coefficient for a particle bed can be found, consequently, Equation 4.2.11 is currently used regardless of Prandtl number. Thus, code users are cautioned against quantified interpretation of results for problems in which a superheated liquid metal (low Prandtl number fluid) flows through a particle bed.

5. Crust Growth (Remelt) and Wall Heatup

Crust deposition on the channel wall is controlled by the competing effects of convective hat transfer from the bulk melt to the crust surface and the conduction limited removal of heat from the crust into the wall. An external coolant may further enhance this heat removal by limiting the temperature increase in the wall.

The solution for the coupled crust-growth (or remelt) and wall heatup is obtained from a numerical solution of the integral energy equations in the crust and wall. The solution procedure assumes that both the crust and wall temperature profiles can be described by second order polynomials (in spatial coordinate) with time-dependent coefficients. User-input constant material properties are used in the analysis. The use of these assumed profiles in the integral energy equations results in a system of coupled first-order differential equations, for the time-dependent coefficients, which must be solved for at each axiial node. The equations account for the time-dependent heat flux from the bulk-melet into the growing (or remelting) crust as well as the possible heat transfer between the outer wall surface and the external coolant.

The time-dependent crust/wall contact temperature at each axial node is uniquely defined by the coupled equations. These temperatures indicate the axial extent over which channel wall melting is to be expected. The PLUGH code as described herein does not account for the effect of wall melting (i.e., heat of fusion) on the crust-growth/wall-heatup solutions. This is not required for the core retention applications. However, a future version of the code will account for this effect for transition-phase applications.

The quantities calculated by the crust-growth/wall-heatup module are the time dependent axial crust-thickness distribution and the crust and wall temperature distributions. The principle parameters needed from the other solution modules are the bulk-melt temperature and the bulk-melt velocity (for determining heat transfer coefficients).

Modeling crust growth (remelt) and wall heatup in a particle bed is a particularly difficult task. Here, the asusmption is made that a typical flow path through a particle bed can be represented by a tube with an equivalent hydraulic diameter, consequently, the tube solutions are used. Section 2.4 describes how to specify the hydraulic diameter and wall thickness for this tube-geometry representatcin of a particle bed.

For completeness, Table 5.1 lists all possible states of wall and crust. Those solutions contained in PLUGH are marked with an X. One distinguishing feature of PLUGH is that the state

Table 5.1. Crust Growth (Remelt) and Wall Heatup Solutions

Solutions		Thin Slit		Tube or Particle Bed	
		infinite wall	finite wall	infinite wall	finite wall
1.	No crust with a solid wall	X	X	X	X
2.	Crust on a solid wall	X	X	X	X
3.	No crust with a partially molten wall				
4.	Crust on a partially molten wall				
5.	No crust with a completely molten wall				
6.	Crust on a completely molten wall				

of wall and crust can change with time and with location in the channel. The integral methods used here define a finite thermal layer thickness in the wall. The terms infinite wall and finite wall distinguish whether the wall thermal layer has passed completely through the wall or not.

5.1 Crust Growth Solutions

The following sections summarize each of the existing solutions shown in Table 5.1. Sufficient detail is provided so that the reader can reproduce any of the working equations. The general procedure is quite repetitious for each case considered.

1. Assume polynomial (2nd order) temperature profiles for the crust and wall that satisfy the relevant temperature boundary conditions.

2. Substitute the assumed temperature profiles into the internal form of the energy equation for both the crust and the wall.

3. Substitute the assumed temperature profiles into the flux matching boundary conditions.

The end result is a system of coupled, 1st order, ordinary differential equations which are solved using simply Euler integration.

5.1.1 Thin Slit Geometry - No Crust with a Nonmelting, Infinitely-Thick Wall.

The geometry, representative temperature profiles, and nomenclature for this problem are shown in Figure 5.1. The unknown, time-dependent parameters that must be solved for are

$$\delta_w \ , \ T_c \ .$$

The solution scheme described below summarizes the FORTRAN coding in the PLUGM subroutine SLITXXI.

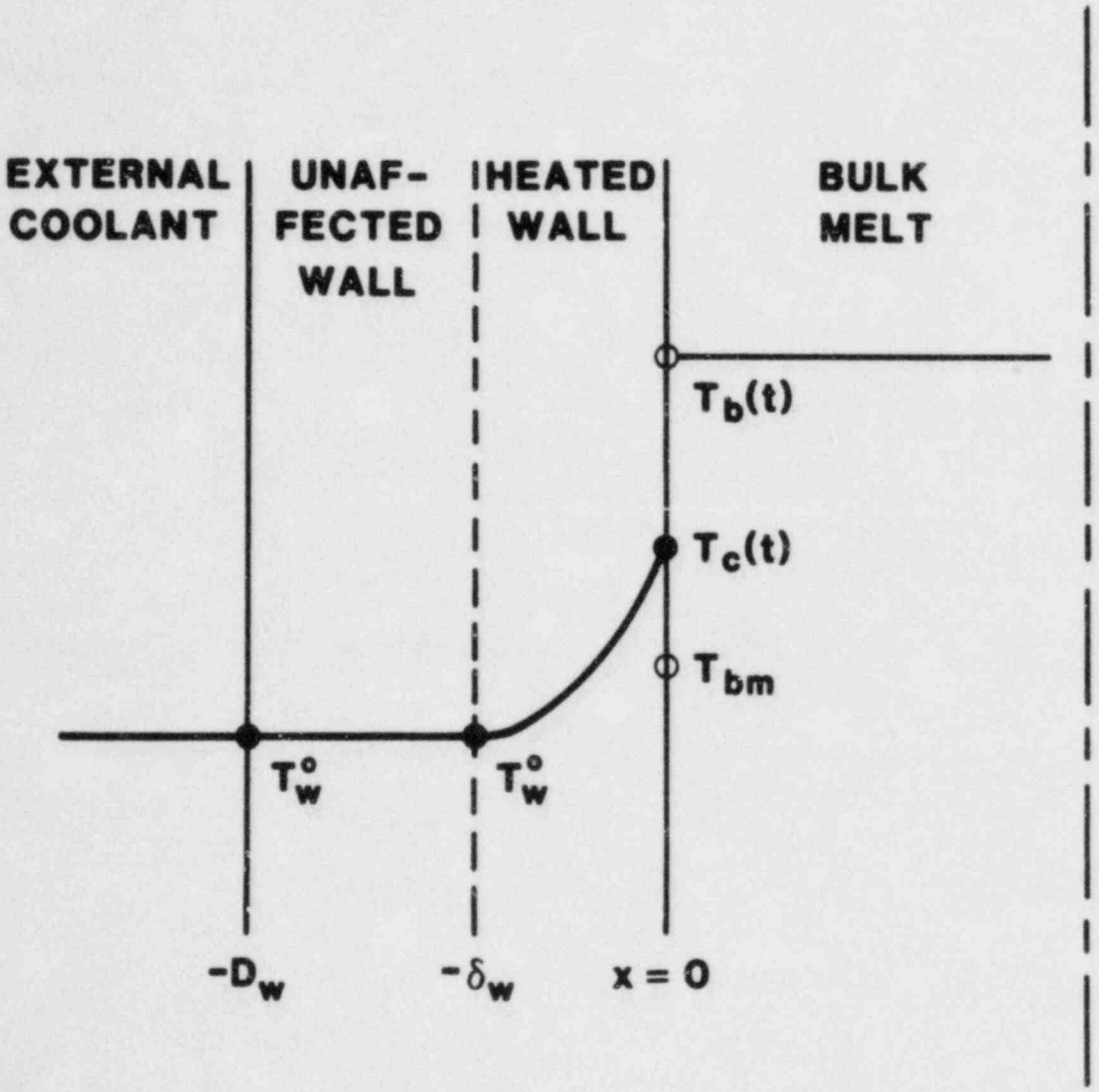

Figure 5.1. Temperature Distribution in Thin Slit Geometry for Case of No Crust / No Wall Melt / Infinite Wall

Assumed Temperature Profile

1) Wall

$$\frac{T_w(x,t) - T_w^o}{T_c(t) - T_w^o} = \left[1 + \frac{x}{\delta_w(t)}\right]^2 \qquad (1)$$

The following boundary conditions are satisfied.

$$T_w(-\delta_w, t) = T_w^o \qquad (2)$$

$$T_w(0,t) = T_c(t) \qquad (3)$$

$$\left.\frac{\partial T_w}{\partial x}\right|_{-\delta_w} = 0 \qquad (4)$$

Governing Equations

1) Wall Energy Equation

$$\int_0^{-\delta_w} \frac{\partial T_w}{\partial t}\, dx = \int_0^{-\delta_w} \alpha_w \frac{\partial^2 T_w}{\partial x^2}\, dx \qquad (5)$$

2) Flux Matching at the Bulk-Melt/Wall Interface

$$k_w \left.\frac{\partial T_w}{\partial x}\right|_0 = h(T_b - T_c) \qquad (6)$$

Derivation of Controlling Differential Equations

The differential equations that must be solved in order to determine the unknown parameters are obtained by substituting the temperature profiles into each of the governing equations above. A brief summary of the steps involved in these derivations and the resulting differential equations are provided below.

1) Starting with the wall energy equation (Eq. 5), move the time derivative outside the left-hand integral, and evaluate the integral of the second-order spatial derivative. Substitute the wall temperature profile (Eq. 1) into the result.

$$A_{11} \frac{d\delta_w^2}{dt} = B_1 \qquad 7$$

where,

$$A_{11} = 1 + \frac{2k_w}{2k_w + h\delta_w} \qquad 8$$

$$B_1 = 12\alpha_w - \frac{2k_w}{2k_w + h\delta_w} \frac{2\delta_w^2}{T_b - T_c} \frac{dT_b}{dt} \qquad 9$$

2) Substitute the wall temperature profile (Eq. 1) into the flux matching condition at the bulk-melt/wall interface (Eq. 6). Differentiate the result with respect to time and use the undifferentiated result to simplify the resulting expression.

$$A_{21} \frac{d\delta_w^2}{dt} + A_{22} \frac{dT_c}{dt} = B_2 \qquad 10$$

where,

$$A_{21} = \frac{T_b - T_c}{T_c - T_w^o} \frac{h\delta_w}{2k_w + h\delta_w} \qquad 11$$

$$A_{22} = \frac{-2\delta_w^2}{T_c - T_w^o} \qquad 12$$

$$B_2 = \frac{h\delta_w}{2k_w + h\delta_w} \frac{2\delta_w^2}{T_c - T_w^o} \frac{dT_b}{dt} \qquad 13$$

Auxiliary Relationship

It is possible to use some of the governing equations to derive simple algebraic expressions for some of the unknown parameters as a function of the other parameters (no time derivatives). A brief summary of the steps involved in these derivations and the resulting consistency relationships are provided below.

1) Contact Temperature - Substitute the wall temperature profile (Eq. 1) into the flux matching condition (Eq. 6) at the bulk-melt/wall interface.

$$T_c = \frac{h\delta_w T_b + 2k_w T_w^o}{h\delta_w + 2k_w} \qquad 14$$

5.1.2 Thin Slit Geometry - No Crust With a Nonmelting, Finite-Thickness Wall

The geometry, representative temperature profiles, and nomenclature for this problem are shown in Figure 5.2. The unknown, time-dependent parameters that must be solved for are

$$T_{wb},\ T_c,\ \beta_w.$$

The solution scheme described below summarizes the FORTRAN coding in the PLUGM subroutine SLITXXF.

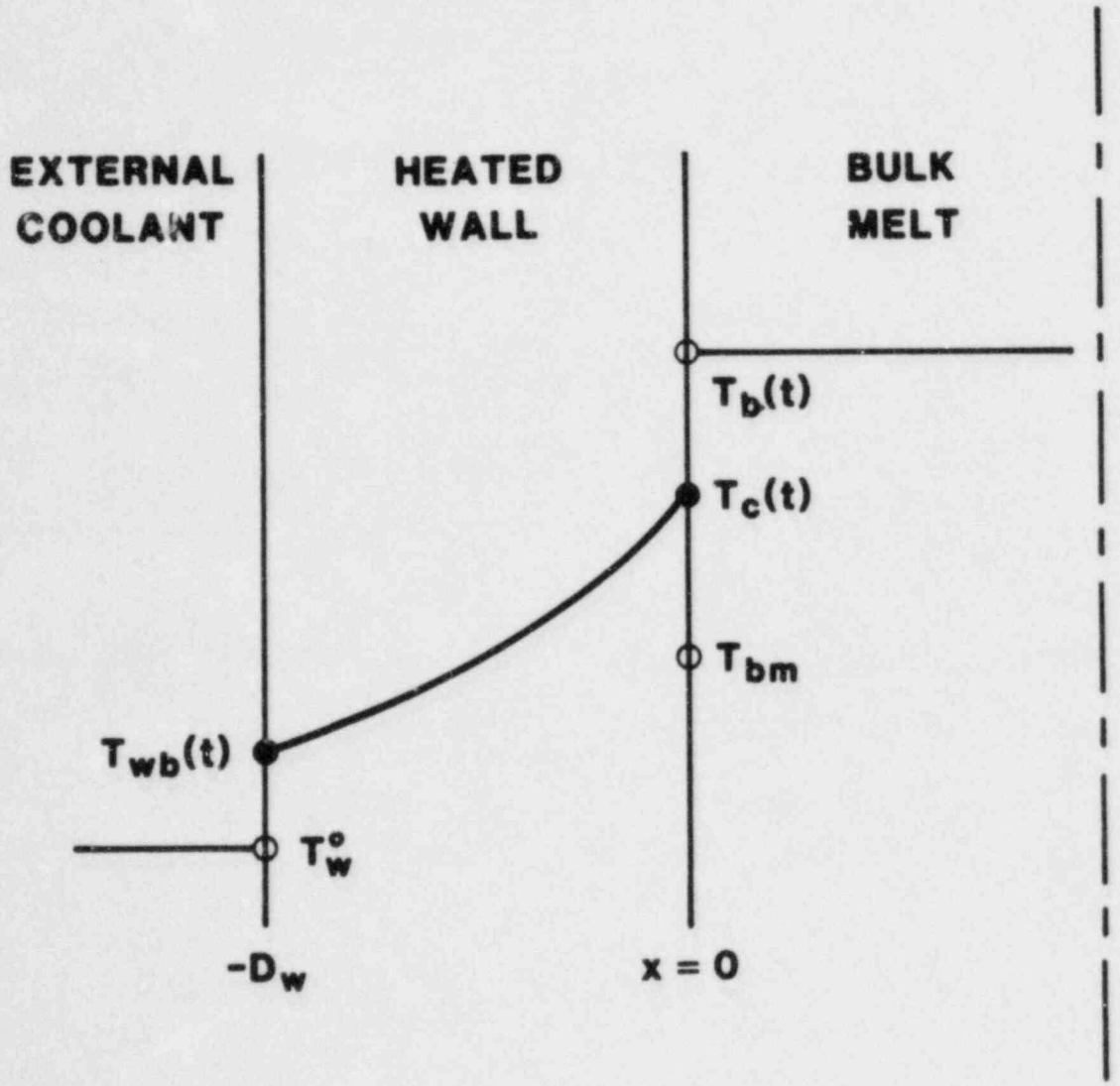

Figure 5.2 Temperature Distribution in Thin Slit Geometry for Case of No Crust / No Wall Melt / Finite Wall

Assumed Temperature Profile

1) Wall

$$\frac{T_w(x,t) - T_{wb}(t)}{T_c(t) - T_{wb}(t)} = \beta_w(t)\left[1 + \frac{x}{D_w}\right] + \left[1 - \beta_w(t)\right]\left[1 + \frac{x}{D_w}\right]^2 \quad (1)$$

The following boundary conditions are satisfied.

$$T_w(-D_w, t) = T_{wb}(t) \quad (2)$$

$$T_w(0, t) = T_c(t) \quad (3)$$

Governing Equations

1) Wall Energy Equation

$$\int_0^{-D_w} \frac{\partial T_w}{\partial t}\, dx = \int_0^{-D_w} \alpha_w \frac{\partial^2 T_w}{\partial x^2}\, dx \quad (4)$$

2) Flux Matching at the Bulk-Melt/Wall Interface

$$k_w \left.\frac{\partial T_w}{\partial x}\right|_0 = h(T_b - T_c) \quad (5)$$

3) Flux Matching at the External-Coolant/Wall Interface

$$k_w \left.\frac{\partial T_w}{\partial x}\right|_{-D_w} = h_w(T_{wb} - T_w^o) \qquad 6$$

Derivation of Controlling Differential Equations

The differential equations that must be solved in order to determine the unknown parameters are obtained by substituting the temperature profiles into each of the governing equations above. A brief summary of the steps involved in these derivations and the resulting differential equations are provided below.

1) Starting with the wall energy equation (Eq. 4), move the time derivative outside the left-hand integral, and evaluate the integral of the second-order spatial derivative. Substitute the wall temperature profile (Eq. 1) into the result.

$$A_{11}\frac{dT_{wb}}{dt} + A_{12}\frac{dT_c}{dt} + A_{13}\frac{d\beta_w}{dt} = B_1 \qquad 7$$

where,

$$A_{11} = D_w^2(4 - \beta_w) \qquad 8$$

$$A_{12} = D_w^2(2 + \beta_w) \qquad 9$$

$$A_{13} = D_w(T_c - T_w) \qquad 10$$

$$B_1 = 12\alpha_w(1 - \beta_w)(T_c - T_{wb}) \qquad 11$$

2) Substitute the wall temperature profile (Eq. 1) into the flux matching condition at the bulk-melt/wall interface (Eq. 6). Differentiate the result with respect to time and use the undifferentiated result to simplify the resulting expression.

$$A_{21}\frac{dT_{wb}}{dt} + A_{22}\frac{dT_c}{dt} + A_{23}\frac{d\beta_w}{dt} = B_2$$

where,

$$A_{21} = \beta_w - 2 \qquad 12$$

$$A_{22} = 2 - \beta_w + \frac{hD_w}{k_w} \qquad 13$$

$$A_{23} = T_{wb} - T_c \qquad 14$$

$$B_2 = \frac{hD_w}{k_w} \qquad 15$$

3) Substitute the wall temperature profile (Eq. 1) into the flux matching condition (Eq. 6) at the external-coolant/wall interface. Differentiate the result with respect to time.

$$A_{31} \frac{dT_{wb}}{dt} + A_{32} \frac{dT_c}{dt} + A_{33} \frac{d\beta_w}{dt} = B_3 \qquad 16$$

where,

$$A_{31} = -\beta_w - \frac{h_w D_w}{k_w} \qquad 17$$

$$A_{32} = \beta_w \qquad 18$$

$$A_{33} = T_c - T_{wb} \qquad 19$$

$$B_3 = 0 \qquad 20$$

Auxiliary Equations

It is possible to use some of the governing equations to derive simple algebraic expressions for some of the unknown parameters as a function of the other parameters (no time derivatives). A brief summary of the steps involved in these

derivations and the resulting consistency relationships are provided below.

1) Contact Temperature - Substitute the wall temperature profile (Eq. 1) into the flux matching condition (Eq. 5) at the bulk-melt/wall interface.

$$T_c = \frac{k_w(2-\beta_w)\ T_{wb} + hD_w\ T_b}{k_w(2-\beta_w) + hD_w} \qquad 21$$

2) Wall Temperature Shape Parameter - Substitute the wall temperature profile (Eq. 1) into the flux matching condition at the external-coolant/wall interface (Eq. 6).

$$\beta_w = \frac{h_w D_w}{k_w} \frac{T_{wb} - T_w^o}{T_c - T_{wb}} \qquad 22$$

5.1.3 Thin Slit Geometry - Crust on a Nonmelting, Infinitely-Thick Wall

The geometry, representative temperature profiles, and nomenclature for this problem are shown in Figure 5.3. The unknown, time-dependent parameters that must be solved for are

$$\delta,\ \delta_w,\ T_c,\ \beta\ .$$

The solution scheme described below summarizes the FORTRAN coding in the PLUGM subroutine SLITCXI.

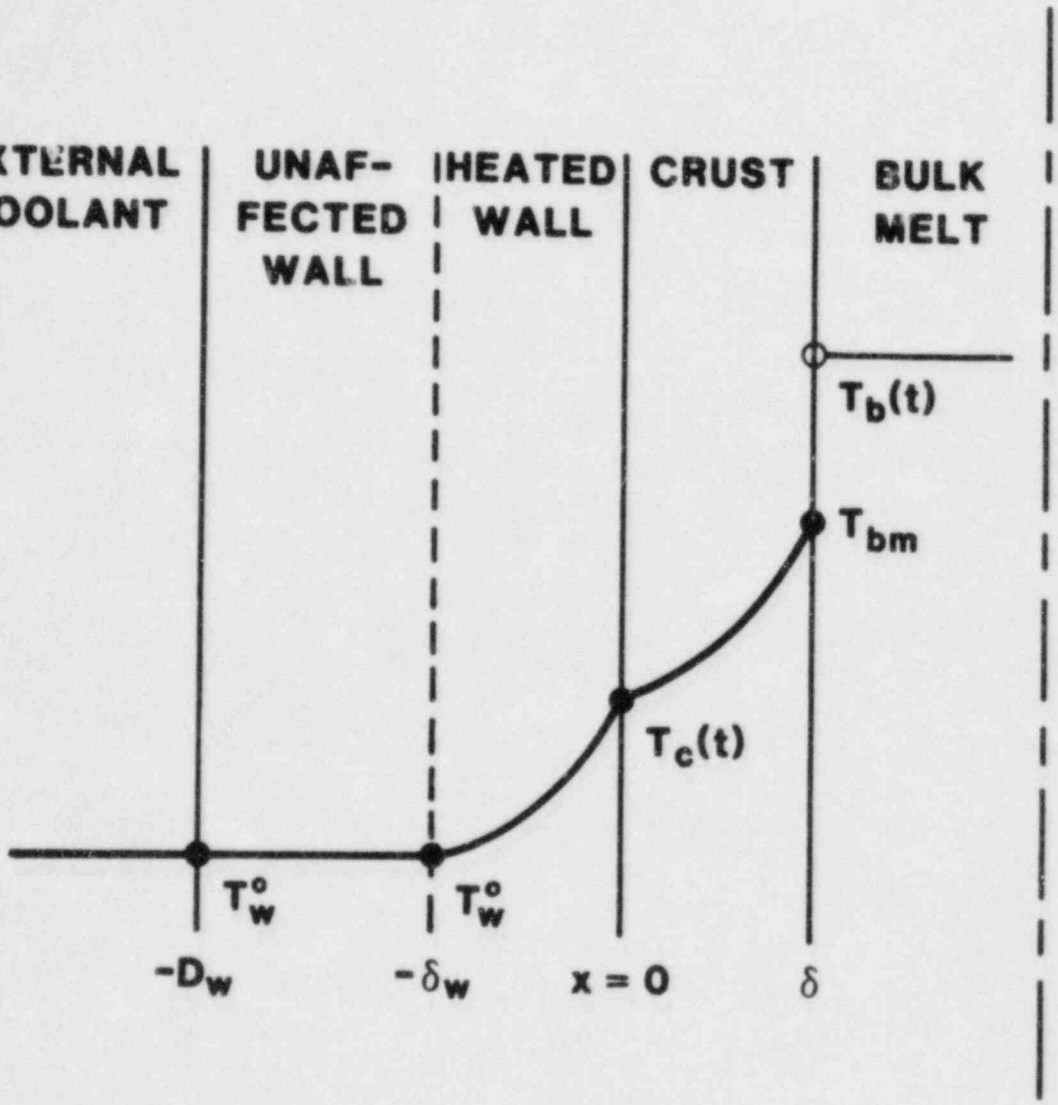

Figure 5.3. Temperature Distribution in Thin Slit Geometry for Case of Crust / No Wall Melt / Infinite Wall

Assumed Temperature Profiles

1) Crust

$$\frac{T(x,t) - T_m}{T_c(t) - T_m} = \beta(t) \left[1 - \frac{x}{\delta(t)} \right] + \left[1 - \beta(t) \right] \left[1 - \frac{x}{\delta(t)} \right]^2 \quad (1)$$

The following boundary conditions are satisfied.

$$T(\delta,t) = T_m \quad (2)$$

$$T(0,t) = T_c(t) \quad (3)$$

2) Wall

$$\frac{T_w(x,t) - T_w^o}{T_c(t) - T_w^o} = \left[1 + \frac{x}{\delta_w(t)} \right]^2 \quad (4)$$

The following boundary conditions are satisfied.

$$T_w(0,t) = T_c(t) \quad (5)$$

$$T_w(-\delta_w,t) = T_w^o \quad (6)$$

$$\left. \frac{\partial T_w}{\partial x} \right|_{-\delta_w} = 0 \quad (7)$$

Governing Equations

1) Crust Energy Equation

$$\int_0^{\delta} \frac{\partial T}{\partial t}\, dx = \int_0^{\delta} \alpha \frac{\partial^2 T}{\partial x^2}\, dx \qquad 8$$

2) Wall Energy Equation

$$\int_0^{-\delta_w} \frac{\partial T_w}{\partial t}\, dx = \int_0^{-\delta_w} \alpha_w \frac{\partial^2 T_w}{\partial x^2}\, dx \qquad 9$$

3) Flux Matching at the Bulk-Melt/Wall Interface

$$\rho h^*_{fb} \frac{d\delta}{dt} = k \left.\frac{\partial T}{\partial x}\right|_{\delta} - h(T_b - T_m) \qquad 10$$

where,

$$h^*_{fb} = h_{fb} + c_{pb}(T_b - T_m) \qquad 11$$

4) Flux Matching at the Crust/Wall Interface

$$k \left.\frac{\partial T}{\partial x}\right|_0 = k_w \left.\frac{\partial T_w}{\partial x}\right|_0 \qquad 12$$

Derivation of Controlling Differential Equations

The differential equations that must be solved in order to determine the unknown parameters are obtained by substituting the temperature profiles into each of the governing equations above. A brief summary of the steps involved in these derivations and the resulting differential equations are provided below.

1) Starting with the crust energy equation (Eq. 8), move the time derivation outside the left-hand integral, and evaluate the integral of the second-order spatial derivative. Substitute the crust temperature profile (Eq. 1) into the result.

$$A_{11} \frac{d\delta^2}{dt} + A_{13} \frac{dT_c}{dt} + A_{14} \frac{d\beta}{dt} = B_1 \qquad 13$$

where,

$$A_{11} = T_m - T_c \qquad 15$$

$$A_{13} = 2\delta^2 \qquad 16$$

$$xA_{14} = -\frac{2\delta^2}{2 + \beta} (T_m - T_c) \qquad 17$$

$$B_1 = 24\alpha \frac{1 - \frac{\beta}{2}}{2 + \beta} (T_m - T_c) \qquad 18$$

2) Starting with the wall energy equation (Eq. 9), move the time derivative outside the left-hand integral, and evaluate the integral of the second-order spatial derivative. Substitute the wall temperature profile (Eq. 4) into the result.

$$A_{22} \frac{d\delta_w^2}{dt} + A_{23} \frac{dT_c}{dt} = B_2 \qquad 19$$

where,

$$A_{22} = 1 \qquad 20$$

$$A_{23} = \frac{2\delta_w^2}{T_c - T_w^o} \qquad 21$$

$$B_2 = 12\alpha_w \qquad 22$$

3) Substitute the crust temperature profile (Eq. 1) into the flux matching condition (Eq. 10) at the bulk-melt/crust interface.

$$A_{31} \frac{d\delta^2}{dt} = B_3 \qquad 23$$

where,

$$A_{31} = 1 \qquad 24$$

$$B_3 = 2\beta \frac{k}{\rho h_{fb}^*} (T_m - T_c) - \frac{2h\delta}{\rho h_{fb}^*} (T_b - T_m) \qquad 25$$

4) Substitute the crust temperature profile (Eq. 1) and the wall temperature profile (Eq. 4) into the flux matching condition at the crust/wall interface (Eq. 12). Differentiate the result with respect to time, and use the undifferentiated result to simplify the resulting expression.

$$A_{41} \frac{d\delta^2}{dt} + A_{42} \frac{d\delta_w^2}{dt} + A_{43} \frac{dT_c}{dt} + A_{44} \frac{d\xi}{dt} = B_4 \qquad 26$$

where,

$$A_{41} = k_w(T_c - T_w^o) \qquad 27$$

$$A_{42} = -\left[\frac{k}{2}(2 - \beta)(T_m - T_c)\right]^2 \frac{1}{k_w(T_c - T_w^o)} \qquad 28$$

$$A_{43} = \delta(2k_w\delta + k\delta_w(2 - \beta)) \qquad 29$$

$$A_{44} = k\delta\delta_w(T_m - T_c) \qquad 30$$

$$B_4 = 0 \qquad 31$$

Auxiliary Relationships

It is possible to use some of the governing equations to derive simple algebraic expressions for some of the unknown parameters as a function of the other parameters (no time derivatives). A brief summary of the steps involved in these derivations and the resulting consistency relationships are provided below.

1) Contact Temperature - Substitute the crust temperature profile (Eq. 1) and the wall temperature profile (Eq. 4) into the flux matching condition at the crust/wall interface (Eq. 12).

$$T_c = \frac{2k_w\delta\ T_w + kD_w(2 - \beta)\ T_m}{2k_w\delta + kD_w(2 - \beta)} \qquad 32$$

2) Crust Temperature Shape Parameter - Form the differential of the temperature boundary condition (Eq. 2) at the bulk-melt/crust interface.

$$\left.\frac{\partial T}{\partial x}\right|_\delta \frac{d\delta}{dt} + \left.\frac{\partial T}{\partial t}\right|_\delta = 0 \qquad 33$$

Solve for $d\delta/dt$. Eliminate $\partial T/\partial t$ by using the differential form of the crust energy equation.

$$\frac{d\delta}{dt} = - \frac{\alpha \left.\frac{\partial^2 T}{\partial x^2}\right|_{\delta}}{\left.\frac{\partial T}{\partial x}\right|_{\delta}} \qquad 34$$

Substitute this result into the flux matching condition (Eq. 10) at the bulk-melt/crust interface.

$$\beta = \frac{1}{2A_1} (2 - A_2 A_1) \left[(1 + A_3)^{1/2} - 1\right] \qquad 35$$

where,

$$A_1 = \frac{c_p (T_m - T_c)}{h^*_{fb}} \qquad 36$$

$$A_2 = \frac{h\delta}{k} \frac{T_b - T_m}{T_m - T_c} \qquad 37$$

$$A_3 = \frac{8A_1}{(2 - A_2 A_1)^2} \qquad 38$$

5.1.4 Thin Slit Geometry - Crust on a Nonmelting, Finite-Thickness Wall

The geometry, representative temperature profiles, and nomenclature for this problem are shown in Figure 5.4. The unknown, time-dependent parameters that must be solved for are

$$\delta,\ T_{wb},\ T_c,\ \beta,\ \beta_w\ .$$

The solution scheme described below summarizes the FORTRAN coding in the PLUGM subroutine SLITCXF.

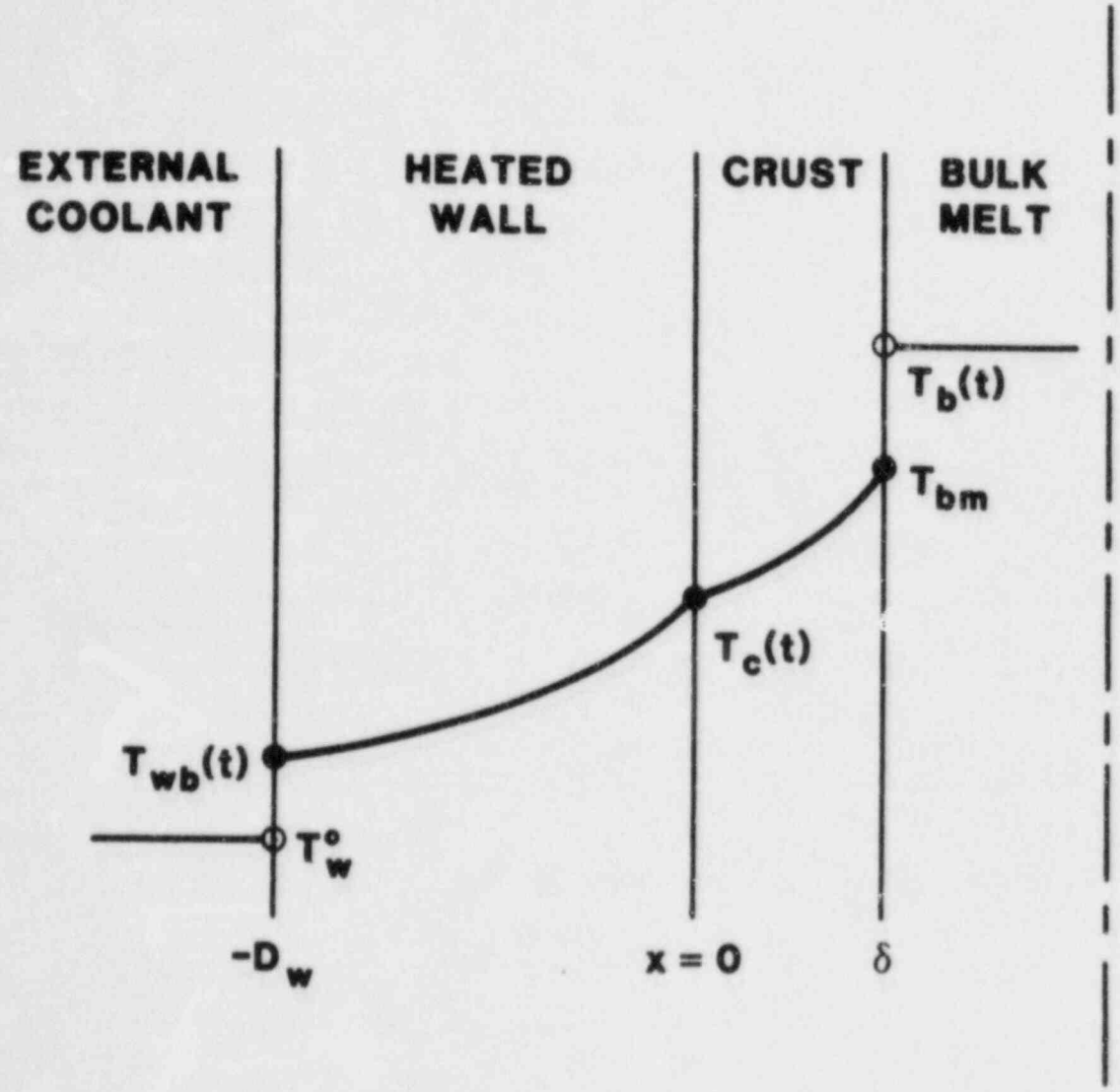

Figure 5.4. Temperature Distribution in Thin Slit Geometry for Case of Crust / No Wall Melt / Finite Wall

Assumed Temperature Profiles

1) Crust

$$\frac{T(x,t) - T_m}{T_c(t) - T_m} = \beta(t) \left[1 - \frac{x}{\delta(t)} \right] + \left[1 - \beta(t) \right] \left[1 - \frac{x}{\delta(t)} \right]^2 \quad (1)$$

The following boundary conditions are satisfied.

$$T(\delta,t) = T_m \quad (2)$$

$$T(0,t) = T_c(t) \quad (3)$$

2) Wall

$$\frac{T_w(x,t) - T_{wb}(t)}{T_c(t) - T_{wb}(t)} = \beta_w(t) \left[1 + \frac{x}{D_w} \right] + \left[1 - \beta_w(t) \right] \left[1 + \frac{x}{D_w} \right]^2 \quad (4)$$

The following boundary conditions are satisfied.

$$T_w(-D_w,t) = T_w(t) \quad (5)$$

$$T_w(0,t) = T_c(t) \quad (6)$$

Governing Equations

1) Crust Energy Equation

$$\int_0^{\delta} \frac{\partial T}{\partial t}\, dx = \int_0^{\delta} \alpha \frac{\partial^2 T}{\partial x^2}\, dx \qquad 7$$

2) Wall Energy Equation

$$\int_0^{-D_w} \frac{\partial T_w}{\partial t}\, dx = \int_0^{-D_w} \alpha_w \frac{\partial^2 T_w}{\partial x^2}\, dx \qquad 8$$

3) Flux Matching at the Bulk-Melt/Wall Interface

$$\rho h^*_{fb} \frac{d\delta}{dt} = k \left.\frac{\partial T}{\partial x}\right|_{\delta} - h(T_b - T_m) \qquad 9$$

where,

$$h^*_{fb} = h_{fb} + c_{pb}(T_b - T_m) \qquad 10$$

4) Flux Matching at the Crust/Wall Interface

$$k \left.\frac{\partial T}{\partial x}\right|_0 = k_w \left.\frac{\partial T_w}{\partial x}\right|_0 \qquad 11$$

5) Flux Matching at the External-Coolant/Wall Interface

$$k_w \left.\frac{\partial T_w}{\partial x}\right|_{-D_w} = h_w(T_{wb} - T_w^o) \qquad 12$$

Derivation of Controlling Differential Equations

The differential equations that must be solved in order to determine the unknown parameters are obtained by substituting the temperature profiles into each of the governing equations above. A brief summary of the steps involved in these derivations and the resulting differential equations are provided below.

1) Starting with the crust energy equation (Eq. 8), move the time derivative outside the left-hand integral, and evaluate the integral of the second-order spatial derivative. Substitute the crust temperature profile (Eq. 1) into the result.

$$A_{11}\frac{d\delta^2}{dt} + A_{13}\frac{dT_c}{dt} + A_{14}\frac{d\beta}{dt} = B_1 \qquad 13$$

where,

$$A_{11} = 1 \qquad 14$$

$$A_{13} = \frac{2\delta^2}{T_m - T_c} \qquad 15$$

$$A_{14} = \frac{2\delta^2}{2 + \beta} \qquad 16$$

$$B_1 = 24\alpha\,\frac{1 - \beta}{2 + \beta} \qquad 17$$

2) Starting with the wall energy equation (Eq. 9), move the time derivative outside the left-hand integral, and evaluate the integral of the second-order spatial derivative. Substitute the wall temperature profile (Eq. 4) into the result.

$$A_{22} \frac{dT_{wb}}{dt} + A_{23} \frac{dT_c}{dt} + A_{25} \frac{d\beta_w}{dt} = B_2 \qquad 18$$

where,

$$A_{22} = D_w^2(4 - \beta_w) \qquad 19$$

$$A_{23} = D_w^2(2 + \beta_w) \qquad 20$$

$$A_{25} = D_w^2(T_c - T_{wb}) \qquad 21$$

$$B_2 = 12\alpha_w(T_c - T_{wb})(1 - \beta_w) \qquad 22$$

3) Substitute the crust temperature profile (Eq. 1) into the flux matching condition (Eq. 9) at the bulk-melt/crust interface.

$$A_{31} \frac{d\delta^2}{dt} = B_3 \qquad 23$$

where,

$$A_{31} = 1 \qquad 24$$

$$B_3 = 2\beta \frac{k}{\rho h^*_{fb}} (T_m - T_c) - \frac{2h\delta}{\rho h^*_{fb}} (T_b - T_m) \qquad 25$$

4) Substitute the crust temperature profile (Eq. 1) and the wall temperature profile (Eq. 4) into the flux matching condition (Eq. 11) at the crust/wall interface. Differentiate the result with respect to time.

$$A_{41}\frac{d\delta^2}{dt} + A_{42}\frac{dT_{wb}}{dt} + A_{43}\frac{dT_c}{dt} + A_{44}\frac{d\beta}{dt} + A_{45}\frac{d\beta_w}{dt} = B_4 \qquad 26$$

where,

$$A_{41} = k_w(2 - \beta_w)(T_c - T_{wb}) \qquad 27$$

$$A_{42} = -2k_w\delta^2(2 - \beta_w) \qquad 28$$

$$A_{43} = 2\delta(k_w\delta(2 - \beta_w) + kD_w(2 - \beta)) \qquad 29$$

$$A_{44} = 2k\delta D_w(T_m - T_c) \qquad 30$$

$$A_{45} = 2k_w\delta^2(T_w - T_c) \qquad 31$$

$$B_4 = 0 \qquad 32$$

5) Substitute the wall temperature profile (Eq. 4) into the flux matching condition at the external-coolant/wall interface (Eq. 12). Differentiate the result with respect to time.

$$A_{52}\frac{dT_{wb}}{dt} + A_{53}\frac{dT_c}{dt} + A_{55}\frac{d\beta_w}{dt} = B_5 \qquad 33$$

where,

$$A_{52} = \frac{h_w D_w}{k_w} + \beta_w \qquad 34$$

$$A_{53} = -\beta_w \qquad 35$$

$$A_{55} = T_{wb} - T_c \qquad 36$$

$$B_5 = 0 \qquad 37$$

Auxiliary Relationships

It is possible to use some of the governing equations to derive simple algebraic expressions for some of the unknown parameters as a function of the other parameters (no time derivatives). A brief summary of the steps involved in these derivations and the resulting consistency relationships are provided below.

1) Contact Temperature - Substitute the crust temperature profile (Eq. 1) and the wall temperature profile (Eq. 4) into the flux matching condition (Eq. 11) at the crust/wall interface.

$$T_c = \frac{k_w\delta(2 - \beta_w)\ T_w + kD_w(2 - \beta)\ T_m}{k_w\delta(2 - \beta_w) + kD_w(2 - \beta)} \qquad 38$$

2) Crust Temperature Shape Parameter - Form the differential of the temperature boundary condition (Eq. 2) at the bulk-melt/crust interface.

$$\left.\frac{\partial T}{\partial x}\right|_{\delta} \frac{d\delta}{dt} + \left.\frac{\partial T}{\partial t}\right|_{\delta} = 0 \qquad 39$$

Solve for $d\delta/dt$. Eliminate $\partial T/\partial t$ by using the differential form of the crust energy equation.

$$\frac{d\delta}{dt} = - \frac{\alpha \left.\frac{\partial^2 T}{\partial x^2}\right|_{\delta}}{\left.\frac{\partial T}{\partial x}\right|_{\delta}} \qquad 40$$

Substitute this result into the flux matching condition (Eq. 5) at the bulk-melt/crust interface.

$$\beta = \frac{1}{2A_1} (2 - A_2 A_1) \left[(1 + A_3)^{1/2} - 1\right] \qquad 41$$

where,

$$A_1 = \frac{c_p (T_m - T_c)}{h^*_{fb}} \qquad 42$$

$$A_2 = \frac{h\delta}{k} \frac{T_b - T_m}{T_m - T_c} \qquad 43$$

$$A_3 = \frac{8A_1}{(2 - A_2 A_1)^2} \qquad 44$$

3) Wall Temperature Shape Parameter - Substitute the wall temperature profile (Eq. 4) into the flux matching condition (Eq. 12) at the external-coolant/wall interface.

$$\beta_w = \frac{h_w D_w}{k_w} \frac{T_{wb} - T^o_w}{T_c - T_{wb}} \qquad 45$$

5.1.5 Cylindrical Geometry - No Crust With a Nonmelting, Infinitely-Thick Wall

The geometry, representative temperature profiles, and nomenclature for this problem are shown in Figure 5.5. The unknown, time-dependent parameters that must be solved for are

$$\delta_w, \; T_c \; .$$

The solution scheme described below summarizes the FORTRAN coding in the PLUGM subroutine TUBEXXI.

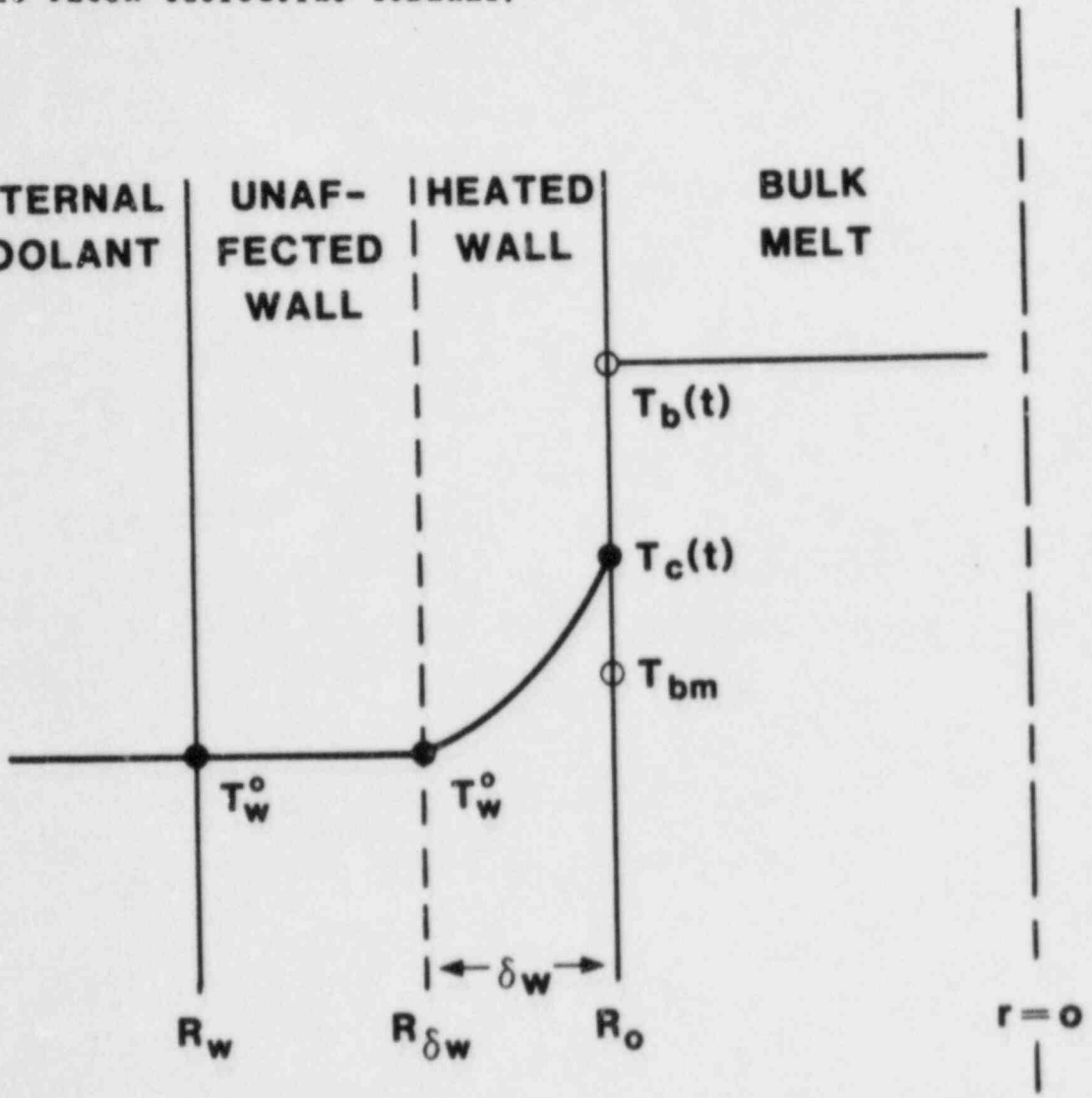

Figure 5.5. Temperature Distribution in Cylindrical Geometry for Case of No Crust / No Wall Melt / Infinite Wall

Assumed Temperature Profile

1) Wall

$$\frac{T_w(r,t) - T_w^o}{T_c(t) - T_w^o} = \left[1 - \frac{\ln(r/R_o)}{\ln(R_{\delta w}/R_o)} \right]^2 \qquad 1$$

The following boundary conditions are satisfied.

$$T_w(R_o,t) = T_c(t) \qquad 2$$

$$T_w(R_{\delta w},t) = T_w^o \qquad 3$$

$$\left.\frac{\partial T}{\partial r}\right|_{R_{\delta w}} = 0 \qquad 4$$

Governing Equations

1) Wall Energy Equation

$$\int_{R_o}^{R_{\delta w}} \frac{\partial T_w}{\partial t}\, r\, dr = \int_{R_o}^{R_{\delta w}} \alpha_w \frac{\partial}{\partial r}\left(r \frac{\partial T_w}{\partial r}\right) dr \qquad 5$$

2) Flux Matching at the Bulk-Melt/Wall Interface

$$h(T_b - T_c) = -k_w \left.\frac{\partial T_w}{\partial r}\right|_{R_o} \qquad 6$$

Derivation of Controlling Differential Equations

The differential equations that must be solved in order to determine the unknown parameters are obtained by substituting the temperature profiles into each of the governing equations above. A brief summary of the steps involved in these derivations and the resulting differential equations are provided below.

It is convenient to express the results for the differential equations in cylindrical geometry in terms of the dimensionless variable

$$x = r/R_o. \qquad 7$$

Thus, in place of the wall thermal-front radius, $R_{\delta w}$, we use the dimensionless variable

$$x_{\delta w} = R_{\delta w}/R_o. \qquad 8$$

1) Starting with the wall energy equation (Eq. 5), move the time derivative outside the left-hand integral, and evaluate the integral of the second-order spatial derivative. Substitute the wall temperature profile (Eq. 1) into the result.

$$A_{11} \frac{dx_{\delta w}}{dt} + A_{12} \frac{dT_c}{dt} = B_1 \qquad 9$$

where,

$$A_{11} = (1 + \ln x_{\delta w}) + x_{\delta w}^2(\ln x_{\delta w} - 1) \qquad 10$$

$$A_{12} = -\frac{x_{\delta w}(\ln x_{\delta w})^3 + x_{\delta w}(\ln x_{\delta w})^2 + \frac{1}{2}x_{\delta w}(1 - x_{\delta w}^2)\ln x_{\delta w}}{T_c - T_w^o} \qquad 11$$

$$B_1 = \frac{4\alpha_w}{R_o^2} x_{\delta w}(\ln x_{\delta w})^2 \qquad 12$$

2) Substitute the wall temperature profile (Eq. 1) into the flux matching condition at the bulk-melt/wall interface (Eq. 6). Differentiate the result with respect to time and use the undifferentiated result to simplify the resulting expression.

$$A_{21} \frac{dx_{\delta w}}{dt} + A_{22} \frac{dT_c}{dt} = B_2 \qquad 13$$

where,

$$A_{21} = \frac{hR_o(T_c - T_b)}{hR_o x_{\delta w} \ln x_{\delta w} + 2k_w x_{\delta w}} \qquad 14$$

$$A_{22} = 1 \qquad 15$$

$$B_2 = \frac{hR_o \ln x_{\delta w}}{hR_o \ln x_{\delta w} + 2k_w} \frac{\partial T_b}{\partial t} \qquad 16$$

Auxiliary Relationship

It is possible to use some of the governing equations to derive simple algebraic expressions for some of the unknown parameters as a function of the other parameters (no time derivatives). A brief summary of the steps involved in these derivations and the resulting consistency relationships are provided below.

1) Contact Temperature - Substitute the wall temperature profile (Eq. 1) into the flux matching condition at the wall/bulk melt interface (Eq. 2).

$$T_c = \frac{hR_o \ln x_{\delta w} T_b + 2k_w T_w^o}{hR_o \ln x_{\delta w} + 2k_w} \qquad 17$$

5.1.6 Cylindrical Geometry - No Crust with a Nonmelting, Finite-Thickness Wall

The geometry, representative temperature profiles, and nomenclature for this problem are shown in Figure 5.6. The unknown parameters that must be solved for are

$$T_c,\ T_{wb},\ \beta_w\ .$$

The solution scheme described below summarizes the FORTRAN coding in the PLUGM subroutine TUBEXXF.

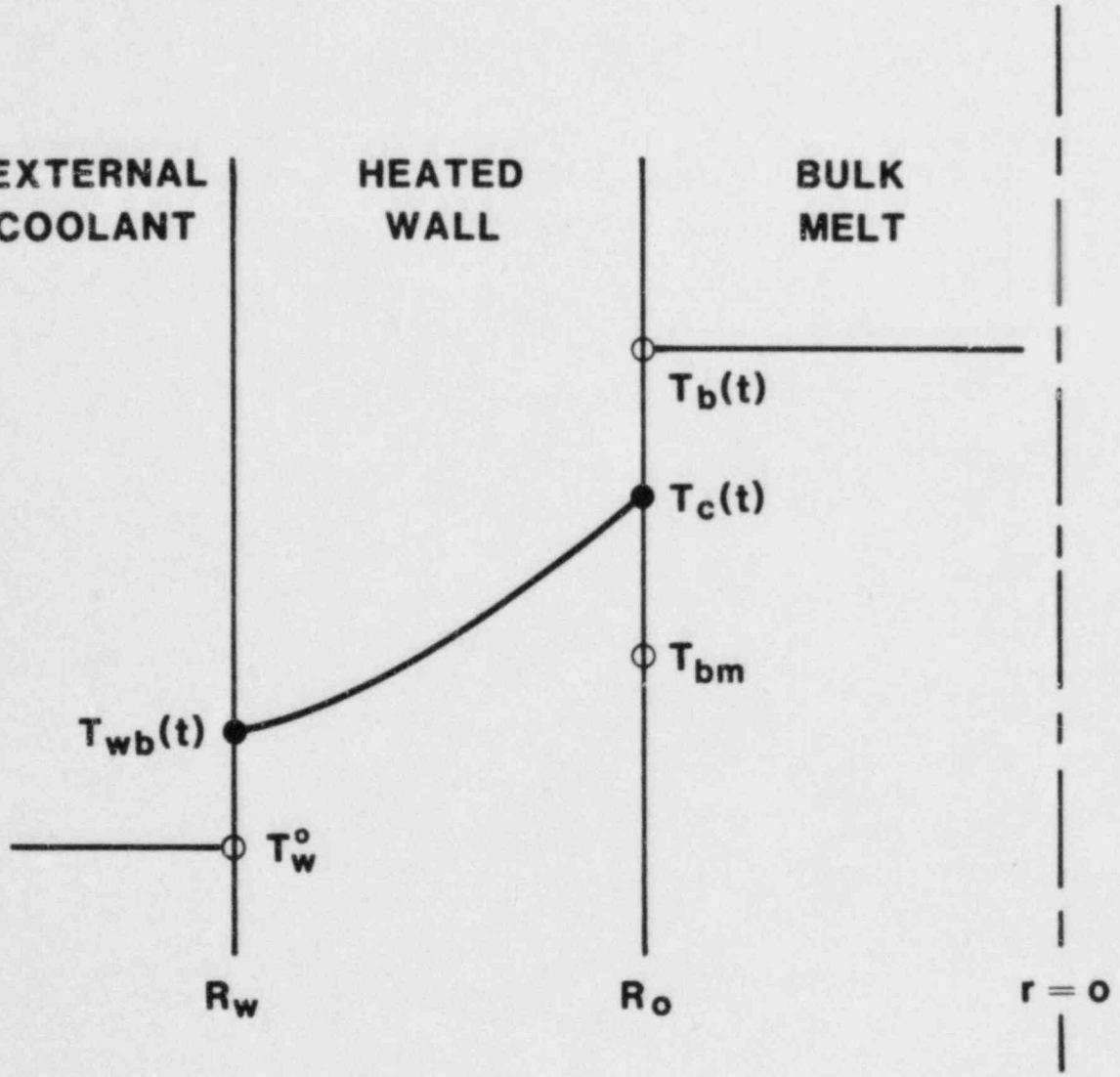

Figure 5.6. Temperature Distribution in Cylindrical Geometry for Case of No Crust / No Wall Melt / Finite Wall

Assumed Temperature Profiles

1) Wall

$$\frac{T_w(r,t) - T_{wb}(t)}{T_c(t) - T_{wb}(t)} = \beta_w(t) \left[1 - \frac{\ln(r/R_o)}{\ln(R_w/R_o)} \right]$$

$$+ \left[1 - \beta_w(t)\right] \left[1 - \frac{\ln(r/R_o)}{\ln(R_w/R_o)} \right]^2 \quad 1$$

The following boundary conditions are satisfied.

$$T_w(R_o,t) = T_c(t) \quad 2$$

$$T_w(R_w,t) = T_{wb}(t) \quad 3$$

Governing Equations

1) Wall Energy Equation

$$\int_{R_o}^{R_w} \frac{\partial T_w}{\partial t} r \, dr = \int_{R_o}^{R_w} \alpha_w \frac{\partial}{\partial r}\left(r \frac{\partial T_w}{\partial r}\right) dr \quad 4$$

2) Flux Matching at the Wall/Bulk-Melt Interface

$$h(T_b - T_c) = -k_w \left.\frac{\partial T_w}{\partial r}\right|_{R_o} \quad 5$$

3) Flux Matching at the Wall/External Coolant Interface

$$h_w(T_{wb} - T_w^o) = -k_w \left.\frac{\partial T_w}{\partial r}\right|_{R_w} \qquad 6$$

Derivation of Controlling Differential Equations

The differential equations that must be solved in order to determine the unknown parameters are obtained by substituting the temperature profiles into each of the governing equations above. A brief summary of the steps involved in these derivations and the resulting differential equations are provided below.

It is convenient to express the results for the differential equations in cylindrical geometry in terms of the dimensionless variable

$$x = r/R_o. \qquad 7$$

Thus, in place of the outer wall radius, R_w, we use the dimensionless variable

$$x_w = R_w/R_o. \qquad 8$$

1) Starting with the wall energy equation (Eq. 4), move the time derivative outside the left-hand integral, and evaluate the integral of the second-order spatial derivative. Substitute the wall temperature profile (Eq. 1) into the result.

$$A_{11} \frac{\partial T_c}{\partial t} + A_{12} \frac{\partial T_{wb}}{\partial t} + A_{13} \frac{\partial \beta_w}{\partial t} = B_1 \qquad 9$$

where,

$$A_{11} = -2\ln x_w + (\beta_w x_w^2 + \beta_w - 2) - \frac{(1 - \beta_w)(1 - x_w^2)}{\ln x_w} \qquad 10$$

$$A_{12} = 2x_w^2 \ln x_w - (\beta_w x_w^2 + \beta_w - 2) - \frac{(1 - \beta_w)(x_w^2 - 1)}{\ln x_w} \qquad 11$$

$$A_{13} = (T_c - T_{wb})(x_w^2 + 1) + \frac{(T_c - T_{wb})(1 - x_w^2)}{\ln x_w} \qquad 12$$

$$B_1 = 8\alpha_w R_o^2 (1 - \beta_w)(T_c - T_{wb}) \qquad 13$$

2) Substitute the wall temperature profile (Eq. 1) into the flux matching condition at the bulk-melt/wall interface (Eq. 5). Differentiate the result with respect to time and use the undifferentiated result to simplify the resulting expression.

$$A_{21} \frac{\partial T_c}{\partial t} + A_{22} \frac{\partial T_{wb}}{\partial t} + A_{23} \frac{\partial \beta_w}{\partial t} = B_2 \qquad 14$$

where,

$$A_{21} = k_w R_o (2 - \beta_w) + h R_o^2 \ln x_w \qquad 15$$

$$A_{22} = k_w R_o (\beta_w - 2) \qquad 16$$

$$A_{23} = k_w R_o (T_{wb} - T_c) \qquad 17$$

$$B_2 = h R_o^2 \ln x_w \frac{dT_b}{dt} \qquad 18$$

3) Substitute the wall temperature profile (Eq. 1) into the flux matching condition at the wall/external-coolant interface (Eq. 6). Differentiate the result with respect to time and use the undifferentiated result to simply the resulting expression.

$$A_{31} \frac{\partial T_c}{\partial t} + A_{32} \frac{\partial T_{wb}}{\partial t} + A_{33} \frac{\partial \beta_w}{\partial t} = B_3 \qquad 19$$

where,

$$A_{31} = -\beta_w \qquad 20$$

$$A_{32} = \frac{h_w R_o x_w \ln x_w}{k_w} + \beta_w \qquad 21$$

$$A_{33} = T_{wb} - T_c \qquad 22$$

$$B_3 = 0 \qquad 23$$

Auxiliary Relationships

It is possible to use some of the governing equations to derive simple algebraic expressions for some of the unknown parameters as a function of the other parameters (no time derivatives). A brief summary of the steps involved in these derivations and the resulting consistency relationships are provided below.

1) Contact Temperature - Substitute the wall temperature profile (Eq. 1) into the flux matching condition at the bulk-melt/wall/interface (Eq. 5).

$$T_c = \frac{hR_o \ln x_w \; T_b + k_w(2 - \beta_w) \; T_{wb}}{hR_o \ln x_w + k_w(2 - \beta_w)} \qquad 24$$

2) Wall Temperature Shape Parameter - Substitute the wall temperature profile (Eq. 1) into the flux matching condition at the wall/external-coolant interface (Eq. 6).

$$\beta_w = \frac{h_w R_o x_w \ln x_w}{k_w} \quad \frac{T_w^o - T_{wb}}{T_{wb} - T_c} \qquad 25$$

5.1.7 Cylindrical Geometry - Crust on a Nonmelting, Infinitely-Thick Wall

The geometry, representative temperature profiles, and nomenclature for this problem are shown in Figure 5.7. The unknown parameters that must be solved for are

$$\delta,\ \delta_w,\ T_c,\ \beta.$$

The solution scheme described below summarizes the FORTRAN coding in the PLUGM subroutine TUBECXI.

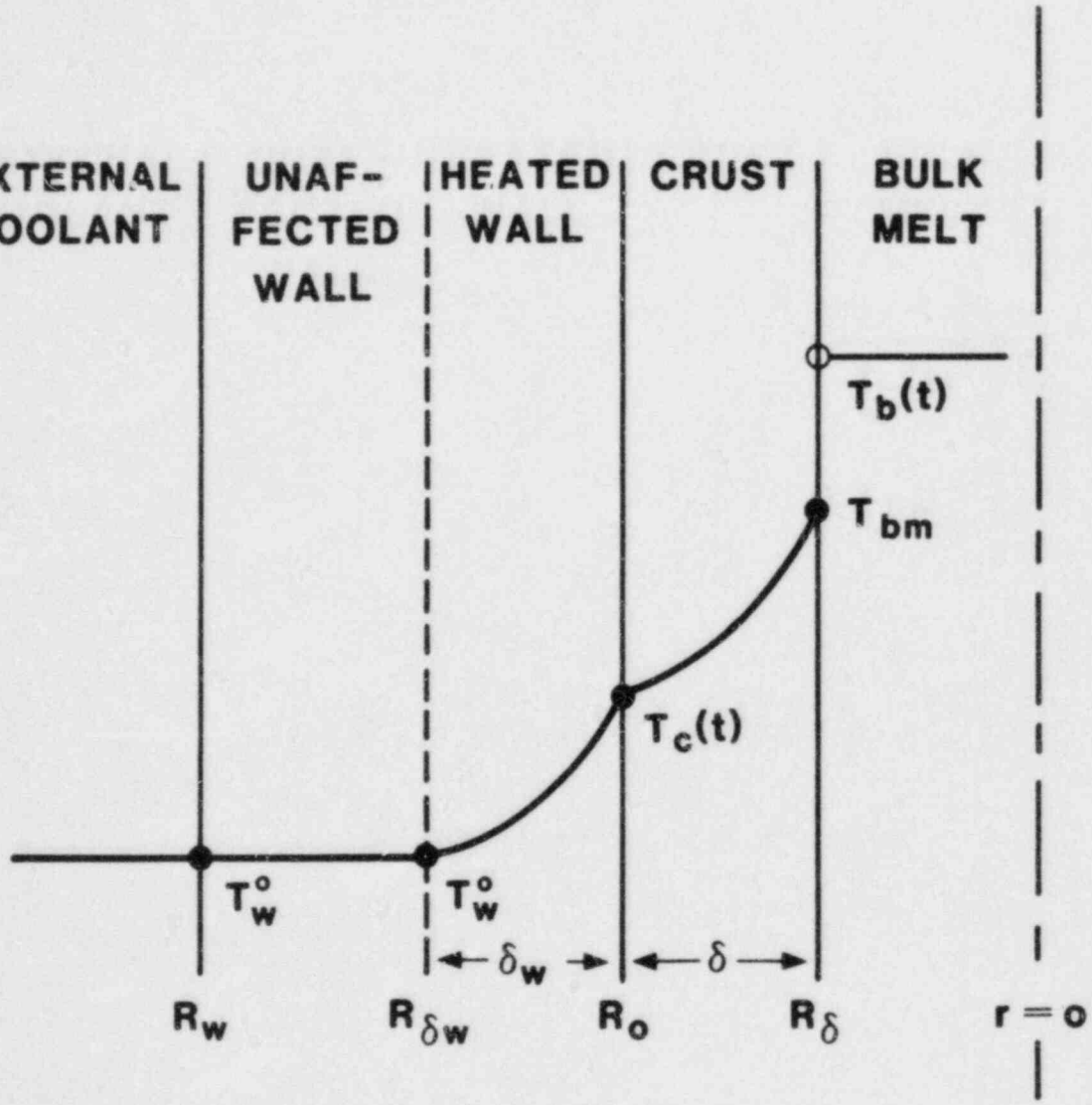

Figure 5.7. Temperature Distribution in Cylindrical Geometry for Case of Crust / No Wall Melt / Infinite Wall

Assumed Temperature Profiles

1) Crust

$$\frac{T(r,t) - T_m}{T_c(t) - T_m} = \beta(t) \left[1 - \frac{\ln(r/R_o)}{\ln(R_\delta(t)/R_o)} \right]$$

$$+ \left[1-\beta(t)\right] \left[1 - \frac{\ln(r/R_o)}{\ln(R_\delta(t)/R_o)} \right]^2 \qquad 1$$

The following boundary conditions are satisfied.

$$T(R_\delta, t) = T_m \qquad 2$$

$$T(R_o, t) = T_c(t) \qquad 3$$

2) Wall

$$\frac{T_w(r,t) - T_w^o}{T_c(t) - T_w^o} = \left[1 - \frac{\ln(r/R_o)}{\ln(R_{\delta w}(t)/R_o)} \right]^2 \qquad 4$$

The following boundary conditions are satisfied,

$$T_w(R_o, t) = T_c(t) \qquad 5$$

$$T_w(R_{\delta w}, t) = T_w^o \qquad 6$$

$$\left.\frac{\partial T_w}{\partial r}\right|_{R_{\delta w}(t)} = 0 \qquad 7$$

Governing Equations

1) Crust Energy Equation

$$\int_{R_\delta}^{R_o} \frac{\partial T}{\partial t}\, r\, dr = \int_{R_\delta}^{R_o} \alpha\, \frac{\partial}{\partial r}\left(r \frac{\partial T}{\partial r}\right) dr \qquad 8$$

2) Wall Energy Equation

$$\int_{R_o}^{R_{\delta w}} \frac{\partial T_w}{\partial t}\, r\, dr = \int_{R_o}^{R_{\delta w}} \alpha_w\, \frac{\partial}{\partial r}\left(r \frac{\partial T_w}{\partial r}\right) dr \qquad 9$$

3) Flux Matching at the Bulk-Melt/Crust Interface

$$\rho h^*_{fb} \frac{\partial R_\delta}{\partial t} = k \left.\frac{\partial T}{\partial r}\right|_{R_\delta} + h(T_b - T_m) \qquad 10$$

where,

$$h^*_{fb} = h_{fb} + c_{pb}(T_b - T_m) \qquad 11$$

4) Flux Matching at the Crust/Wall Interface

$$k \left.\frac{\partial T}{\partial r}\right|_{R_o} = k_w \left.\frac{\partial T_w}{\partial r}\right|_{R_o} \qquad 12$$

Derivation of Controlling Differential Equations

The differential equations that must be solved in order to determine the unknown parameters are obtained by substituting the temperature profiles into each of the governing equations above. A brief summary of the steps involved in these derivations and the resulting differential equations are provided below.

It is convenient to express the results for the differential equations in cylindrical geometry in terms of the dimensionless variable

$$x = r/R_o. \qquad 13$$

Thus, in place of the outer crust radius, R_δ, we use the dimensionless variable

$$x_\delta = R_\delta/R_o \qquad 14$$

and in place of the wall thermal front radius, $R_{\delta w}$, we use the dimensionless variable

$$x_{\delta w} = R_{\delta w}/R_o. \qquad 15$$

1) Starting with the crust energy equation (Eq. 8), move the time derivative outside the left-hand integral, and evaluate the integral of the second-order spatial derivative. Substitute the crust temperature profile (Fq. 1) into the result.

$$A_{11} \frac{dx_\delta}{dt} + A_{13} \frac{\partial T_c}{\partial t} + A_{14} \frac{\partial \beta}{\partial t} = B_1 \qquad 16$$

where,

$$A_{11} = \left[\frac{1 + x_\delta^2}{x_\delta \ln x_\delta} + \frac{1 - x_\delta^2}{x_\delta (\ln x_\delta)^2}\right] \qquad 17$$

$$+ \beta \left[x_\delta - \frac{1 + 3x_\delta^2}{2x_\delta \ln x_\delta} - \frac{1 - x_\delta^2}{x_\delta (\ln x_\delta)^2}\right]$$

$$A_{13} = \left[\frac{\beta}{2}\left[1 + x_\delta^2 + \frac{1 - x_\delta^2}{\ln x_\delta}\right]\right. \qquad 18$$

$$\left. - \left[1 + \ln x_\delta + \frac{1 - x_\delta^2}{2 \ln x_\delta}\right]\right] / (T_c - T_m)$$

$$A_{14} = \frac{1}{2}\left[1 + x_\delta^2 + \frac{1 - x_\delta^2}{\ln x_\delta}\right] \qquad 19$$

$$B_1 = \frac{4\alpha}{R_o^2}(1 - \beta) \qquad 20$$

2) Starting with the wall energy equation (Eq. 9), move the time derivative outside the left-hand integral, and evaluate the integral of the second-order spatial derivative. Substitute the wall temperature profile (Eq. 4) into the result.

$$A_{22} \frac{\partial x_{\delta w}}{\partial t} + A_{23} \frac{\partial T_c}{\partial t} = B_2 \qquad 21$$

where,

$$A_{22} = (1 + \ln x_{\delta w}) + x_{\delta w}^2 (\ln x_{\delta w} - 1) \qquad 22$$

$$A_{23} = \frac{-1}{T_c - T_w^o} \left[x_{\delta w} (\ln x_{\delta w})^3 + \right.$$

$$\left. x_{\delta w} (\ln x_{\delta w})^2 + \frac{x_{\delta w}}{2} (1 - x_{\delta w}^2) \ln x_{\delta w} \right] \qquad 23$$

$$B_2 = \frac{4 a_w}{R_o^2} x_{\delta w} (\ln x_{\delta w})^2 \qquad 24$$

3) Substitute the crust temperature profile (Eq. 1) into the flux matching condition (Eq. 10) at the bulk-melt/crust interface.

$$A_{31} \frac{dx_\delta}{dt} = B_3 \qquad 25$$

where,

$$A_{31} = 1 \qquad 26$$

$$B_3 = \frac{\beta}{R_o^2 x_\delta \ln x_\delta} \frac{k}{\rho h_{fb}^*} (T_m - T_c) + \frac{h}{R_o \rho h_{ft}^*} (T_b - T_m) \qquad 27$$

4) Sub titute the crust temperature profile (Eq. 1) and the wall temperature profile (Eq. 4) into the flux matching condition (Eq. 12) at the crust/wall interface. Differentiate the result with respect to time, and use the undifferentiated result to simplify the resulting expression.

$$A_{41} \frac{dx_\delta}{dt} + A_{42} \frac{dx_{\delta w}}{dt} + A_{43} \frac{dT_c}{dt} + A_{44} \frac{d\beta}{dt} = B_4 \qquad 28$$

where,

$$A_{41} = \frac{2 - \beta}{x_\delta \ln x_\delta} \qquad 29$$

$$A_{42} = \frac{\beta - 2}{x_{\delta w} \ln x_{\delta w}} \qquad 30$$

$$A_{43} = (2 - \beta) \frac{T_w^o - T_m}{(T_c - T_w^o)(T_c - T_m)} \qquad 31$$

$$A_{44} = 1 \qquad 32$$

$$B_4 = 0 \qquad 33$$

Auxillary Relationships

It is possible to use some of the governing equations to derive simple algebraic expressions for some of the unknown parameters as a function of the other parameters (no time derivatives). A brief summary of the steps involved in these derivations and the resulting consistency relationships are provided below.

1) Contact Temperature - Substitute the crust temperature profile (Eq. 1) and the wall temperature profile (Eq. 4) into the flux matching condition (Eq. 12) at the crust/wall interface.

$$T_c = \frac{2k_w \ln x_\delta \; T_w^o + (\beta - 2) k \ln x_{\delta w} \; T_m}{2k_w \ln x_\delta + (\beta - 2) k \ln x_{\delta w}} \qquad 34$$

2) Crust Temperature Shape Parameter - Form the differential of the temperature boundary condition (Eq. 2) at the bulk-melt/crust interface.

$$\left.\frac{\partial T}{\partial r}\right|_{R_\delta} \frac{dR_\delta}{dt} + \left.\frac{\partial T}{\partial t}\right|_{R_\delta} = 0 \qquad 35$$

Solve for dR_δ/dt. Eliminate $\partial T/\partial t$ by using the differential form of the crust energy equation.

$$\frac{dR_\delta}{dt} = - \frac{\frac{\alpha}{r} \frac{\partial}{\partial r}\left(r \frac{\partial T}{\partial r}\right)\Big|_{R_\delta}}{\left.\frac{\partial T}{\partial x}\right|_{R_\delta}} \qquad 36$$

Substitute this result into the flux matching condition at the bulk-melt/crust interface (Eq. 10).

$$\beta = \frac{1}{2A_1}(2 - \ln x_\delta - A_1 A_2)[(1 + A_3)^{1/2} - 1] \qquad 37$$

where,

$$A_1 = \frac{c_p(T_m - T_c)}{h^*_{fb}} \qquad 38$$

$$A_2 = \frac{hR_o}{k} \frac{T_b - T_m}{T_c - T_m} x_\delta \ln x_\delta \qquad 39$$

$$A_3 = \frac{8A_1}{(2 - \ln x_\delta - A_1 A_2)^2} \qquad 40$$

5.1.8 Cylindrical Geometry - Crust on a Nonmelting, Finite-Thickness Wall

The geometry, representative temperature profiles, and nomenclature for this problem are shown in Figure 5.8. The unknown parameters that must be solved for are

$$\delta,\ T_c,\ T_{wb},\ \beta,\ \beta_w.$$

The solution scheme described below summarizes the FORTRAN coding in the PLUGM subroutine TUBECXF.

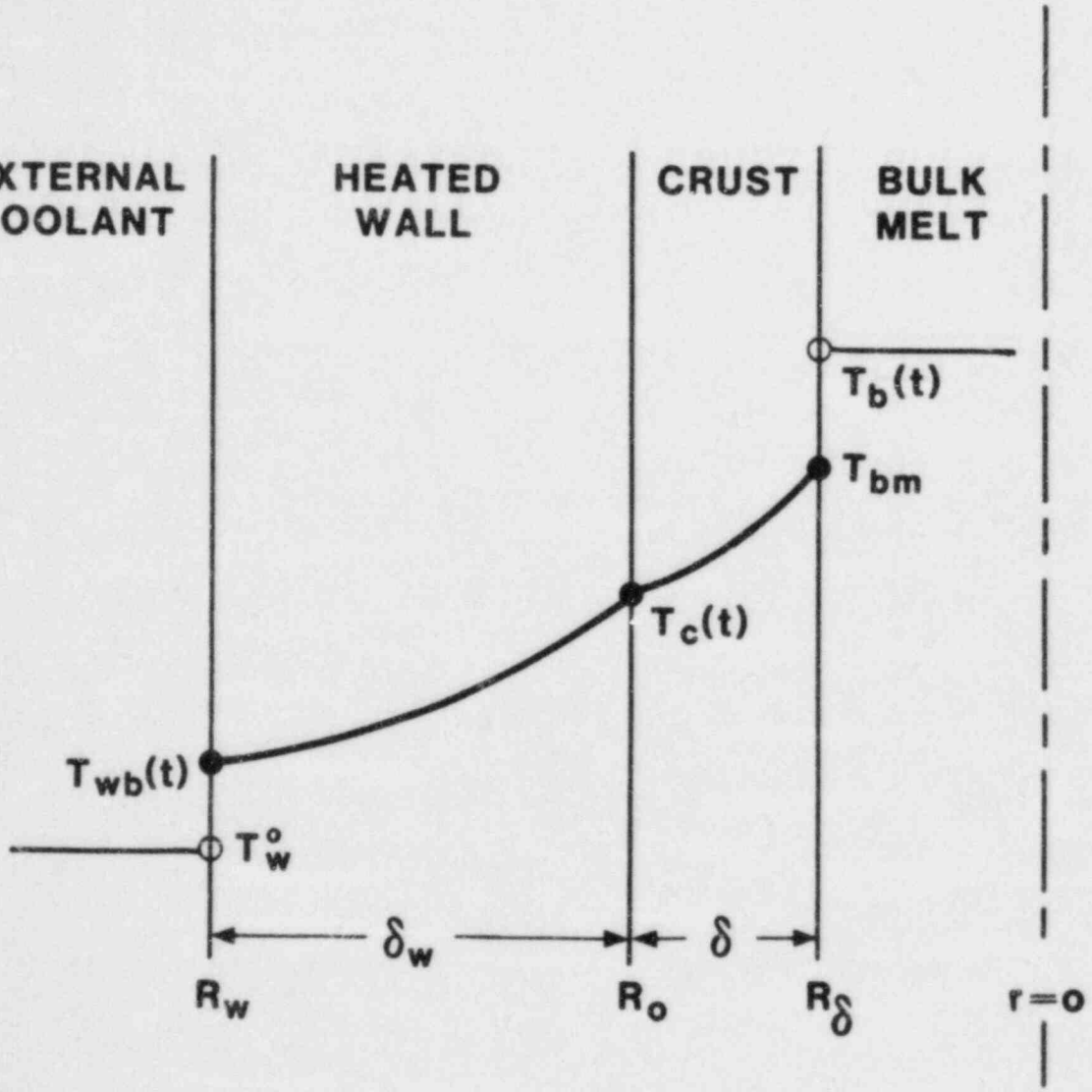

Figure 5.8. Temperature Distribution in Cylindrical Geometry for Case of Crust / No Wall Melt / Finite Wall

Assumed Temperature Profiles

1) Crust

$$\frac{T(r,t) - T_m}{T_c(t) - T_m} = \beta(t) \left[1 - \frac{\ln(r/R_o)}{\ln(R_\delta(t)/R_o)} \right]$$

$$+ \left[1 - \beta(t)\right] \left[1 - \frac{\ln(r/R_o)}{\ln(R_\delta(t)/R_o)} \right]^2 \qquad 1$$

The following boundary conditions are satisfied.

$$T(R_\delta, t) = T_m \qquad 2$$

$$T(R_o, t) = T_c(t) \qquad 3$$

2) Wall

$$\frac{T_w(r,t) - T_{wb}(t)}{T_c(t) - T_{wb}(t)} = \beta_w(t) \left[1 - \frac{\ln(r/R_o)}{\ln(R_w/R_o)} \right]$$

$$+ \left[1 - \beta_w(t)\right] \left[1 - \frac{\ln(r/R_o)}{\ln(R_w/R_o)} \right]^2 \qquad 4$$

The following boundary conditions are satisfied,

$$T_w(R_o, t) = T_c(t) \qquad 5$$

$$T_w(R_w, t) = T_{wb}(t) \qquad 6$$

Governing Equations

1) Crust Energy Equation

$$\int_{R_o}^{R_\delta} \frac{\partial T}{\partial r}\, r\, dr = \int_{R_o}^{R_\delta} \alpha \frac{\partial}{\partial r}\left(r\frac{\partial T}{\partial r}\right) dr \qquad 7$$

2) Wall Energy Equation

$$\int_{R_w}^{R_o} \frac{\partial T_w}{\partial r}\, r\, dr = \int_{R_w}^{R_o} \alpha \frac{\partial}{\partial r}\left(r\frac{\partial T_w}{\partial r}\right) dr \qquad 8$$

3) Flux Matching at the Bulk-Melt/Crust Interface

$$\rho h^*_{fb} \frac{\partial R_\delta}{\partial t} = k \left.\frac{\partial T}{\partial r}\right|_{R_\delta} + h(T_b - T_m) \qquad 9$$

where,

$$h^*_{fb} = h_{fb} + c_{pb}(T_b - T_m) \qquad 10$$

4) Flux Matching at the Crust/Wall Interface

$$k \left.\frac{\partial T}{\partial r}\right|_{R_o} = k_w \left.\frac{\partial T_w}{\partial r}\right|_{R_o} \qquad 11$$

5) Flux Matching at the Wall/External Coolant Interface

$$-k_w \left.\frac{\partial T_w}{\partial r}\right|_{R_w} = h_w(T_{wb} - T_w^o) \qquad 12$$

Derivation of Controlling Differential Equations

The differential equations that must be solved in order to determine the unknown parameters are obtained by substituting the temperature profiles into each of the governing equations above. A brief summary of the steps involved in these derivations and the resulting differential equations are provided below.

It is convenient to express the results for the differential equations in cylindrical geometry in terms of the dimensionless variable

$$x = r/R_o \; . \qquad 13$$

Thus, in place of the outer crust radius, R_δ, we use the dimensionless variable

$$x_\delta = R_\delta/R_o \qquad 14$$

and in place of the wall radius, R_w, we use the dimensionless variable

$$x_w = R_w/R_o. \qquad 15$$

1) Starting with the crust energy equation (Eq. 8), move the time derivative outside the left-hand integral, and evaluate the integral of the second-order spatial derivative. Substitute the crust temperature profile (Eq. 1) into the resulting equation and evaluate the result.

$$A_{11}\frac{dx_\delta}{dt} + A_{12}\frac{\partial T_c}{\partial t} + A_{14}\frac{\partial \beta}{\partial t} = B_1 \qquad 16$$

where,

$$A_{11} = \left[\frac{1 + x_\delta^2}{x_\delta \ln x_\delta} + \frac{1 - x_\delta^2}{x_\delta (\ln x_\delta)^2}\right]$$

$$+\beta\left[x_\delta - \frac{1 + 3x_\delta^2}{2x_\delta \ln x_\delta} - \frac{1 - x_\delta^2}{x_\delta (\ln x_\delta)^2}\right] \qquad 17$$

$$A_{12} = \left[\frac{\beta}{2}\left[1 + x_\delta^2 + \frac{1 - x_\delta^2}{\ln x_\delta}\right]\right. \qquad 18$$

$$\left.-\left[1 + \ln x_\delta + \frac{1 - x_\delta^2}{2\ln x_\delta}\right]\right](T_c - T_m)$$

$$A_{14} = \frac{1}{2}\left[1 + x_\delta^2 + \frac{1 - x_\delta^2}{\ln x_\delta}\right] \qquad 19$$

$$B_1 = \frac{4\alpha}{R_o^2}(1 - \beta) \qquad 20$$

2) Starting with the wall energy equation (Eq. 9), move the time derivative outside the left-hand integral, and evaluate the integral of the second-order spatial derivative. Substitute the wall temperature profile (Eq. 4) into the result.

$$A_{22}\frac{dT_c}{dt} + A_{23}\frac{dT_{wb}}{dt} + A_{25}\frac{d\beta_w}{dt} = B_2 \qquad (21)$$

where,

$$A_{22} = -2\ln x_w + (\beta_w x_w^2 + \beta_w - 2) - \frac{(1-\beta_w)(1-x_w^2)}{\ln x_w} \qquad (22)$$

$$A_{23} = 2x_w^2 \ln x_w - (\beta_w x_w^2 + \beta_w - 2) - \frac{(1-\beta_w)(x_w^2-1)}{\ln x_w} \qquad (23)$$

$$A_{25} = (1+x_w^2)(T_c - T_{wb}) + \frac{(1-x_w^2)(T_c - T_{wb})}{\ln x_w} \qquad (24)$$

$$B_2 = 8\alpha_w R_o^2 (1-\beta_w)(T_c - T_{wb}) \qquad (25)$$

3) Substitute the crust temperature profile (Eq. 1) into the flux matching condition (Eq. 10) at the bulk-melt/crust interface.

$$A_{31}\frac{dx_\delta}{dt} = B_3 \qquad (26)$$

where,

$$A_{31} = 1 \qquad (27)$$

$$B_3 = \frac{\beta}{R_o^2 x_\delta \ln x_\delta}\frac{k}{\rho h_{fb}^*}(T_m - T_c) + \frac{h}{R_o \rho h_{fb}^*}(T_b - T_m) \qquad (28)$$

4) Substitute the crust temperature profile (Eq. 1) and the wall temperature profile profile (Eq. 4) into the flux matching condition (Eq. 22) at the crust/wall interface. Differentiate the result with respect to time.

$$A_{41}\frac{dx_\delta}{dt} + A_{42}\frac{dT_c}{dt} + A_{43}\frac{dT_{wb}}{dt} + A_{44}\frac{d\beta}{dt} + A_{45}\frac{d\beta_w}{dt} = B_4 \qquad 29$$

where,

$$A_{41} = k_w(2 - \beta_w)(T_c - T_{wb}) \qquad 30$$

$$A_{42} = x_\delta\left[k_w(2 - \beta_w)\ln x_\delta - k(2 - \beta)\ln x_w\right] \qquad 31$$

$$A_{43} = -k_w x_\delta \ln x_\delta (2 - \beta_w) \qquad 32$$

$$A_{44} = -k x_\delta \ln x_w (T_m - T_c) \qquad 33$$

$$A_{45} = -k_w x_\delta \ln x_\delta (T_c - T_{wb}) \qquad 34$$

$$B_4 = 0 \qquad 35$$

5) Substitute the wall temperature profile (Eq. 4) into the flux matching condition at the wall/external-coolant interface (Eq. 12). Differentiate the result with respect to time.

$$A_{52}\frac{dT_c}{dt} + A_{53}\frac{dT_{wb}}{dt} + A_{55}\frac{d\beta_w}{dt} = B_5 \qquad 36$$

where,

$$A_{52} = -\beta_w \qquad 37$$

$$A_{53} = \frac{h_w R_o x_w \ln x_w}{k_w} + \beta_w \qquad 38$$

$$A_{55} = T_{wb} - T_c \qquad 39$$

$$B_5 = 0 \qquad 40$$

Auxiliary Relationships

It is possible to use some of the governing equations to derive simple algebraic expressions for some of the unknown parameters as a function of the other parameters (no time derivatives). A brief summary of the steps involved in these derivations and the resulting consistency relationships are provided below.

1) Contact Temperature - Substitute the crust temperature profile (Eq. 1) and the wall temperature profile (Eq. 4) into the flux matching condition (Eq. 11) at the crust/wall interface.

$$T_c = \frac{k(\beta - 2)\ln x_w \, T_m + k_w(2 - \beta_w)\ln x_\delta \, T_{wb}}{k(\beta - 2)\ln x_w + k_w(2 - \beta_w)\ln x_\delta} \qquad 41$$

2) Crust Temperature Shape Parameter - Form the differential of the temperature boundary condition (Eq. 2) at the bulk-melt/crust interface.

$$\left.\frac{\partial T}{\partial r}\right|_{R_\delta} \frac{dR_\delta}{dt} + \left.\frac{\partial T}{\partial t}\right|_{R_\delta} = 0 \qquad 42$$

Solve for dR_δ/dt. Eliminate $\partial T/\partial t$ by using the differential form of the crust energy equation.

$$\frac{dR_\delta}{dt} = - \frac{\frac{a}{r}\frac{\partial}{\partial r}\left(r\frac{\partial T}{\partial r}\right)\Big|_{R_\delta}}{\frac{\partial T}{\partial r}\Big|_{R_\delta}} \qquad 43$$

Substitute this result into the flux matching condition at the bulk-melt/crust interface (Eq. 10).

$$\beta = \frac{1}{2A_1}(2 - \ln x_\delta - A_1 A_2)[(1 + A_3)^{1/2} - 1] \qquad 44$$

$$\text{where, } A_1 = \frac{c_p(T_m - T_c)}{h^*_{fb}} \qquad 45$$

$$A_2 = \frac{hR_o}{k}\frac{T_b - T_m}{T_c - T_m} x_\delta \ln x_\delta \qquad 46$$

$$A_3 = \frac{8A_1}{(2 - \ln x_\delta - A_1 A_2)^2} \qquad 47$$

3) Wall Temperature Shape Parameter - Substitute the wall temperature profile (Eq. 4) into the flux matching condition at the wall/external-coolant interface (Eq. 12).

$$\beta_w = \frac{h_w R_o x_w \ln x_w}{k_w}\frac{T_w^o - T_{wb}}{T_{wb} - T_c} \qquad 48$$

5.2 Initial Conditions

Certain crust growth and wall heatup parameters must be specified when melt enters a node that previously contained no melt. One of two things can occur: crust does not begin to grow instantaneously, or crust does begin to grow instantaneously.

Following initial bulk-melt/wall contact, the radius of curvature of the channel cross section is large compared to the thickness of any wall thermal-layer (δ_w) or crust (δ) that may begin to grow--regardless of geometry. Therefore, initial conditions derived for thin-slit geometry (infinitely thick wall) are equally applicable for any other geometry.

5.2.1 No Instantaneous Crust Growth

Instantaneous growth of crust does not occur if the fusion temperature (T_{bm}) of the bulk melt is less than the initial temperature of the wall (T_w^o).

$$T_{bm} < T_w^o \qquad (1)$$

Water (T_m = 273 K) flowing through a warm pipe (say, T_w^o = 300 K) is an example where instantaneous growth of crust does not occur. For this case, the parameters that must be initialized are 1) δ_w^o, the wall thermal-layer thickness, and 2) T_c^o, the bulk-melt/wall interface temperature.

Initial conditions for the case of no instantaneous crust growth are given below.

$$\delta_w^o = 0 \qquad (2)$$

$$T_c^o = T_w^o \qquad (3)$$

5.2.2 Instantaneous Crust Growth

Instantaneous growth of crust occurs when the initial temperature of the wall (T_w^o) is less than the fusion temperature (T_m) of the bulk melt

$$T_w^o < T_{bm}. \quad (1)$$

The following parameters must be initialized: 1) δ^o, crust thickness, 2) $\delta_w{}^o$, wall thermal-layer thickness, 3) $T_c{}^o$, crust/wall contact temperature, and 4) β^o, shape parameter for the temperature profile in the crust.

The first two parameters are easily initialized.

$$\delta^o = 0 \quad (2)$$

$$\delta_w^o = 0 \quad (3)$$

Short-time estimates for δ and δ_w are obtained by integrating Equation 5.1.3.23 and Equation 5.1.3.19, respectively.

$$\delta = \Delta^* t^{1/2} \quad (4)$$

$$\delta = \Delta_w^* t^{1/2} \quad (5)$$

where,

$$\Delta^* = \left[2\beta\alpha \, S_n^* \right]^{1/2} \quad (6)$$

$$\Delta_w^* = \left[12\alpha_w \right]^{1/2} \quad (7)$$

$$S_n^* = \frac{\rho c_p \, (T_{bm} - T_c)}{h_{fb}^*} \quad (8)$$

$$h_{fb}^* = h_{fb} + c_{pb} \, (T_b - T_{bm}) \quad (9)$$

An alternate expression short-time crust growth is obtained by integrating Equation 5.1.3.13.

$$\delta = \left[24\alpha \frac{1-\beta}{2+\beta} t \right]^{1/2} \qquad 10$$

Equating Equation 4 and Equation 10 yields a short time estimate of β^o in terms of the still undetermined contact temperature, T_c^o.

$$\beta^o = \left[1 + \frac{6}{S_n^*} \right] \left[1 + \frac{12}{S_n^* \left(1 + \frac{6}{S_n^*}\right)^2} \right]^{1/2} \qquad 11$$

A nonlinear expression for the crust/wall contact temperature is obtained by substituting the short-time solutions for δ and δ_w (Eqs. 4 and 5) and the result for β^o (Eq. 11) into Equation 5.1.3.32.

$$T_c^o = \frac{2k_w\Delta^o T_w + k\Delta_w{}^o(2 - \beta^o) T_m}{2k_w\Delta^o + k\Delta_w{}^o(2 - \beta^o)} \qquad 12$$

An interval halving method is then used to find the root (T_c^o) of Equation 12. Substitute T_c^o into Equation 11 to obtain an estimate of β^o.

5.3 Procedure for Treatment of Crust Remelting

The use of simple polynomials to describe the temperature profiles in the crust and in the wall works well as long as there are no sudden perturbations in the heat flux at the various boundaries. If sudden perturbations in the heat flux do occur, potential problems may arise. The case of complete crust remelting represents such a perturbation.

Consider a wall, crust and bulk-melt environment such that heat transfer from the bulk melt to the crust is large enough to cause crust remelting. So long as crust is still present, it is acting as a heat sink via the heat of fusion, and the heat transfer into the wall from the crust is limited. When the crust completely remelts and disappears, however, the crust heat of fusion is no longer available as a heat sink and the heat flux into the wall abruptly increases.

Physically what would happen at this point is that the bulk-melt/wall interface temperature (had been the wall/crust contact temperature) would rapidly increase with only limited early effect on the wall temperature distribution away from the wall surface. Because of the assumed polynomial temperature profile in the wall, however, such a localized perturbation can only be treated in an approximate fashion. Conservation of energy in the wall thermal layer thickness will cause a sudden rise in wall surface temperature to be accompanied by a decrease in the wall thermal layer thickness (for the case of semi-infinite wall) or a change in the wall temperature shape parameter and wall outer surface temperature (for the case of a finite wall).

To avoid problems with the algorithm that solves the differential equations discussed in Section 5.2, a special procedure is used at the time of crust remelting to reset the wall temperature profile parameters. For the case of a semi-infinite wall, the conditions of

1) flux matching at the wall/bulk-melt interface, and

2) conservation of wall energy just prior to crust remelt vs. just after crust remelt

are used to define new, self consistent values of T_c and δ_w. For the case of a finite wall, the conditions of

1) flux matching at the wall/bulk-melt interface,

2) flux matching at the wall/external-coolant interface, and

3) conservation of wall energy just prior to crust remelt vs. just after crust remelt

are used to define new, self consistent values of T_c, T_{wb}, and β_w.

The details of these calculations are described in the following sections.

5.3.1 Crust Remelt - Slit Geometry, Infinitely-Thick Wall

Just prior to crust remelt, the temperature distribution in the wall is given by

$$\frac{T_w(x,t) - T_w^o}{T_m - T_w^o} = \left[\frac{x + \delta_w}{\delta_w} \right]^2 . \qquad 1$$

This temperature distribution satisfies the flux matching condition at the crust/wall interface (see Eq. 5.1.3.12).

Just after crust remelt, the temperature distribution is given by

$$\frac{T_w'(x,t) - T_w^o}{T_c'(t) - T_w^o} = \left[\frac{x + \delta_w'}{\delta_w'} \right]^2 . \qquad 2$$

The new values T_c' and δ_w' are determined such that the new flux matching condition at the bulk-melt/wall interface (Eq. 5.1.1.6) is satisfied without changing the internal energy content of the wall thermal layer.

Flux Matching Condition at the Bulk-Melt/Wall Interface

$$T_c' - T_w^o = \frac{h\delta_w'}{h\delta_w' + k} (T_b - T_w^o) \qquad 3$$

Wall Energy Conservation at Time of Remelt

$$\int_0^{-\delta_w} (T_w(x,t) - T_w^o)\, dx = \int_0^{-\delta_w'} (T_w'(x,t) - T_w^o)\, dx \qquad 4$$

Substituting for the old and new temperature profiles as given by Eqs. (1) and (2) the energy conservation relation simplies to

$$T_c' - T_w^o = \frac{\delta_w}{\delta_w'} (T_m - T_{wo}) \qquad 5$$

The flux matching condition (Eq. 3) and energy conservation condition (Eq. 4) are then solved simultaneously to yield an expression for the new wall thermal layer thickness.

$$\delta_w' = \frac{h\delta_w + \left[h^2\delta_w^2 + 4hk\delta_w \frac{T_{wb} - T_w^o}{T_m - T_w^o}\right]^{1/2}}{2h \frac{T_{wb} - T_w^o}{T_m - T_w^o}} \qquad 6$$

The new contact temperature is obtained directly from Eq. 3.

5.3.2 Crust Remelt - Slit Geometry, Finite-Thickness Wall

Just prior to crust remelt, the temperature distribution in the wall is given by

$$\frac{T_w(x,t) - T_{wb}(t)}{T_m - T_{wb}(t)} = \beta_w(t) \left[\frac{x + D_w}{D_w}\right] + \left[1 - \beta_w(t)\right] \left[\frac{x + D_w}{D_w}\right]^2. \qquad 1$$

This temperature distribution satisfies the flux matching condition at the crust/wall interface (Eq. 5.1.7.12).

Just after crust remelt, the temperature distribution is given by

$$\frac{T'_w(x,t) - T'_{wb}(t)}{T'_c(t) - T'_{wb}(t)} = \beta'_w(t) \left[\frac{x + D_w}{D_w} \right] + \left[1 - \beta'_w(t) \right] \left[\frac{x + D_w}{D_w} \right]^2 . \quad (2)$$

The new values T'_{wb}, T'_c, and β'_w are determined such that the new flux matching conditions at the bulk-melt/wall interface (Eq. 5.1.2.5) and at the wall/external-coolant interface (Eq. 5.1.2.6) are satisfied without changing the internal energy content of the wall thermal layer.

Flux Matching at the Bulk-Melt/Wall Interface

$$T'_c = \frac{k_w(2 - \beta'_w)\, T'_{wb} + hD_w\, T_b}{k_w(2 - \beta'_w) + hD_w} \quad (3)$$

Flux Matching at the Wall/External-Coolant Interface

$$\beta'_w = \frac{h_w D_w}{k_w} \frac{T'_{wb} - T^o_w}{T'_c - T'_{wb}} \quad (4)$$

Wall Energy Conservation at Time of Remelt

$$\int_0^{-D_w} (T_w(x,t) - T_w^o)\, dx = \int_0^{-D_w} (T'_w(x,t) - T_w^o)\, dx \qquad 5$$

Substituting for the old and new temperature profiles as given by Eqs. 1 and 2, the energy conservation relation simplifies to

$$T'_{wb} = \frac{\frac{2+\beta'_w}{6} + \left[\frac{2+\beta_w}{6} - 1\right] T_{wb} - \frac{2+\beta_w}{6} T_c}{\frac{2+\beta_w}{6} - 1} \qquad 6$$

The flux matching conditions (Eqs. 3 and 4) and simplified energy conservation equation (Eq. 5) are then solved iteratively to yield new values for T'_c, β'_w, and T'_{wb}.

5.3.3 Crust Remelt - Cylindrical Geometry, Infinitely-Thick Wall

Just prior to crust remelt, the temperature distribution in the wall is given by

$$\frac{T_w(r,t) - T_w^o}{T_m - T_w^o} = \left[1 - \frac{\ln(r/R_o)}{\ln x_{\delta w}} \right]^2 . \qquad 1$$

where,

$$x_{\delta w} = R_{\delta w}/R_o \qquad 2$$

This temperature distribution satisfies the flux matching condition at the crust/wall interface (see Eq. 5.1.7.12).

Just after crust remelt, the temperature distribution is given by

$$\frac{T'_w(r,t) - T^o_w}{T'_c(t) - T^o_w} = \left[1 - \frac{\ln(r/R_o)}{\ln x'_{\delta w}} \right]^2 . \qquad 3$$

where,

$$x'_{\delta w} = R'_{\delta w}/R_o \qquad 4$$

The new values T'_c and x'_γ are determined such that the new flux matching condition at the bulk-melt/wall interface (Eq. 5.1.5.6) is satisfied without changing the internal energy content of the wall thermal layer.

Flux Matching Condition at the Wall/Bulk Melt Interface

$$T'_c - T^o_w = \frac{hR_o \ln x'_\delta}{k + hR_o \ln x'_\delta} (T_b - T^o_w) \qquad 5$$

Wall Energy Conservation at the Time of Remelt

$$\int_{R_o}^{R_{\delta w}} (T_w(r,t) - T^o_w) r dr = \int_{R_o}^{R'_{\delta w}} (T'_w(r,t) - T^o_w) r dr \qquad 6$$

Substituting for the old and new temperature profiles as given by Eqs. 1 and 2, the energy conservation relation simplies to

$$(T_m - T^o_w) \left[1 + \frac{1}{\ln x_{\delta w}} + \frac{1 - x_{\delta w}^2}{2(\ln x_{\delta w})^2} \right] =$$

$$(T_c' - T_w^o)\left[1 + \frac{1}{\ln x_{\delta w}'} + \frac{1 - x_{\delta w}'^2}{2(\ln x_{\delta w}')^2}\right] \qquad 7$$

The flux matching condition (Eq. 5) and energy conservation condition (Eq. 7) are then solved iteratively to yield the new values for T_c' and $x_{\delta w}'$.

5.3.4 Crust Remelt - Cylindrical Geometry, Finite-Thickness Wall

Just prior to crust remelt, the temperature distribution in the wall is given by

$$\frac{T_w(r,t) - T_{wb}(t)}{T_m - T_{wb}(t)} = \beta_w(t)\left[1 - \frac{\ln(r/R_o)}{\ln(R_D/R_o)}\right] \qquad 1$$

$$+ \left[1 - \beta_w(t)\right]\left[1 - \frac{\ln(r/R_o)}{\ln(R_D/R_o)}\right]^2 .$$

This temperature distribution satisfies the flux matching condition at the crust/wall interface (Eq. 5.1.8.11).

Just after crust remelt, the temperature distribution is given by

$$\frac{T_w'(r,t) - T_{wb}'(t)}{T_c'(t) - T_{wb}'(t)} = \beta_w'(t)\left[1 - \frac{\ln(r/R_o)}{\ln(R_D/R_o)}\right]$$

$$+ \left[(1 - \beta_w'(t)\right]\left[1 - \frac{\ln(r/R_o)}{\ln(R_D/R_o)}\right]^2 . \qquad 2$$

The new values T_c', T_{wb}', and β_w' are determined such that the new flux matching conditions at the bulk-melt/wall interface

(Eq. 5.1.6.5) and at the wall/external-coolant interface (Eq. 5.1.6.6) are satisfied without changing the internal energy content of the wall thermal layer.

Flux Matching at the Bulk-Melt/Wall Interface

$$T_c' = \frac{hR_o \ln x_w \, T_b + k_w(2 - \beta_w') \, T_{wb}'}{hR_o \ln x_w + k_w(2 - \beta_w')} \qquad 3$$

Flux Matching at the Wall/External-Coolant Interface

$$\beta_w' = \frac{h_w R_o x_w}{k_w} \ln x_w \, \frac{T_w^o - T_{wb}'}{T_{wb}' - T_c'} \qquad 4$$

Wall Energy Conservation at the Time of Remelt

$$\int_{R_o}^{R_w} (T_w(r,t) - T_w^o) \, r \, dr = \int_{R_o}^{R_w} (T_w'(r,t) - T_w^o) \, r \, dr \qquad 5$$

Substituting for the old and new temperature profiles as given by Eqs. 1 and 2, the energy conservation relation simplifies to

$$T_{wb}' = \frac{-T_c' A_2' + T_c A_2 + T_{wb}(A_1 - A_2)}{A_1 - A_2')} \qquad 6$$

where,

$$A_1 = \frac{x_w^2 - 1}{2} \qquad 7$$

$$A_2 = \beta_w A_3 + (1 - \beta_w) A_4 \qquad 8$$

$$A_2' = \beta_w' A_3 + (1 - \beta_w') A_4 \qquad 9$$

$$A_3 = \frac{x_w^2 - 1}{2} \frac{\ln x_w - 1}{\ln x_w} \qquad 10$$

$$A_4 = \frac{6x_w^2 \ln x_w - 7x_w^2 + 7}{8 \ln x_w} \qquad 11$$

The flux matching conditions (Eqs. 3 and 4) and the simplified energy conservation equation (Eqs. 6 through 11) are then solved iteratively to yield new values for T_c', β_w', and T_{wb}'.

6.0 Conclusions

The PLUGM code as described in this report is unique in its ability to model the conduction-limited freezing and plugging of melt-flow in a nonmelting channel, accounting for all relevant driving forces and pressure losses. Thus, PLUGM fully treats the problems associated with ex-vessel core retention assessment, because these core-retention devices (bricks or particle beds) are made of high melt-temperature oxides that typically do not melt when contacted with molten corium. Further, PLUGM is currently suited for the analysis of many LMFBR transition-phase problems that involve low enough steel wall temperatures such that steel melting would not occur.

PLUGM offers a sound basis on which a new code will be developed that addresses specific needs of the LMFBR transition-phase problem: wall melting in particular. Three major additions are required to handle wall melting problems:

- crust growth/wall heatup solutions that account for wall melting
- crust and wall-melt stability/entrainment criteria
- hydrodynamics treatment that considers bulk-melt mixtures (original melt, crust, wall melt) that may vary as a function of time and axial location.

Sample problems from the areas of core retention and LMFBR transition phase are presented in Appendices B, C, and D. PLUGM's capabilities are exercised for each of the three available geometry options: tube, thin slit, and particle bed. The sample problems demonstrate PLUGM's versatility in answereing reactor safety questions involving the flow and freezing of molten materials.

References

1. Babcock and Wilcox, Steam, its Generation and Use, 38th Edition, Babcock and Wilcox, (1972).

2. L. Baker, Jr., R. E. Faw, and F. A. Kulacki, "Postaccident Heat Removal - Part I: Heat Transfer within an Internally Heated Nonboiling Liquid Layer," Nucl. Sci. Eng., 61, 222 (1976).

3. L. Baker, Jr., F. B. Cheung, and J. D. Bingle, "Growth of Internally-Heated Core Debris Pools Into Soluble and Insoluble Structures," European Applied Research Reports, 1(6), 211, (1979).

4. L. Baker et al, "Thermal Interaction of Molten Core Debris Pool with Surrounding Structural Materials," Proc. Int. Meeting on Fast Reactor Safety, Seattle, Wash., Vol. 1, (Aug. 19-23, 1979).

5. T. Baumeister, E. A. Avallone, and T. Baumeister, III, Marks' Standard Handbook for Mechanical Engineers, 8th Edition, McGraw-Hill, (1978).

6. R. B. Bird, W. E. Stewart, and E. N. Lightfoot, Transport Phenomena, John Wiley and Sons, (1960).

7. Hans K. Fauske, W. D. Ford, and Michael A. Grolmes, "Liquid Film Thickness for Slug Ejection," Trans. Am. Nuc. Soc. 13, 646, (1970).

8. J. D. Fish, M. Pilch, and F. E. Arellano, "Demonstration of Passively-Cooled Particle-Bed Core Retention," Proceedings of International Topical Meeting on Liquid Metal Fast Breeder Reactor Safety and Related Design and Operational Aspects, Lyon, France, July 19-23, 1982.

9. J. D. Fish, M. Pilch, and F. E. Arellano, "Particle-Bed Core Retention Concept: Preliminary Assessment," SAND82-2545, To Be Published.

10. R. D. Gasser and W. T. Pratt, "Thermal Response of a Molten Pool with Stefan Type Boundary Conditions," ASME Paper 80-HT-9, presented at Joint ASME/AICHE National Heat Transfer Conference, Orlando, Florida (July 27-30, 1980).

11. Michael A. Grolmes, George A. Lambert, and Hans K. Fauske, "Liquid Film Thickness for Single-Bubble Slug Ejection," Trans. Am. Nuc. Soc. 14, 242 (1971).

12. J. E. A. John and W. Haberman, Introduction To Fluid Mechanics, Prentice-Hall, (1971).

13. D. A. McArthur, N. K. Hayden, and P. K. Mast, "In-Core Fuel Freezing and Plugging Experiments: Preliminary Results of the Sandia TRAN Series I Experiments," SAND81-1726, (to be published).

14. Offshore Power Systems, "FNP Core Ladle Design and Safety Evaluation," Topical Report No. 36A59, April 1979.

15. H. J. Reilly, et al, "Conceptual Design of a Core Melt Mitigation System for a PWR with an Ice-Condenser Containment," EGG-PR-5633, February 1982.

16. S. K. Rhow, et al., "An Assessment of HCDA Energetics in the CRBRP Heterogeneous Reactor Core," CRBRP-GEFR-00523, General Electric Company, (Dec. 1981).

17. W. M. Rohsenow and J. P. Hartnett, Handbook of Heat Transfer, McGraw-Hill, (1973).

18. D. G. Swanson and I. Catton, "Core Melt Materials Interactions Evaluations," First Annual Progress Report Contract No. NRC-03-80-104, ASAI-81-001, March 1981.

19. D. G. Swanson, I. Catton, V. K. Dhir, and A. R. Marchese, "A Thoria Rubble Bed for Post Accident Core Retention," Proceedings of the Fifth Post Accident Heat Removal Information Exchange Meeting, Nuclear Research Centere Karlsruhe, July 28-30, 1982.

20. Graham B. Wallis, One Dimensional Two-Phase Flow, McGraw-Hill, (1969).

21. Westinghouse Electric Corporation, "Ex-vessel Core Catcher Concept Evaluation Report, "WARD-D-0103, October 1975.

22. Stephen Whitaker, "Forced Convection Heat Transfer Correlations for Flow in Pipes, Past Flat Plates, Single Cylinders, Single Spheres, and for Flow in Packed Beds and Tube Bundles," AIChe J., 18(2), 261-371, (March 1972).

Appendix A - PLUGM Input Description

```
C**********************************************************************
C**** PROBLEM SETUP ***************************************************
C
C     LINE 1 (10A8) TITLE
C          TITLE: ALPHA NUMERIC PROBLEM DESCRIPTION
C
C     LINE 2 (6I12) IGEOM,NREG,IRESOP,IDMPOP,IHTOP,IVELOP
C          IGEOM: 1 THIN SLIT GEOMETRY
C                 2 TUBE GEOMETRY (INTERNAL FLOW)
C                 3 TUBE GEOMETRY (EXTERNAL FLOW)
C                 4 PARTICLE BED
C                 NOTE: LOGIC EXISTS FOR OPTION 3, HOWEVER, NO
C                       WORKING EQUATIONS CURRENTLY EXIST IN
C                       THE CODE
C          NREG: NUMBER OF REGIONS FOR WHICH ALL CHANNEL PARAMETERS
C                ARE CONSTANT. EACH REGION CONSISTS OF ONE OR MORE
C                NODES
C          IRESOP: 0 RIGID BOUNDARY RESERVOIR - TREAT AS CHANNEL
C                  1 POOL TYPE RESERVOIR WITH NO FIXED BOUNDARIES
C                    - NO FRICTION LOSSES
C                    - NO HEAT TRANSFER TO BOUNDARY
C                  2 POOL TYPE RESERVOIR AS IN OPTION (1) - NO MASS
C                    ADDITION OR DEPLETION CALCULATED FOR THIS OPTION
C          IDMPOP: 0 RIGID BOUNDARY CATCH TANK - TREAT AS CHANNEL
C                  1 POOL TYPE CATCH TANK WITH NO FIXED BOUNDARIES
C                    - NO FRICTION LOSSES
C                    - NO HEAT TRANSFER TO BOUNDARY
C                  2 TREAT LAST DEFINED NODE AS CATCH TANK WITH
C                    - NO FRICTION LOSSES
C                    - NO HEAT TRANSFER
C                    - NO AREA-CHANGE LOSSES (SQUIRTS OUT CHANNEL)
C          IHTOP:  0 HYDRODYNAMIC CALCULATIONS ONLY
C                  1 FULLY COUPLED THERMAL HYDRAULIC CALCULATIONS
C          IVELOP: 0 TRANSIENT CALCULATION WITH INERTIAL EFFECTS
C                    - INITIAL VELOCITY OF ZERO
C                  1 TRANSIENT VELOCITY WITH INERTIAL EFFECTS
C                    - INITIAL VELOCITY QUASI-STEADY-STATE
C                  2 QUASI-STEADY VELOCITY USED THROUGHOUT
C
C     LINE 3 (I6) NPSTEP
C          NPSTEP: OUTPUT RESULTS EVERY NPSTEP*DLTMAX SECONDS
C                  - 0 FOR THIS PARAMETER PRODUCES INITIAL-CONDITIONS
C                      SUMMARY AND FINAL TIME-STEP SUMMARY FOR EACH NODE
C          IFILMOP: 0 NO FILM DEPOSITION
C                   1 FILM DEPOSITION
C                   2 FILM DEPOSITION ENHANCED BY RAYLEIGH-TAYLOR
C                     INSTABILITY
C
C     LINE 4 (6E12.6) DLTMIN,DLTMAX, DZMIN , PENMAX , TFIN
```

```
C          DLTMIN: MINIMUM TIME STEP ALLOWED FOR USE IN THE CRUST GROWTH
C                  SOLUTION
C          DLTMAX: MAXIMUM TIME STEP ALLOWED FOR USE IN THE CRUST GROWTH
C                  SOLUTION
C          DZMIN: THE CALCULATIONS END WHEN THE TOTAL LENGTH OF THE
C                 MELT SLUG IS LESS THAN OR EQUAL TO DZMIN
C          PENMAX: MAXIMUM PENETRATION LENGTH STOPPING CRITERION
C          TFIN:   TOTAL TIME STOPPING CRITERION
C
C***** GEOMETRY AND INITIAL CONDITIONS **********************************
C
C     FOR I=1 TO NREG
C
C     LINE 5.I (6I12) ZLEN,NODES,IGDEX
C          ZLEN: LENGTH OF REGION I
C          NODES: NUMBER OF NODES IN REGION I
C          IGDEX: FLOW DIRECTION FOR REGION I
C                  1 DOWN (WITH GRAVITY)
C                  0 HORIZONTAL (NORMAL TO GRAVITY)
C                 -1 UP (AGAINST GRAVITY)
C
C     LINE 6.I (6E12.6) DCHANL,WCHANL,TBLK,DWLL,TWALL,HCOOLN
C          DCHANL: CHARACTERISTIC CHANNEL DIMENSION FOR REGION I
C                  FOR IGEOM=1, SLIT SPACING
C                      IGEOM=2, TUBE DIAMETER
C                      IGEOM=3, FLOW CHANNEL HYDRAULIC DIAMETER
C                      IGEOM=4, PARTICLE BED HYDRAULIC DIAMETER
C          WCHANL: 2ND CHARACTERISTIC CHANNEL DIMENSION FOR REGION I
C                  FOR IGEOM=1, SLIT WIDTH
C                      IGEOM=2, (LEAVE BLANK)
C                      IGEOM=3, (LEAVE BLANK)
C                      IGEOM=4, (LEAVE BLANK)
C          TBLK: MELT BULK TEMPERATURE FOR REGION I. A ZERO VALUE
C                INDICATES THAT NO MELT EXISTS IN THAT REGION AT THE
C                START OF THE PROBLEM.
C          DWLL: WALL THICKNESS FOR REGION I
C                LEAVE BLANK IF POOL TYPE RESERVOIR (IRESOP=1,2)
C          TWALL: INITIAL WALL TEMPERATURE FOR REGION I
C                 LEAVE BLANK IF POOL TYPE RESERVOIR (IRESOP=1,2)
C          HCOOLN: WALL-TO-EXTERNAL-COOLANT HEAT TRANSFER COEFFICIENT
C                  LEAVE BLANK IF POOL TYPE RESERVOIR (IRESOP=1,2)
C
C     NEXT I
C
C***** BOUNDARY CONDITIONS - DELTA P ************************************
C
C     LINE 7 (6E12.6) PTRAIL, PLEAD
C          PTRAIL: APPLIED PRESSURE ON TRAILING EDGE OF MELT SLUG
C          PLEAD: APPLIED PRESSURE ON LEADING EDGE OF MELT SLUG
C
C***** BOUNDARY CONDITIONS - MASS ADDITION ******************************
C
```

```
C     LINE 8 (6E12.6) XMDOT, TCUT
C          XMDOT: CONSTANT MASS ADDITION FLUX INTO TRAILING EDGE NODE
C          TCUT: MASS IS ADDED TO TRAILING EDGE NODE FROM
C                TIME=0.0 TO TIME=TCUT
C
C**** MATERIAL PROPERTIES ***********************************************
C
C     LINE 9 (6E12.6) K, RHO, CP
C          K: BULK MELT THERMAL CONDUCTIVITY
C          RHO: BULK MELT DENSITY
C          CP: BULK MELT SPECIFIC HEAT
C
C     LINE 10 (6E12.6) TBMELT, HFB, VISCB, SIGB
C          TBMELT: BULK MELT FUSION TEMPERATURE
C          HFB: BULK MELT HEAT OF FUSION
C          VISCB: BULK MELT DYNAMIC VISCOSITY (MU)
C          SIGB: BULK MELT SURFACE TENSION
C                - USE A POSITIVE VALUE FOR WETTING FLUIDS
C                  AND A NEGATIVE VALUE FOR NONWETTING FLUIDS
C
C     LINE 11 (6E12.6) KC, RHOC, CPC
C          KC: CRUST THERMAL CONDUCTIVITY
C          RHOC: CRUST DENSITY
C          CPC: CRUST SPECIFIC HEAT
C
C     LINE 12 (6E12.6) KWM, RHOWM, CPWM
C          KWM: WALL MELT THERMAL CONDUCTIVITY
C          RHOWM: WALL MELT DENSITY
C          CPWM: WALL MELT SPECIFIC HEAT
C
C     LINE 13 (6E12.6) TWMELT, HFW, VISCW, SIGW
C          TWMELT: WALL MELT FUSION TEMPERATURE
C          HFW: WALL MELT HEAT OF FUSION
C          VISCW: WALL MELT DYNAMIC VISCOSITY (MU)
C          SIGW: WALL MELT SURFACE TENSION
C                - USE A POSITIVE VALUE FOR WETTING FLUIDS
C                  AND A NEGATIVE VALUE FOR NONWETTING FLUIDS
C               NOTE: HFW, VISCW, AND SIGW ARE NOT CURRENTLY USED
C                     IN THE CODE
C
C     LINE 14 (6E12.6) KW, RHOW, CPW
C          KW: WALL THERMAL CONDUCTIVITY
C          RHOW: WALL DENSITY
C          CPW: WALL SPECIFIC HEAT
C
C***********************************************************************
C***********************************************************************
```

Appendix B. Particle-Bed Core Retention

Three sample problems illustrate how PLUGM can be applied to particle-bed problems. First, design features of a particle-bed core retention device are illustrated. Second, surface tension effects are demonstrated when molten steel is poured onto an alumina bed. The third problem demonstrates that plugging cannot always be expected in a particle bed.

These sample problems exercise the use of the following code options and input parameters:

1. particle-bed geometry,
2. time-dependent gravity head associated with a pour onto the particle bed,
3. gravity-driven, inertia-limited initial acceleration of melt into the bed,
4. surface tension for wetting and nonwetting fluids, and
5. change in channel diameter.

B.1 Design Features of A Particle Bed Core Retention Device

Consider a core retention device that is composed of .02 m diameter alumina particles; bed porosity is 40%. Section 2.4 show how to characterize particle bed geometry for code input: for the reservoir D_h(res) = DCHANL = 1.405E-2, and for the particle bed D_h = DCHANL = 8.889E-3, DWLL = 2.583E-3.

Molten core debris is ejected from the reactor vessel in 4 s (reactor transient accident); this debris would fill the cavity to a depth of .33 m if melt did not flow into the particle bed (XMDOT = $\rho_b dh/dt$ = 5.775E2, TCUT = 4); however, melt flows under gravity the instant it contacts the particle bed. The unit cell over a typical flow channel into the bed is represented as a pool type reservoir (IRESOP =1). A transient inertia-limited hydrodynamics calculation has been specified (IVELOPP =0). The particles are initially at room temperature (TWALL = 300), and the molten debris is either saturated (TBLK = 2225) or superheated by 200K (TBLK = 2425).

How far does the melt penetrate? Table B.1 shows the input file for this problem. PLUGM predicts that molten core debris will penetrate .346 m for the saturated melt and .486 m for the superheated melt.

Table B.1 - Listing of Input File for the Single Sized Particle Problem

```
CORIUM MELT ON  ALUMINA PARTICLES
          4           2           1           0           1           0
          0           1
      1.0E-3      1.0E-2       .0001         .99         15.
       .010           1           1
   1.405E-2                    2425.
        1.0         100           1
   8.889E-3                     0.0   2.583E-3         300.      1.0E-6
          0           0.0
   5.775E2           4.0
       11.0        7000.        485.
       2225.      2.08E5    4.34E-3          .5
        2.31        7070.        402.

       3098.
       8.90        4000.        1213.
```

The actual depth of a particle bed must exceed the expected melt penetration so that pathways necessary for bottom cooling of the bed are assured. A particle bed composed of single size particles represents an impractical design because the required particle bed depth may be too great for the available room in the reactor cavity. Smaller size particles would partially alleviate this problem, but small particles can impede the supply of water necessary for bottom cooling of the debris. An effective solution to this problem is to consider a stratified particle bed.

Consider now the design of a stratified particle bed that is [illegible] m deep. The top .25 m of the bed and the bottom .20 m of the bed are composed of .02 m diameter particle while the .05 m thick middle layer is composed of small particles. The stratified bed is modeled as a four region problem in PLUGM (NREG =4): reservoir, top channel region (ZLEN = .25), middle channel region (ZLEN = .05), bottom channel region (ZLEN = .20). The molten debris has 200K of superheat.

How small should the middle layer particles be in order to control melt penetration into the bed? Table B.2 shows the input file for this stratified bed problem. Figure B.1 shows the expected penetration of melt into the particle bed as a function of middle-layer particle size. As expected, large particles in

Table B.2 - Listing of Input File for Stratified Particle Bed Problem

```
CORIUM MELT ON STRATIFIED BED OF ALUMINA PARTICLES
          4           4           1           0           1           0
          0           1
    1.0E-3      1.0E-2       .0001         .99         15.
       .010           1           1
  1.405E-2                    2425.
       .25          15           1
  8.889E-3                     0.0    2.583E-3        300.      1.0E-6
       .05          20           1
  1.111E-3                     0.0    3.229E-4        300.      1.0E-6
       .20          20           1
  8.889E-3                     0.0    2.583E-3        300.      1.0E-6
        0.0         0.0
     5.775E2        4.0
       11.0        7000.       485.
      2225.      2.08E5    4.34E-3          .5
       2.31        7070.       402.

      3098.
       8.90        4000.      1213.
```

the middle layer enable the melt to approach the concrete basemat; in which case, the device has failed its appointed task.

At the other extreme, small particles (D_p < 5 mm) are very effective at stopping the melt. This comes about by three processes. First, melt flows very slowly through a packed bed composed of small particles because of increased friction. A slower penetration rate translates into more time for melt to freeze while negotiating the same incremental penetration. Lastly, small particles means small flow channels, which are more quickly plugged. For these reasons, a thin layer of small particles is a simple and effective way of controlling the initial penetration of molten core debris into a particle-bed core-retention device.

B.2 Surface Tension

Several particle bed experiments at Sandia were performed using steel melts instead of corium melts. Consider an experiment using a saturated steel melt (1700 K) and a particle bed composed of single sized .01 m diameter alumina particles. All other aspects are the same as the first part of the previous problem. Table B.3 shows the input file.

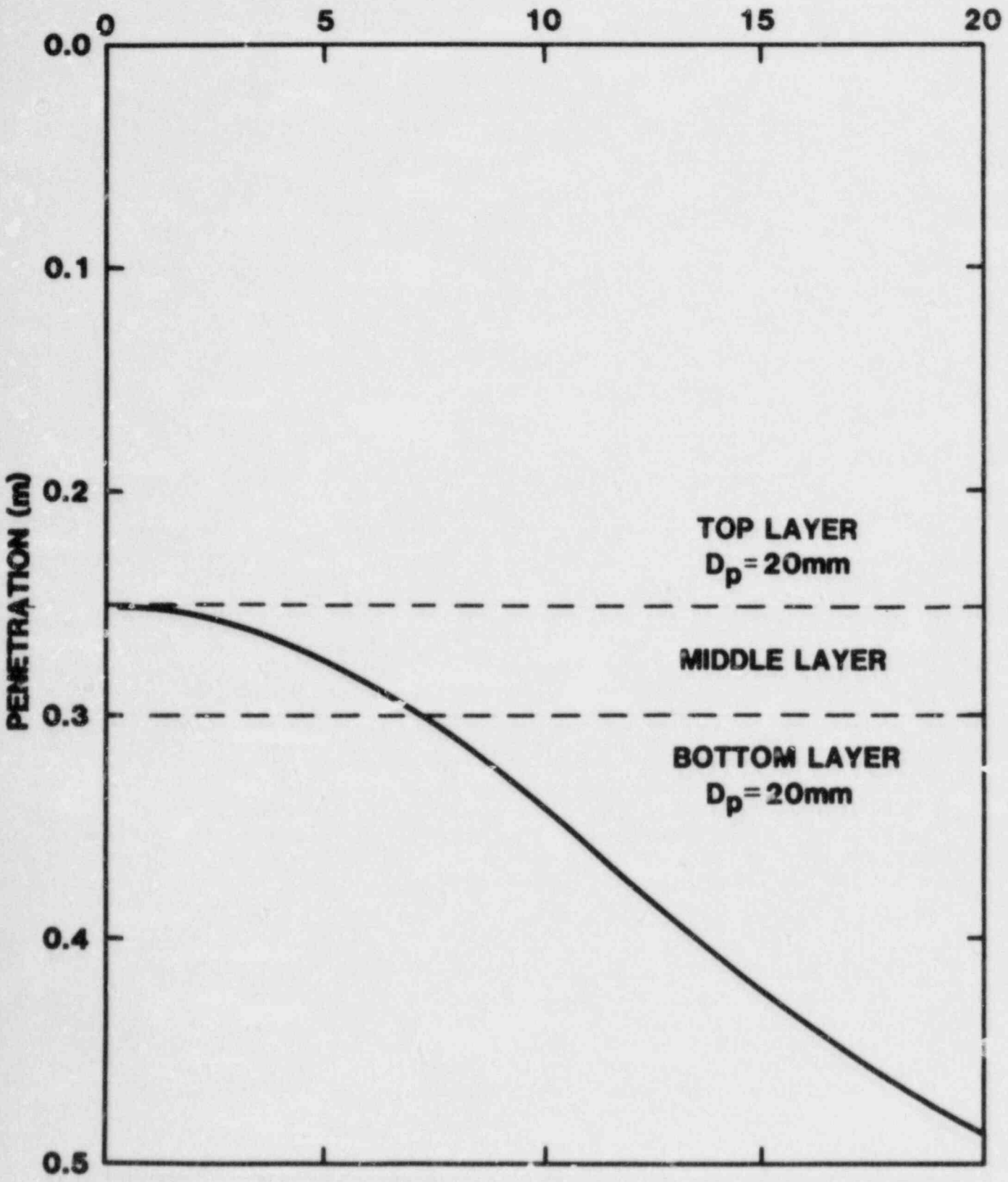

Figure B.1 Stratified Particle Bed

Table B.3 - Listing of Input File for Problem Illustrating Surface Tension Effects

```
STEEL MELT ON ALUMINA PARTICLE BED
        4          2          1          0          1          0
        0          1
   1.0E-4     1.0E-2      .0001       .19         3.
     .001          1          1
 7.026E-3                 1700.
      .20         25          1
 4.444E-3                    0.0  1.291E-3      1375.     1.0E-6
      0.0        0.0
 5.775E2        4.0
     18.0       7000.       776.
    1700.     2.70E5    6.42E-3       -1.7
     25.0       7624.       396.

    2345.
     8.90       4000.       1213.
```

Figure B.2 shows the penetration history for this problem. Note that there is a delay of .27 s before melt penetration into the particle bed begins. This occurs because molten steel does not wet alumina particles, and a period of time must elapse before sufficient melt head (.0224 m) can accumulate during the pour to overcome the surface tension (SIGB = -1.7) resistance to flow into the be Surface tension must then be considered when interpreting experiment results obtained from steel melts because surface tension influences the gravity head during melt flow, which in turn affects the rate and extent of melt penetration.

B.3 Plugging is Not Always Possible

Flow channels involving finite-thickness walls, such as a particle bed, do not necessarily plug. Figure B.3 shows how the initial temperature of particles influences melt penetration for the steel melt problem just discussed. Clearly, there is an initial particle temperature at which plugging will not occur.

For some wall temperatures, code calculations show that the particles and solidified crust can come to thermal equilibrium at the fusion temperature of the melt before the channel is completely plugged. In short, the particles do not have sufficient heat capacity to accommodate the heat of fusion that

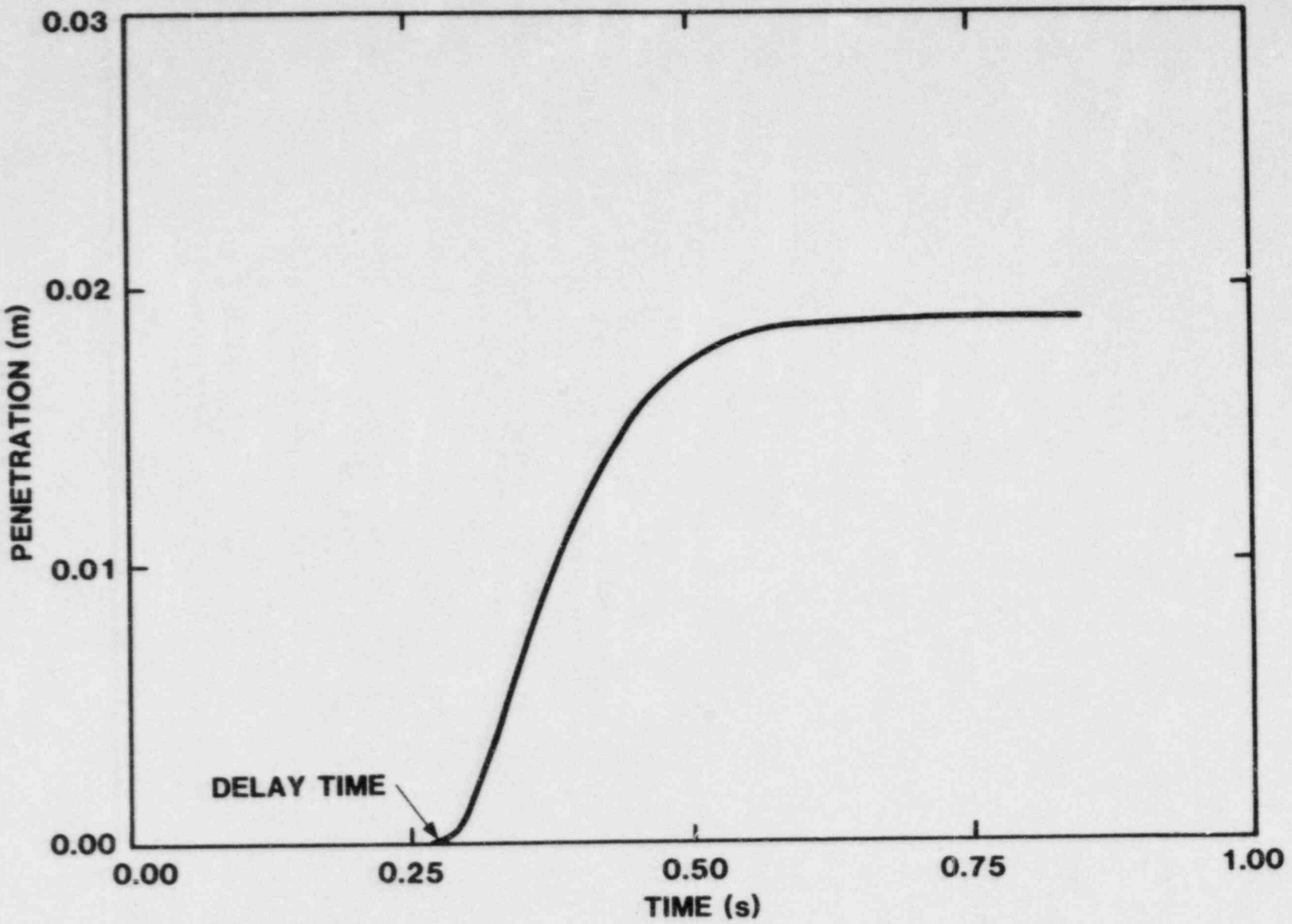

Figure B.2 Melt Penetration Can Be Influenced by Surface Tension

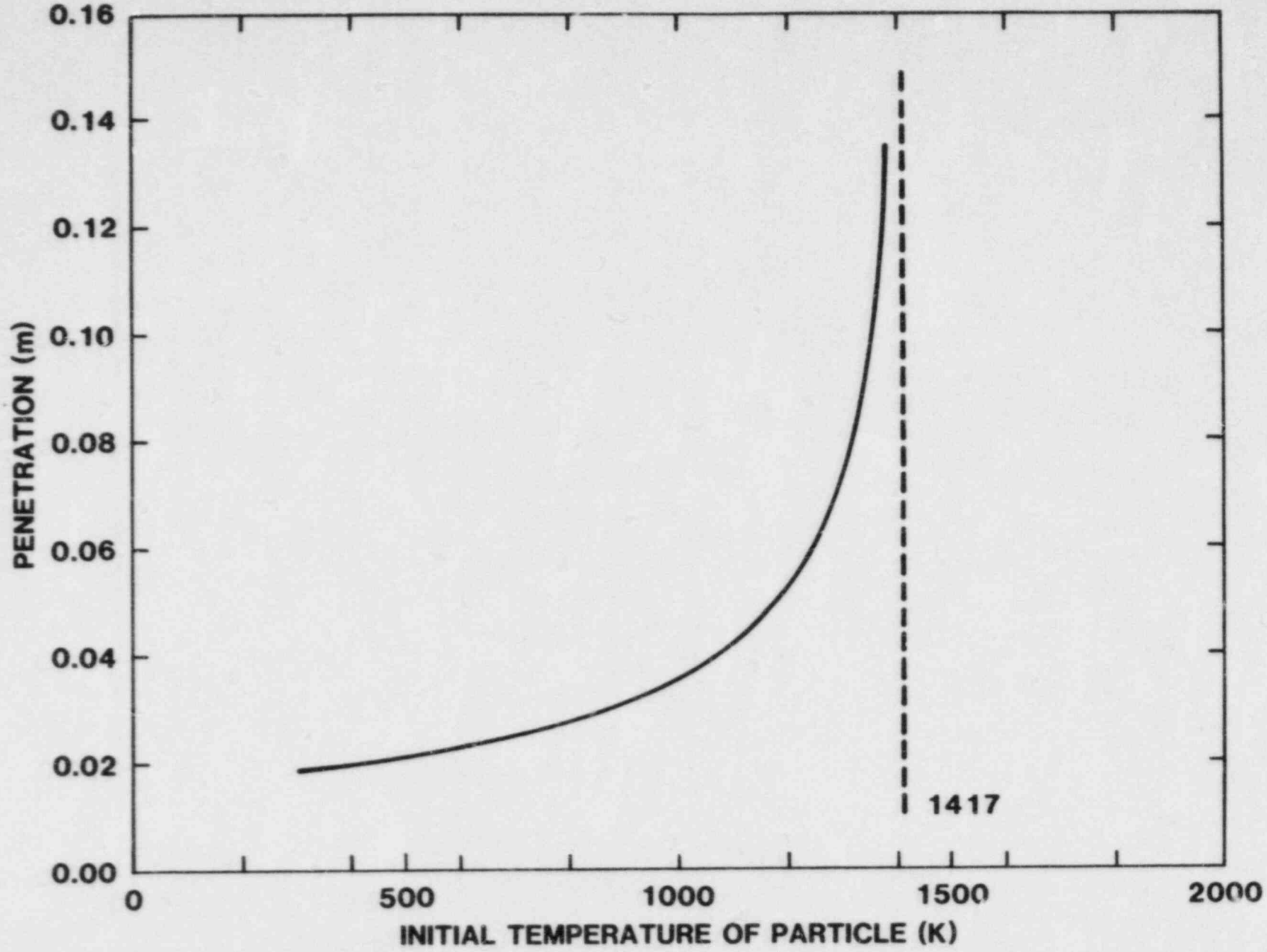

Figure B.3 Melt Does Not Always Plug in a Particle Bed

must be stripped from the melt if the channel is to be completely plugged. This occurs when the wall temperature exceeds 1417 K for the sample problem discussed here.

Appendix C. Refractory-Brick Crucible Core Retention

Two sample problems illustrate how PLUGM can be used in the assessment of core retention devices composed of refractory bricks. First, melt flow and freezing in long vertical cracks is investigated. Second, the influence of flow direction changes associated with the tortuous flow paths of a brick matrix is studied.

These sample problems exercise the use of the following code options and input parameters:

1. thin-slit geometry,
2. time-dependent gravity head associated with a pour onto the bricks,
3. gravity-driven quasi-steady flow of melt into the cracks, and
4. changes in flow direction.

C.1 Vertical Crack

PLUGM is used to investigate melt seepage into a long, thin vertical crack in a refractory brick crucible. Such a crack might be formed by thermal or mechanical stresses when the melt falls onto the core retention device. The crucible is composed of Harklase bricks with the following dimensions: A = 13.5 in. (.3429 m), B = 3 in. (.0762 m), and C = 6 in. (.1524 m). Molten core debris is ejected from the reactor vessel in 4s (reactor transient accident), this debris would fill the cavity to a depth of .33 m if the melt did not flow into the crack, however, melt flows under gravity the instant it contacts the bricks. A pool type reservoir is still specified (IRESOP = 1), but here a quasi steady initial velocity is used followed by an inertia limited transient hydrodynamics calculation (IVELOP = 2). The bricks are initially at room temperature, and the molten debris either is saturated or has 200 K of superheat.

How far does the melt penetrate? Table C.1 shows the input file for this problem. Predicted penetrations as a function of crack spacing and melt superheat are shown in Figure C.1 , which shows that melt penetration into a crack is a sensitive function of both crack spacing and melt superheat. PLUGM predicts that the initial constriction occurs at that point in the channel where all superheat is stripped from the bulk melt. This is at the channel entrance for a saturated melt and progressively further downstream for increasing melt superheats.

Table C.1 - Listing of Input File for Corium Flow in a Vertical Crack

```
CORIUM MELT ON HARKLASE BRICKS - VERTICLE CRACK
         1           2           1           0           1           1
         0           1
   1.0E-5      1.0E-3      .0001         1.0         5.0
      .001           1           1
 7.620E-2    3.429E-1      2225.
       .50         250           1
 .5000E-3    3.429E-1         0.0    3.810E-3        300.      1.0E-6
       0.0         0.0
    5.775E2         4.0
       11.0        7000.        485.
      2225.      2.08E5    4.34E-3          .5
       2.31        7070.        402.

      3098.
       7.92        2760.        1265.
```

C.2 Brick Matrix

Consider now the more complicated problem of melt flow in a brick stack where the interbrick gap is everywhere the same. Melt flows down the face of one brick across its bottom, and then flows down the face of another brick. Table C.2 shows the input file for this problem.

Figure C.2 shows the predicted penetration depth as a function of interbrick gap. Three features distinguish this problem from the previous one. First, pressure losses due to sudden changes in flow direction impede flow into the brick stack. Secondly, an increment of melt flow along a horizontal brick surface does not result in an increment in total gravity head; this also results in less flow. Thirdly, horizontal flow does not contribute to an increase in actual depth of penetration. This last point is represented by horizontal segments in Figure C.2. Clearly, melt flow through a brick stack is more constrained than melt flow through a straight, vertical crack.

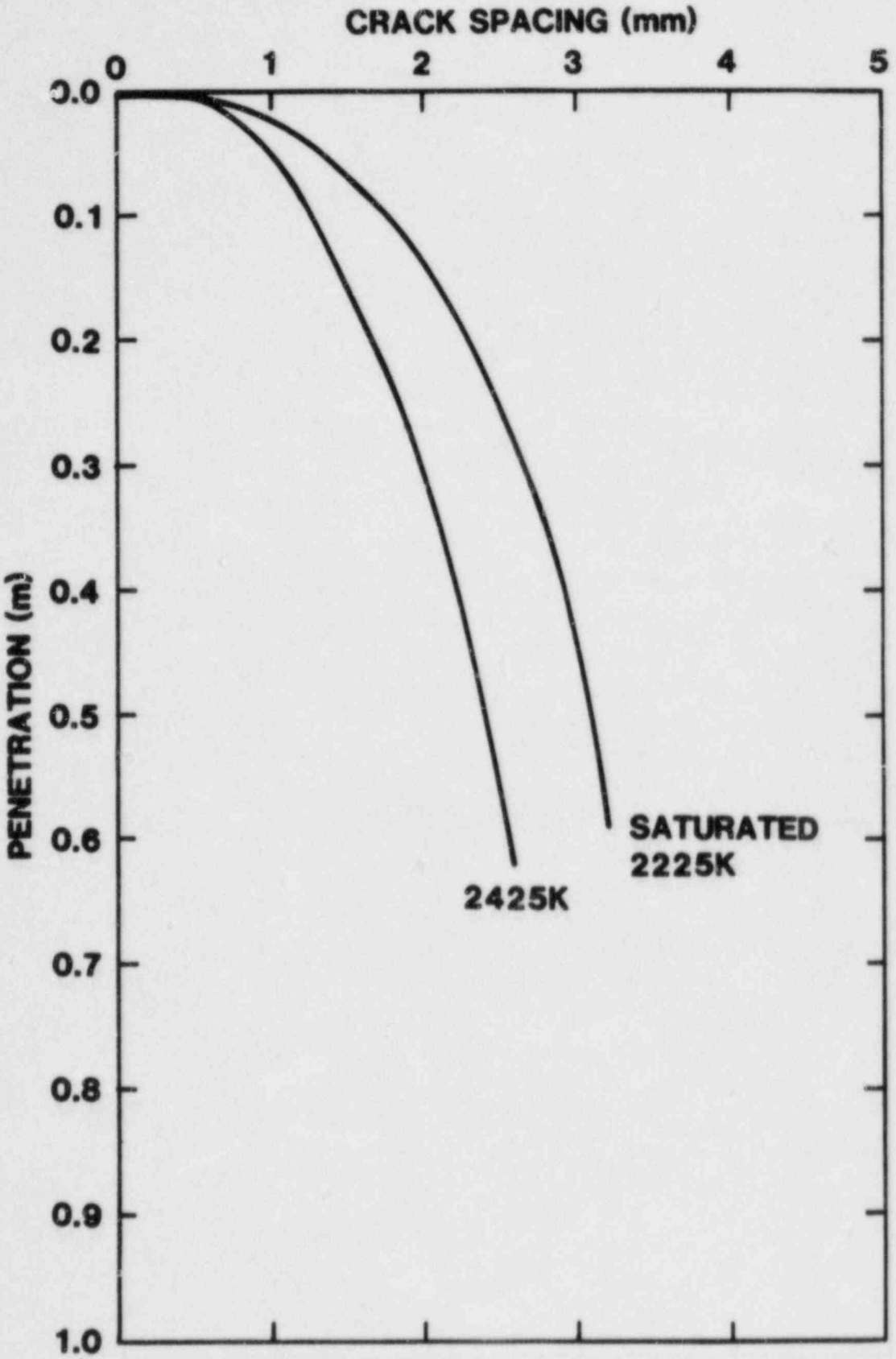

Figure C.1 Pentetration of Corium Melt Through a Vertical Crack

Table C.2 - Listing of Input File for Corium Flow in a Brick Matrix

```
CORIUM MELT ON HARKLASE BRICKS - BRICK MATRIX
          1          10           1           0           1           1
          0           1
     1.0E-5      1.0E-3       .0001         1.0          5.
       .001           1           1
   7.620E-2    3.429E-1       2425.
   1.524E-1          10           1
   1.000E-3    3.429E-1         0.0    3.810E-2        300.      1.0E-6
   7.620E-2           5           0
   1.000E-3    3.429E-1         0.0    7.620E-2        300.      1.0E-6
   1.524E-1          10           1
   1.000E-3    3.429E-1         0.0    3.810E-2        300.      1.0E-6
   7.620E-2           5           0
   1.000E-3    3.429E-1         0.0    7.620E-2        300.      1.0E-6
   1.524E-1          10           1
   1.000E-3    3.429E-1         0.0    3.810E-2        300.      1.0E-6
   7.620E-2           5           0
   1.000E-3    3.429E-1         0.0    7.620E-2        300.      1.0E-6
   1.524E-1          10           1
   1.000E-3    3.429E-1         0.0    3.810E-2        300.      1.0E-6
   7.620E-2           5           0
   1.000E-3    3.429E-1         0.0    7.620E-2        300.      1.0E-6
   1.524E-1          10           1
   1.000E-3    3.429E-1         0.0    3.810E-2        300.      1.0E-6
        0.0         0.0
     5.775E2         4.0
       11.0       7000.        485.
      2225.      2.08E5     4.34E-3          .5
       2.31       7070.        402.

      3098.
       7.92       2760.       1265.
```

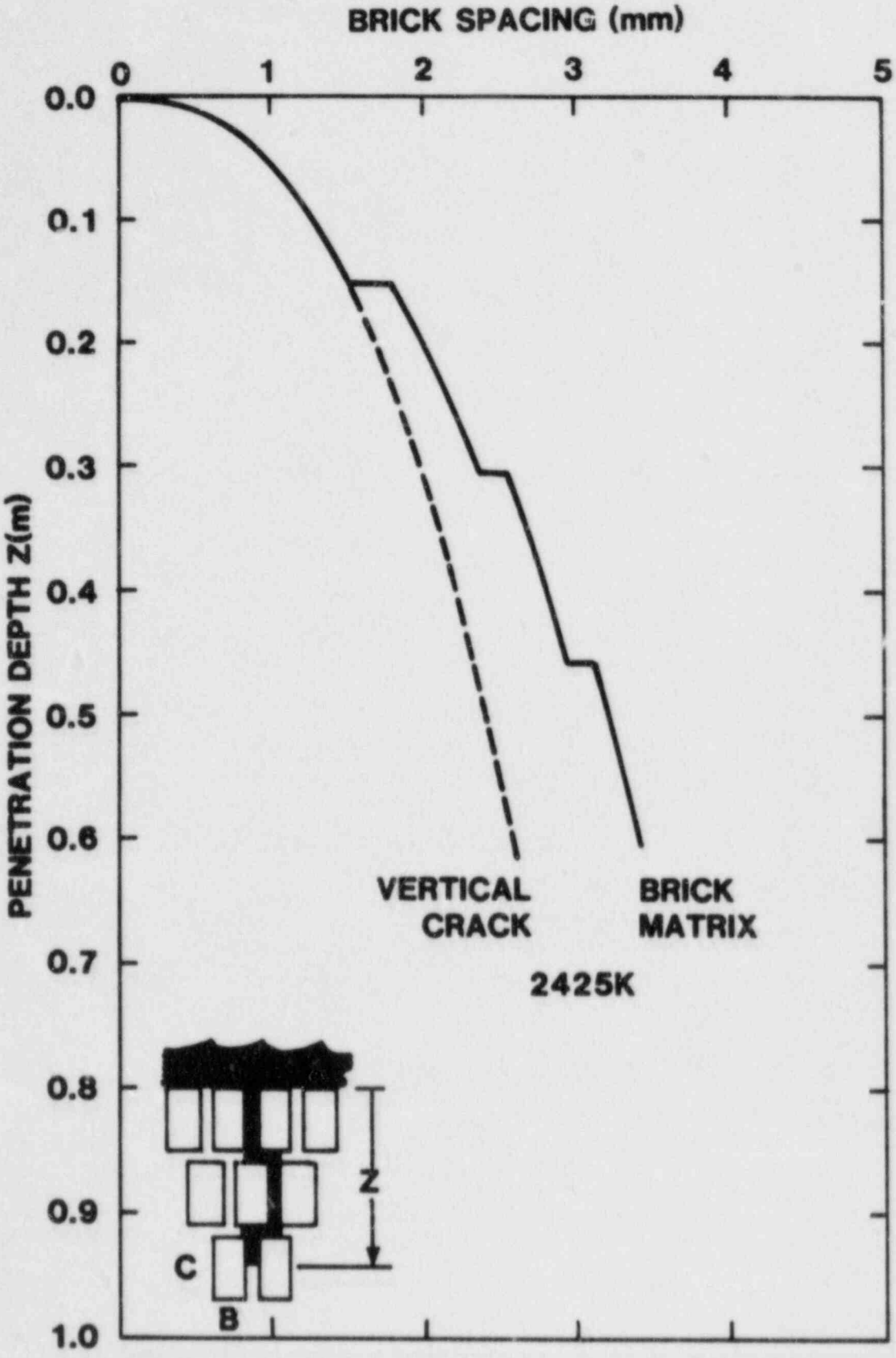

Figure C.2 Penetration of Corium Melt Through a Brick Matrix

Appendix D. Analysis of TRAN-1 Transition Phase Experiment

The PLUGM sample problem described in this appendix is the simulation of the TRAN-1 transition-phase experiment. TRAN-1 was the first experiment done in Sandia National Laboratories' LMFBR Transition-Phase program [13]. In this experiment, a sample of UO_2 was nuclear heated beyond its melting point and then vertically injected into a cylindrical flow channel with high-pressure helium gas. This sample problem illustrates several features of the PLUGM code including:

1. the use of the cylindrical geometry option,
2. the inertia-limited initial acceleration of the melt by the applied pressure differential, and
3. the depletion of the initial liquid slug by crust growth and liquid film deposition.

The geometry for this TRAN-1 experiment is shown in Figure D.1. A listing of the PLUGM input file for this case is shown in Table D.1. As can be seen from Figure D.1, there are three cylindrical (IGEOM = 2) regions in this PLUGM representation of the TRAN-1 geometry (NREG = 3); the fuel melt chamber, a short transition region, and the freezing channel. Only the first, reservoir region (melt chamber) is initially filled with fuel at 3200K (TBLK = 3200). The other three regions are initially empty (TBLK = 0.0).

Because the reservoir region has real boundaries (as opposed to the pool-type reservoirs used in Appendix B and C), it is treated as part of the overall flow channel relative to the calculation of crust growth, film deposition, heat transfer, friction losses, etc. (IRESOP = 0). The catch tank (by definition the last specified region) in this sample problem is actually the long fuel freezing channel. Thus, the last region is also treated as part of the overall flow channel (IDMPOP = 0) rather than as a special catch tank.

The input for this problem specifies a fully-coupled thermal-hydraulic/heat-transfer/crust-growth calculation (IHTOP = 1). A transient hydrodynamics calculation has been specified with an initial velocity of zero (IVELOP = 0). The calculation of film deposition accounts for steady-state film deposition as well as Taylor instabilities (IFILMOP = 2). Three stopping criteria are specified in the input, however, the one that is relevant for this problem is the minimum slug length criterion. This criterion specifies problem termination when the slug length in the channel decreases below 3 cm (DZMIN = 0.03).

	REGION 1	REGION 2	REGION 3
REGION LENGTH (cm)	4.500	0.940	100.000
CHANNEL DIAMETER (mm)	8.200	5.670	3.174
WALL THICKNESS (mm)	20.000	20.000	20.000

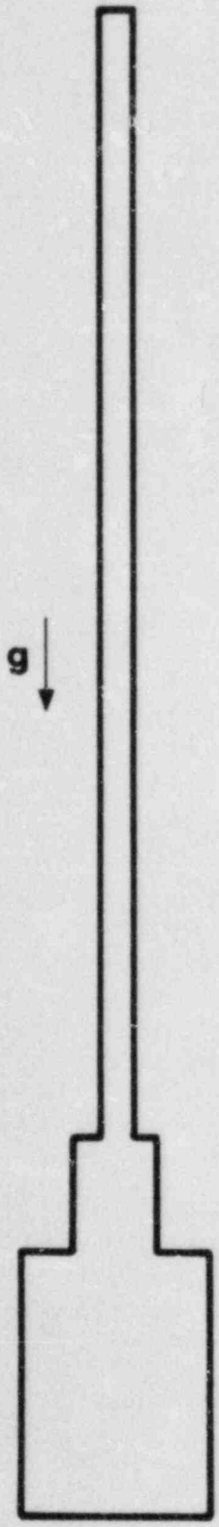

Figure D.1 - TRAN-1 Geometry as Modeled by PLUGM

Table D.1 - Listing of TRAN-1 Input File

```
TRAN1
         2             3             0             0             1             0
        20             2
1.0000E-05   1.0000E-04   3.0000E-02   1.0000E 00   2.5000E-01
4.5000E-02            10           -1
8.2000E-03                 3.2000E 03   2.0000E-02   6.7300E 02   1.0000E 00
0.9400E-02             1           -1
5.6700E-03                 0.0000E 00   2.0000E-02   6.7300E 02   1.0000E 00
1.0000E 00           200           -1
3.1740E-03                 0.0000E 00   2.0000E-02   6.7300E 02   1.0000E 08
1.6000E 06   0.0000E 00
0.0000E 00   0.0000E 00
1.1000E 01   8.6996E 03   4.8500E 02
3.1380E 03   2.8000E 05   4.3400E-03   0.0000E 00
3.4300E 00   9.7200E 03   6.1700E 02

1.7000E 03
3.4400E 01   7.3110E 03   6.7700E 02
```

The flow in this problem is driven by an applied driving pressure difference of 1.6 MPa (PTRAIL = 1.6E6, PLEAD = 0.0) that is assumed to persist in time. The flow direction is upward in each region (IGDEX = -1). No mass addition is specified (MFLUX = 0.0).

Note that the wall thickness specified for all three regions is 2 cm. For the time scale of this TRAN-1 problem, this 2 cm wall thickness represents an "infinite" wall thickness relative to the crust-growth solution procedures discussed in Chapter 5. Thus, the crust growth solutions described in Section 5.1.3 are the ones automatically used in this problem.

Selected results for the PLUGM calculation of this TRAN-1 sample problem are summarized in Figures D.2 - D.5. Figure D.2 shows the final axial distribution of fuel crust and liquid film thickness on the freezing channel wall. The crust thickness shows a fairly strong axial dependence whereas the liquid film thickness is nearly constant over the axial penetration length (dominated by steady-state film deposition). The axial crust distribution peaks at about 10 cm into the freezing channel. The crust thickness near the channel entrance is slightly lower than the peak value because of the small amount of initial superheat

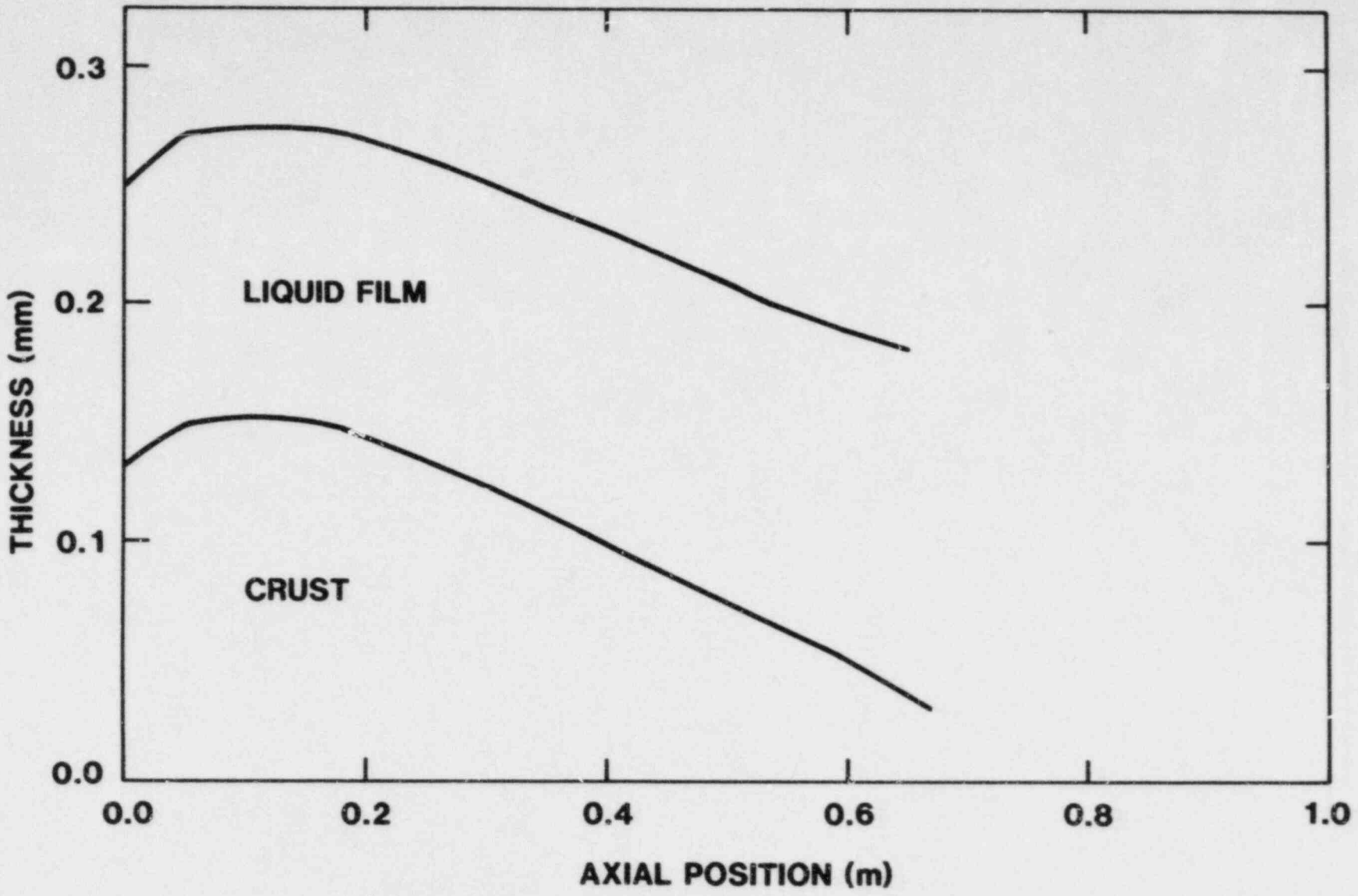

Figure D.2 Calculated Final Crust and Film Axial Distribution in TRAN-1

in the bulk melt. The effect of this superheat is felt most strongly near the channel entrance before the bulk melt cools as a result of heat transfer to the channel wall. Beyond the crust thickness peak at ~10 cm, the crust thickness decreases steadily to the point of maximum penetration. The reason for this is the steady acceleration of the liquid slug caused by mass depletion and the decrease in lug length with time (and with penetration into the channel). Thus, the time that the liquid slug is in contact with (adjacent to) the channel wall decreases with penetration into the channel, thereby leaving less time for crust growth to occur prior to being passed by the trailing edge of the flow.

Figure D.3 shows the leading edge and trailing edge of the liquid fuel slug as a function of time. As can be seen in this figure, the length of the slug is continually decreasing with penetration into the channel because of crust growth and film deposition. The effect of Taylor instabilities on the film deposition is significant. Rerunning this same problem with only steady-state film deposition (IFILMOP = 1) results in a calculated penetration distance that is 8 cm longer than the nominal result.

Figures D.4 and D.5 show the calculated leading edge velocity as a function of time. Shown for comparison in each case is the leading edge velocity that would be calculated for a quasi-steady velocity calculation (IVELOP = 2). Figure D.4 shows the comparison for the first 4 ms of the flow and Figure D.5 shows the comparison for the duration of the flow until mass depletion occurs.

For the early-time results (Figure D.4), the quasi-steady calculation starts at velocity of about 21 m/s (primarily determined by the pressure drop at the entrance to the transition region), and thus the leading edge of the flow reaches the entrance to the freezing channel at ~0.5 ms. The added area-change pressure drop at that point results in an instantaneous decrease in velocity such that the leading edge velocity at that point is about 19 m/s. From there on, the velocity decreases steadily with penetration into the freezing channel because of the added friction length. By comparison, the full transient calculation starts at time zero with zero velocity, and the liquid fuel slug accelerates because of the applied pressure differential. Because the average early-time velocity is lower in this case, it takes ~1.5 ms for the leading edge of the flow to reach the entrance to the freezing channel (compared to 0.5 ms in the quasi-steady case). Continuity of mass flux and a decrease in channel flow area by a factor of ~3.5 at that point result in an initial penetration velocity of ~35 m/s in the freezing channel. However, the large pressure drop

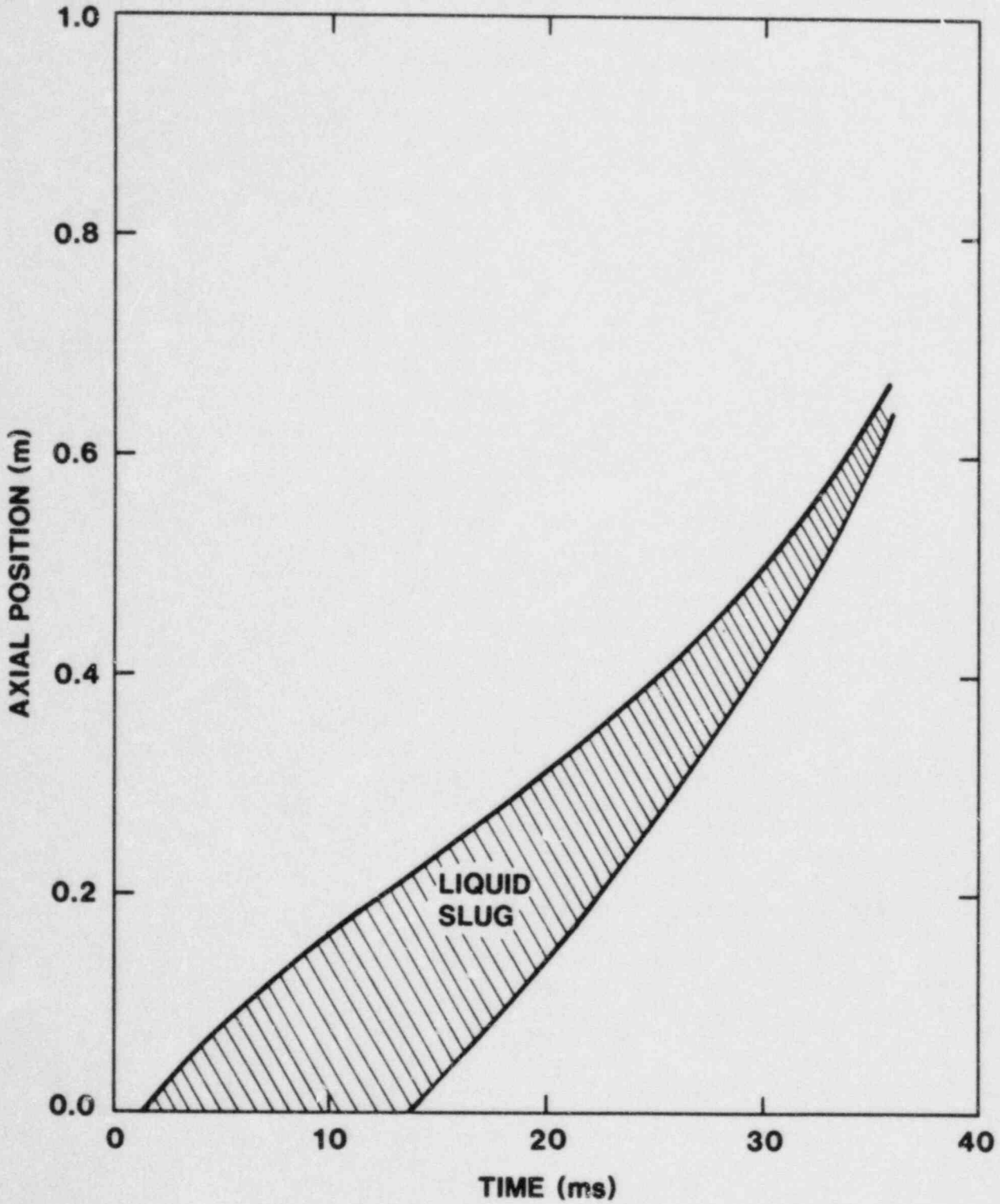

Figure D.3 - Slug Position as a Function of Time in TRAN-1 (Steady-State Deposition Plus Taylor Instabilities)

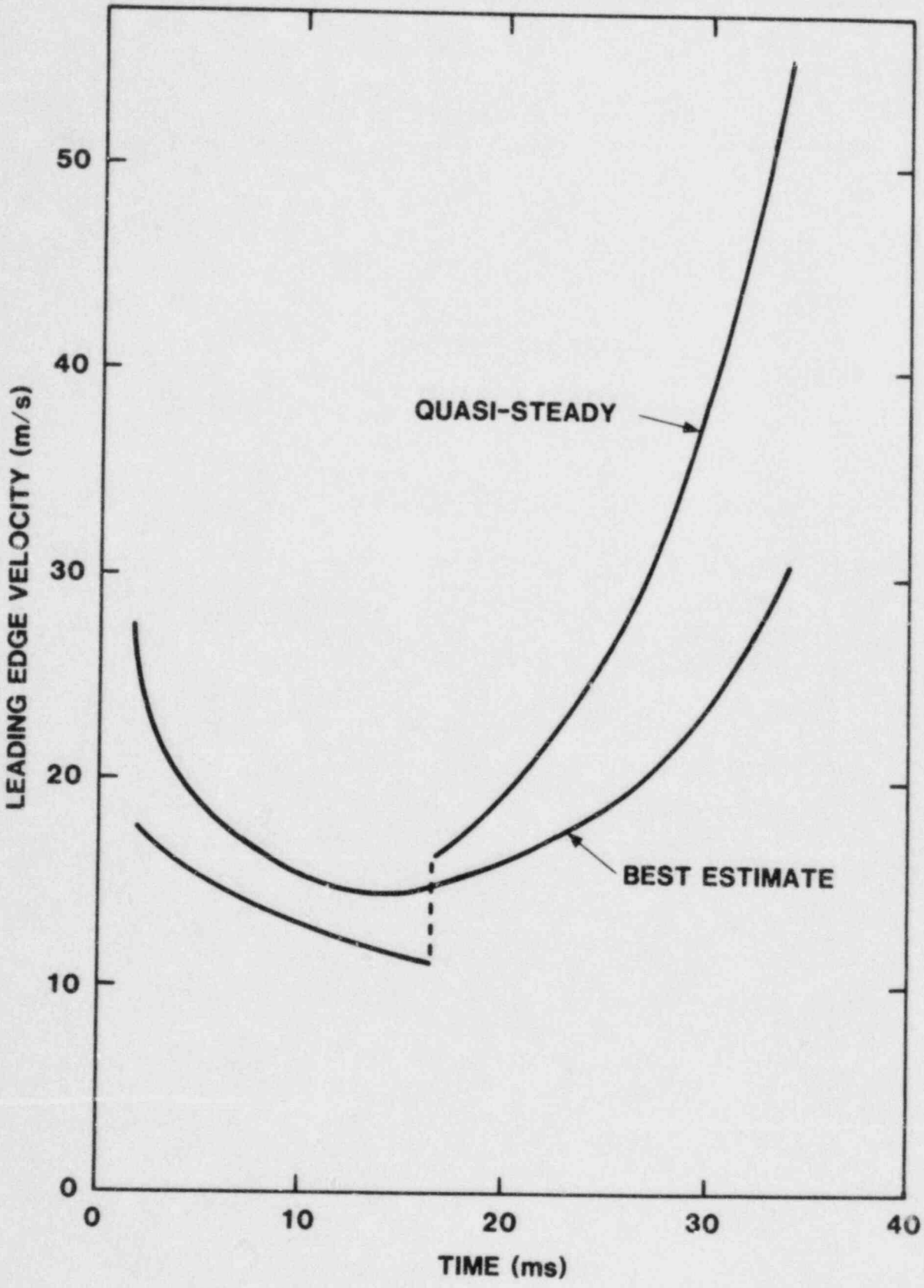

Figure D.4 – Slug Leading-Edge Velocity in TRAN-1

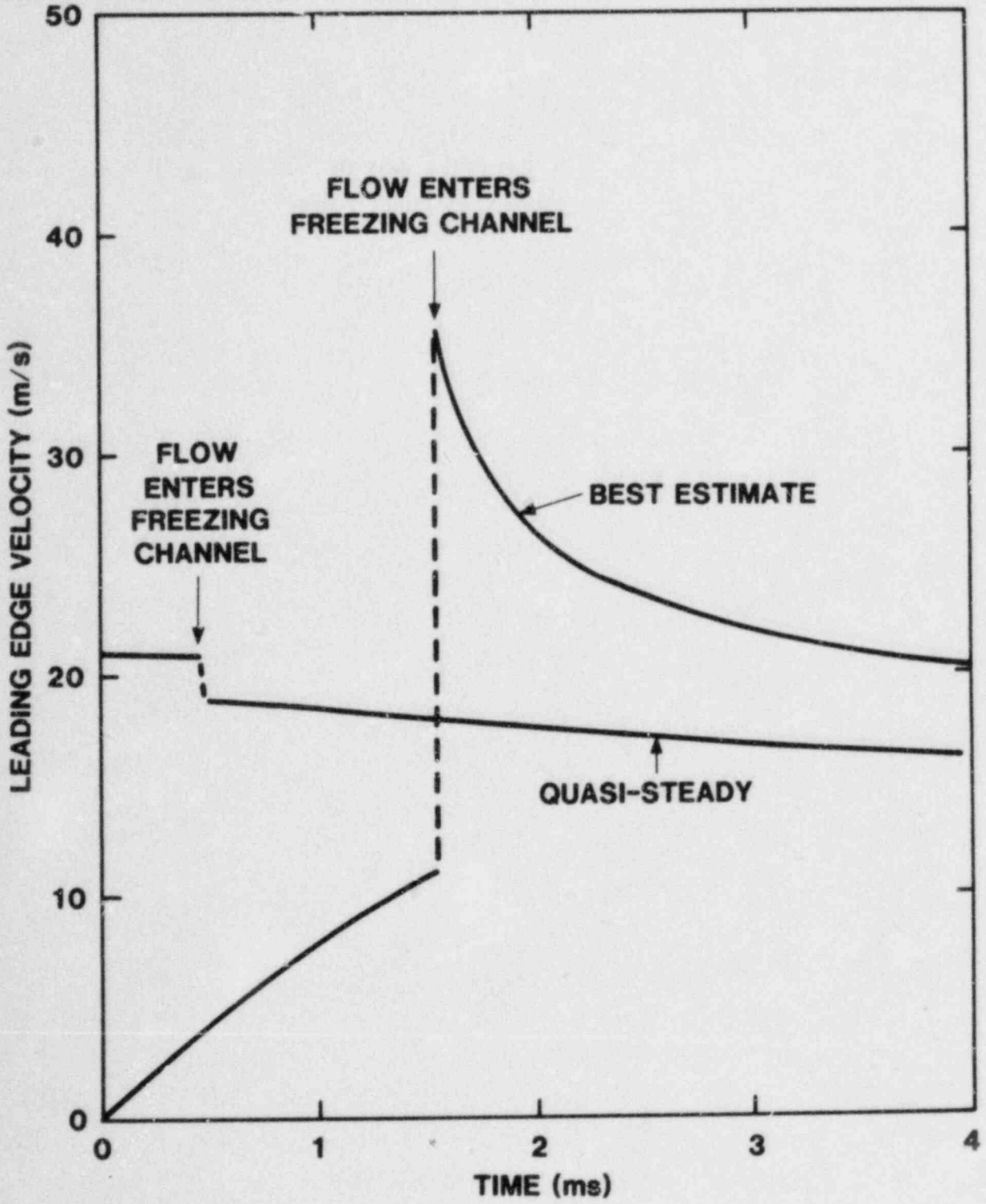

Figure D.5 - Short-Time Leading-Edge Velocity in TRAN-1

resulting from that area change causes a rapid deceleration of the fuel slug such that the velocity tends towards the quasi-steady result.

Figure D.5 shows the velocity comparison for the duration of the fuel flow. In both cases, the velocity decreases with time until the trailing edge of the flow enters the freezing channel (at ~14 ms for the full transient case and ~16.5 ms for the quasi-steady case). The velocity then increases (by definition this increase is instantaneous for the quasi-steady case) because the slug flow no longer sees the large area change (and pressure drop) at the entrance to the freezing channel. Late in time, the velocity increases rapidly because of rapid mass depletion. Inertial effects in the best estimate case limit this acceleration substantially relative to the quasi-steady results.

As is apparent from the comparisons shown in Figures D.4 and D.5, there are substantial differences between a best-estimate velocity history and one that would be obtained from a quasi-steady flow approximation. These differences in velocity result in a calculated penetration distance for the quasi-steady case that is about 10 cm longer than the nominal result. Thus, inertial effects on the velocity are important for the understanding of problems such as the TRAN-1 experiment.

DISTRIBUTION:

U.S. NRC Distribution Contractor (CDSI) (365 copies)
7300 Pearl Street
Bethesda, MD 20014
340 copies for R3
25 copies for NTIS

U.S. Nuclear Regulatory Commission (16)
Office of Nuclear Regulatory Research
Washington, D.C. 20555
Attn: O. E. Bassett
B. S. Burson
R. T. Curtis
C. N. Kelber
J. Larkins
T. Lee (5)
G. Marino
D. F. Ross
M. Silberberg
R. W. Wright
T. Walker
P. Wood
W. Pasedag

U.S. Nuclear Regulatory Commission (4)
Office of Nuclear Regulatory Regulation
Washington, DC 20555
Attn: L. G. Hulman
P. Easky
J. Rosenthal
J. Mitchell

U.S. Nuclear Regulatory Commission
Office of Nuclear Reactor Research
Clinch River Breeder Reactor Program Office
Washington, DC 20555
Attn: C. Allen

U.S. Department of Energy (3)
Albuquerque Operations Office
P.O. Box 5400
Albuquerque, NM 87185
Attn: J. R. Roeder, Director
Operational Safety Division
D. K. Nowlin, Director
Special Programs Division
For: C. B. Quinn
D. Plymale
D. L. Krenz, Director
Energy Technologies Division
For: C. B. Quinn
R. L. Clark

U.S. Department of Energy
Office of Nuclear Safety Coordination
Washington, DC 20545
Attn: R. W. Barber

Electric Power Research Institute
3412 Hillview Avenue
Palo Alto, CA 94303
Attn: R. Vogel
R. Sehgal

Los Alamos National Laboratory
P.O. Box 1663
Los Alamos, NM 87145
Attn: C. R. Bell, Q-7

General Electric Corporation (5)
310 DeGuigne Drive
Sunnyvale, CA 94086
Attn: S. M. Davies, Mgr., LSPB Project
T. I. Temme, Mgr., Probabilistic Risk Assessment
D. M. Switick, Mgr., Plant Safety
S. Rhow

Battelle Columbus Laboratory (4)
505 King Avenue
Columbus, OH 43201
Attn: P. Cybulskis
R. Denning
J. Gieseke
G. Greene

J. E. Antill
Berkeley Nuclear Laboratory
Berkeley GL 139 PB
Gluocestershire
United Kingdom

W. G. Cunliffe
Bldg. 396
British Nuclear Fuels, Ltd.
Springfields Works
Salwick, Preston
Lancs
United Kingdom

Power Reactor and Nuclear Fuel (4)
Development Corporation (PNC)
Oarai Engineering Center
Oarai, Ibaraki-ken
Japan 311-13
Attn: Dr. K. Takahashi
Dr. N. Tanaka
Dr. M. Saito
Dr. A. Furutani

Centre d'Etudes Nucleaires de Cadarache (4)
Boite Postale No. 1
13115 St. Paul lez Durance
France
Attn: A. Meyer-Heine DERS/SIES
J. Cl. Melis DERS/SIES
M. Schwarz DERS/SIES
C. LeRigoleur DRNR/SYTC

Dr. Carl A. Erdman
Nuclear Engineering Department
Texas A and M University
College Station, TX 77843

University of Virginia
Department of Nuclear Engineering
and Engineering Physics
Attn: A. B. Reynolds

Massachusetts Institute of Technology
Department of Nuclear Engineering
Cambridge, Mass.
Attn: M. Kazimi

Professor T. Theofanous
Purdue University
School of Engineering
West Lafayette, IN 47907

Fauske Associates (3)
16W070 West 83rd Street
Burr-Ridge, IL 60521
Attn: R. Henry
M. Grolmes
M. Epstein

I. Catton
UCLA
Nuclear Energy Laboratory
405 Hilgard Avenue
Los Angeles, CA 90024

EG&G, Idaho Inc.
P.O. Box 1625
Idaho Falls, ID 83401
Attn: F. M. Haggag

Brookhaven National Laboratory (4)
Upton, NY 11973
Attn: R. A. Bari
T. Pratt
G. Greene
T. Ginsberg

Professor R. Seale
Department of Nuclear Engineering
University of Arizona
Tucson, AZ

Oak Ridge National Laboratory (3)
OakRidge, TN
Attn: T. Kress
S. Hodge
K. S. Norwood

K. Holtzclaw
General Electric - San Jose
Mail Code 682
175 Kurtner Avenue
San Jose, CA 95125

Argonne National Laboratory (9)
9700 S. Cass Avenue
Argonne, IL 60439
Attn: L. W. Deitrich
C. Dickerman
A. E. Klickman
T. E. Kraft
J. M. Kramer
D. Pedersen
J. J. Sienicki
B. W. Spencer
D. P. Weber

Reactor Development Division (4)
UKAEA - Atomic Energy Establishment
Winfrith, Dorchester
Dorset
United Kingdom
Attn. R. G. Tyror, Head
T. Briggs
R. Potter
A. Nichols

UKAEA Safety and Reliability Directorate (4)
Wigshaw Lane
Culcheth
Warrington WA3 4NE
Cheshire
England
Attn: Dr. J. Gittus, Director
Dr. M. J. Hnyn
Mr. H. Teague
Dr. R. S. Peckover

AERE Harwell
Didcot
Oxfordshire OX11 ORA
England
Attn: Dr. J. R. Matthews,
Theoretical Physics Division

UKAEA (2)
Risley
Warrington WA3 6AT
Cheshire
England
Attn: Dr. B. Cowking, FRDD
Dr. D. Hicks, TRDD

Dr. F. Briscoe
Culham Laboratory
Culham
Abingdon
Oxfordshire OX14 X
England

Mr. C. P. Gratton
Division Head, SESD
Atomic Energy Eestablishment
Winfrith,
Dorset DTZ 8DH
England

Projekt Nucleare Sicherheit (3)
Kerforschungszentrum Karlsruhe
Postfach 3640
75 Karlsruhe
Federal Republic of Germany
Attn: J. P. Hoseman
Albrecht
H. H. Rininsland

Projekt Schneller Brueter (8)
Kernforschungszentrum Karlsruhe GMBH
Postfach 3640
D75 Karlsruhe
West Germany
Attn: Dr. Kessler (2)
Dr. Heusener (2)
Dr. Froelich
Dr. Werle
Dr. Kuhn
Dr. Groetzbach
Dr. Ohnemus

Mr. G. Petrangeli
Direzione Centrale della Srcurezza
Nucleare e della Protezione Sanitaria (DISP)
Entre Nazionnle Energie Alternative (ENEA)
Vrale Regina Margherita, 125
Casella Postale N. 2358
I-00100 Roma A.D., ITALY

Dr. K. J. Brinkman
Reactor Centrum Nederland
P.O. Box 1
1755 ZG Petten
THE NETHERLANDS

Joint Research Centre (2)
Ispra Establishment
21020 Ispra (Varese)
Italy
Attn: H. Holtbecker
P. Fasoli-Stella

Power Reactor and Nuclear Fuel (3)
Development Corporation (PNC)
Fast Breeder Reactor Development Project (FBR)
9-13, 1-Chome, Akasaka
Minato-Ku, Tokyo
Japan
Attn: Dr. A. Watanabe (3)

Technology Management Center (3)
Argonne National Laboratory
Building 207
9700 S. Cass Avenue
Argonne, IL 60439
Attn: L. Baker
S. S. Borys
D. R. Ferguson

Cathy Anderson
Nuclear Safety Oversight Commission
1133 15th Street, NW
Washington, DC 20005

Mr. H. Bairiot, Chief
Department LWR Fuel
Delgonucleaire
Rue de Champde Mars. 25
B-1050 BRUSSELS, BELGIUM

Dr. S. Saito
Japan Atomic Energy Research Institute
Takai Research Establishment
Tokai-Mura, Naku-Gun
Ibaraki-ken
JAPAN

Wang Lu
TVA
400 Commerce, W9C157-CK
Knoxville, TN 37902

M. Fontana
Director, IDCOR Program
Technology for Energy, Inc.
P.O. Box 22996
10770 Dutchtown Road
Knoxville, TN 37922

H. J. Teague (3)
UKAEA
Safety and Reliability Directorate
Wigshaw Lane
Culcheth
Warrington, WA3 4NE
United Kingdom

Dr. Fran Reusenbach
Gesellschaft fur Reaktorsicherheit (GRS mbH)
Postfach 101650
Glockengasse 2
5000 Koeln 1
Federal Republic of Germany

1230 J. E. Powell
1830 M. J. Davis
1840 R. J. Eagan
1846 R. K. Quinn
1846 R. A. Sallach (5)
3141 C. M. Ostrander (5)
3151 W. L. Garner
3431 B. N. Tates
6000 E. H. Beckner
6255 D. O. Lee
6400 A. W. Snyder
6410 D. J. McCloskey
6412 J. W. Hickman
6420 J. V. Walker
6420 J. B. Rivard
6420 M. Watkins
6420 M. Hasti
6421 T. R. Schmidt
6421 Hitchcock
6422 D. A. Powers
6422 F. E. Arellano
6422 J. E. Brockmann
6422 R. M. Elrick
6422 E. R. Copus
6422 J. E. Gronager
6422 W. Tarbell
6423 P. S. Pickard (2)
6423 R. O. Gauntt
6423 S. A. Wright
6425 W. J. Camp
6425 M. Pilch (5)
6425 P. K. Mast (5)
6425 J. E. Kelly
6425 R. J. Lipinski
6427 M. Berman
6440 D. A. Dahlgren
6442 W. A. Von Riesemann
6449 K. D. Bergeron
6450 J. A. Reuscher
6451 T. F. Luera
6453 W. J. Whitfield
6454 G. L. Cano
7100 C. D. Broyles
7530 T. B. Lane
7537 N. R. Keltner
7550 F. W. Neilson
8424 M. A. Pound

NRC FORM 335 (16-83) U.S. NUCLEAR REGULATORY COMMISSION

BIBLIOGRAPHIC DATA SHEET

1 REPORT NUMBER (Assigned by TIDC add Vol. No. if any)
SAND82-1580
NUREG/CR-3190

2 Leave blank

3 TITLE AND SUBTITLE
PLUGM: A Coupled Thermal-Hydraulic Computer Model for Freezing Melt Flow in a Channel

4 RECIPIENT'S ACCESSION NUMBER

5 DATE REPORT COMPLETED
MONTH: April YEAR: 1984

6 AUTHOR(S)
M. Pilch, Sandia National Laboratories
P. K. Mast, Science Applications, Inc.

7 DATE REPORT ISSUED
MONTH: April YEAR: 1984

8 PERFORMING ORGANIZATION NAME AND MAILING ADDRESS (Include Zip Code)
Sandia National Laboratories
Albuquerque, NM 87185

9 PROJECT/TASK/WORK UNIT NUMBER

10 FIN NUMBER
A1247

11 SPONSORING ORGANIZATION NAME AND MAILING ADDRESS (Include Zip Code)
Div. of Engineering Technology &
Division of Accident Evaluation
Office of Nuclear Regulatory Research
U.S. Nuclear Regulatory Commission
Washington, DC 20555

12a TYPE OF REPORT
Computer Model

12b PERIOD COVERED (Inclusive dates)

13 SUPPLEMENTARY NOTES

14 ABSTRACT

PLUGM models the flow and freezing of molten material in a nonmelting channel. PLUGM is being developed for applications in Sandia's Ex-Vessel Core Retention Materials Assessment Program and in Sandia's LMFBR Transition-Phase Program.

PLUGM models time-dependent flow from a reservoir, through a channel and possibly into a catch tank. Three user-specified geometry options enable realistic modeling of melt flow and freezing in tubes, thin slits, and particle beds. Axial variation of relevant channel parameters is possible.

Melt flow is driven or hindered by gravity, applied pressure, and capillary pressure. Hydrodynamic losses due to friction, area changes, and flow direction changes are modeled. Also modeled are the competing effects of mass addition to the reservoir, mass drainage into the channel, and slug depletion by film and crust deposition on the channel wall.

Cooldown of a superheated melt occurs by material transport down the channel and by convective heat transfer to the channel walls or crust. Axial conduction and volumetric heating within the bulk melt are not modeled.

Crust deposition on the channel wall is controlled by the competing effects of convective heat transfer from the bulk melt to the crust surface and the conduction limited removal of heat from the crust into the wall. An external coolant may further enhance this heat removal by limiting the temperature increase in the wall.

Sample problems, pertaining to ex-vessel core retention and LMFBR transition phase, illustrate features and capabilities of the code.

15a KEY WORDS AND DOCUMENT ANALYSIS 15b DESCRIPTORS

Plugging, Freezing, Core Catcher, LMFBR Transition Phase

16 AVAILABILITY STATEMENT
Unlimited

17 SECURITY CLASSIFICATION (This report)
U

18 NUMBER OF PAGES

19 SECURITY CLASSIFICATION (This page)
U

20 PRICE
$